



## Durham E-Theses

---

### *Optimizing the performance of an atmospheric Cherenkov telescope*

Roberts, Ian David

#### How to cite:

---

Roberts, Ian David (1998) *Optimizing the performance of an atmospheric Cherenkov telescope*, Durham theses, Durham University. Available at Durham E-Theses Online: <http://etheses.dur.ac.uk/4685/>

#### Use policy

---

The full-text may be used and/or reproduced, and given to third parties in any format or medium, without prior permission or charge, for personal research or study, educational, or not-for-profit purposes provided that:

- a full bibliographic reference is made to the original source
- a [link](#) is made to the metadata record in Durham E-Theses
- the full-text is not changed in any way

The full-text must not be sold in any format or medium without the formal permission of the copyright holders.

Please consult the [full Durham E-Theses policy](#) for further details.

# Optimizing the Performance of an Atmospheric Cherenkov Telescope

by Ian David Roberts, M.Sc.

A thesis submitted to the University of Durham in  
accordance with the regulations for admittance to

the degree of Doctor of Philosophy

The copyright of this thesis rests  
with the author. No quotation  
from it should be published  
without the written consent of the  
author and information derived  
from it should be acknowledged.

Department of Physics

University of Durham

September 1998



22 JUN 1999

## Abstract

This thesis is concerned with the performance of the Mark 6 atmospheric Cherenkov telescope, which is the latest triple-coincidence VHE gamma-ray telescope built by the Durham group.

Chapter 3 describes the Durham telescopes, with particular reference to the Mark 6 telescope. It goes on to describe the procedures which are involved in taking and processing data and the subsequent analysis of such data using imaging techniques to distinguish between gamma-rays and the cosmic-ray background.

The quality and quantity of data recorded are dependent upon the performance of various components of the telescope and also on the environment in which it operates. Chapter 4 discusses the effects of such parameters on the performance of the telescope and describes the efforts made to minimize the variations in the data caused by changes in these conditions. Chapter 5 describes the improvements made to the telescope design and operation post-construction in order to increase the rate of data acquisition and to improve the quality of the data, particularly with a view to enhancing the telescope sensitivity to low energy gamma-rays.

Data taken with 2 separate and simple light collectors/detectors can be combined to use differences in the distribution of light from gamma-ray and hadronic induced showers to discriminate between them. Chapter 6 contains the results of such a study of the stereoscopic properties of Cherenkov signals using the Durham Mark 6 and Mark 5A telescopes and highlights the use of data taken using the well-separated left and right detectors of the Mark 6 telescope for a similar purpose.

The final chapter reviews the achievements to date in terms of the improvements made to the telescope and the sources detected during its operation. It goes on to describe future developments to further enhance the telescope performance.

## Contents

Chapter 1 - Introduction	1
1.1 An Introduction to Cosmic Ray Astrophysics	1
1.2 The Development of TeV Gamma Ray Astronomy	2
1.3 Candidate Gamma Ray Sources and Interaction Mechanisms	2
1.3.1 Cosmic Gamma-Ray Sources	4
1.3.2 Gamma-Ray Production Mechanisms	4
1.3.3 Gamma-Ray Absorption Mechanisms	6
1.4 Ground Based Gamma-Ray Astronomy	7
1.5 Motivations for Observations at Lower Energies	8
1.6 Summary	9
Chapter 2 - Ground Based Gamma-Ray Astronomy	10
2.1 Introduction	10
2.2 Cherenkov Light	10
2.2.1 The Physical Basis of Cherenkov Radiation	10
2.2.2 Cherenkov Radiation as an Astronomical Tool	13
2.3 Extensive Air Showers	14
2.3.1 Detection of EAS via the Atmospheric Cherenkov Technique	18
2.4 Atmospheric Cherenkov Telescopes	20
2.5 Summary	21
Chapter 3 - The Durham Atmospheric Cherenkov Telescopes	23
3.1 Introduction	23
3.1.1 Historical Background	23
3.1.1.1 The Triple-Coincidence Technique	23
3.1.2 The Bohena Observatory	24
3.2 The Durham Atmospheric Cherenkov Telescopes	25
3.2.1 The Mark 3A Telescope	26
3.2.2 The Mark 5A Telescope	27

3.3 The Mark 6 Telescope	29
3.3.1 Overview	29
3.3.2 Flux Collectors	30
3.3.3 Light Detecting Packages	30
3.3.3.1 The Imaging Camera	30
3.3.3.2 The Triggering System	33
3.3.4 Electronics	33
3.3.5 Data Logging	38
3.3.6 Routine Monitoring	38
3.3.7 Steering	38
3.3.7.1 CCD Camera	38
3.4 The Control Room	39
3.5 Methods of Observation	39
3.5.1 Tracking Mode	40
3.5.2 Chopping Modes	40
3.5.3 Drift Scans	40
3.6 Timekeeping	41
3.7 Data Recording	41
3.8 Data Calibration	42
3.8.1 PM Tube Response Calibration	42
3.8.2 Accurate Measurement of the Telescope Attitude	45
3.8.3 Adjustment of Event Times to the Centre of the Solar System	47
3.8.4 Adjustment of Event Times for an Object in a Binary System	48
3.9 Analysis of Data from Individual Telescopes	49
3.9.1 Imaging Analysis	49
3.9.2 Timing Analysis for Pulsed Sources	54
3.9.3 Compensation for Differences Between On- and Off-Source Fields	55
3.10 Quality Control	55
3.11 Observing Campaigns for 1994-7	56
3.12 Summary	57

Chapter 4 - The Stability and Operation of Atmospheric Cherenkov Telescopes	58
4.1 Introduction	58
4.2 Nominal Performance of the Mark 6 Telescope	59
4.3 Factors Influencing the Performance of Atmospheric Cherenkov Telescopes	61
4.3.1 Telescope Design and Operation	63
4.3.1.1 Mirror Characteristics	64
4.3.1.2 Telescope Pointing Accuracy	65
4.3.1.3 Electronics Stability	67
4.3.1.4 Variation in Laser Calibration	68
4.3.2 Photomultiplier Tube Performance	70
4.3.2.1 Performance Variations across the Photocathode of an XP3422 PM tube	72
4.3.2.2 Summary	74
4.3.3 Effects of Changes in the Telescope Environment	75
4.3.3.1 Ambient Temperature	75
4.3.3.2 Background Illumination	77
4.3.3.3 Photomultiplier Tube Orientation Relative to the Earth's Magnetic Field	79
4.3.4 Sky Clarity	81
4.4 Systems for Monitoring Telescope Performance and Environment	82
4.4.1 Telescope Performance Parameters	82
4.4.2 Monitoring the Telescope Environment	82
4.4.3 Sky Clarity	85
4.5 Stabilization of Telescope Operating Conditions	87
4.6 Conclusions	88
Chapter 5 - Enhancements to the Performance of the Durham Mark 6 Atmospheric Cherenkov Telescope	89
5.1 Introduction	89
5.2 Reduction in the Energy Threshold of the Telescope	90

5.2.1 Optimization of Trigger Capability by Choice of PM tubes	92
5.2.2 Threshold Energy Reduction using Light Collecting Cones	94
5.2.2.1 Laboratory Measurement of Efficiency of Light Collecting Cones	96
5.2.2.2 Field Testing of Light Collecting Cones	99
5.2.3 Minimization of Sky Noise Using Light Baffles	102
5.3 Improving the Detection Efficiency for Smaller Events	105
5.3.1 The Standard 4-fold Digital Trigger System	105
5.3.2 Alternative Methods for Telescope Triggering	106
5.3.2.1 Triggering on the Response of the Imaging Camera	106
5.3.2.2 An Analogue Trigger	107
5.3.3 Comparison of Analogue and Digital Trigger Systems	108
5.3.3.1 Specification of an Analogue Trigger System	109
5.3.3.2 Additional Tests of the Analogue Trigger Concept	110
5.4 Increasing the Duty Cycle of the Telescope	111
5.4.1 Prevention of Condensation on the Mirrors	111
5.4.2 Mirror Heating to Prevent Freezing	112
5.5 Conclusions	118
Chapter 6 - Stereo Techniques in Ground Based Gamma-Ray Astronomy	119
6.1 Introduction	119
6.2 Event Parameterization Using Two Widely Spaced Telescopes	120
6.2.1 The Geometric Height of Maximum ( $H_c$ )	120
6.2.2 Image Centroid Separation ( $D_{miss}$ )	121
6.2.3 Primary Energy Ratio ( $R_{ep}$ )	123
6.3 Stereo Observations Using the Durham Mark 3A and Mark 5A Telescope Pair	125

6.3.1 Observations of the Cataclysmic Variable AE Aquarii	125
6.3.2 Limitations of the Mark3/Mark5 Telescopes as a Long Baseline Stereo Pair	126
6.4 Adapting Stereo Techniques to Data from the Mark 5A and Mark 6 Telescope Pair	128
6.5 Analysis of Mark 6 Telescope Data from Centaurus X-3	128
6.6 Observations of Centaurus X-3 using the Mark 5A and Mark 6 Telescopes	131
6.6.1 Analysis Procedures	132
6.6.2 Discussion of Results	133
6.6.3 Expectation of a Successful Detection of Gamma-Rays with the Mark 5 and Mark 6 Telescopes	137
6.7 Short Baseline Stereo Measurements using the Mark 6 Telescope	138
6.8 Summary	141
Chapter 7 - Conclusions and Future Work	142
7.1 Introduction	142
7.2 Achievements to Date	142
7.3 Detections of VHE Gamma-Ray Sources	143
7.4 Further Modifications to the Durham Atmospheric Cherenkov Telescopes	144
7.4.1 Future Improvements to the Mark 6 Telescope	145
7.5 Future Prospects for VHE Gamma-Ray Astronomy	147
References	148

## Preface

All of the work described in this thesis has been part of the programme of study with the atmospheric Cherenkov telescopes operated at the University of Durham Gamma-Ray Observatory, Narrabri, New South Wales, Australia. The author spent seven dark moon periods at Narrabri as part of teams involved in data collection and telescope improvement projects.

In Durham, the author has been involved in the testing and commissioning of the photomultiplier tubes used in the triggering detectors of the telescopes and also in the evaluation of the properties of those used in the high-resolution imaging detector of the Mark 6 telescope. The author has also investigated the effects of changes in the telescope environment - particularly temperature change - on its operation. He has been involved in the implementation of measures to control and minimize the influence of such variations on the data.

An investigation has been made into the possibility of using the Mark 5A telescope in conjunction with the Mark 6 telescope to provide stereoscopic measurements of Cherenkov images as a further discriminant against the cosmic ray background. Such techniques have been applied to a dataset recorded during observation of Centaurus X-3.

None of the material presented in this thesis has been submitted previously for admittance to a degree in this or any other university, except where due reference is made.

The copyright of this thesis rests with the author. No quotation from it should be published without his prior written consent and information derived from it should be acknowledged.

## Acknowledgements

I would like to thank Professor Brian Tanner for the provision of the facilities of the Department of Physics and the Particle Physics and Astronomy Research Council for their financial support.

I would also like to thank my supervisor, Professor Ted Turver, for his support and guidance throughout my study. Thanks also to Lowry McComb and Steve Rayner for their advice and to the rest of the Durham group, past and present, particularly Mark Dickinson, Simon Shaw and Jamie Holder and everyone I have met and through my work in Durham and Australia.

Thanks also to my family and friends, particularly those who know me better than I do! To the University Staff Football and Cricket teams and everyone who played for the Astrophysics 5-a-side football team, thanks for reminding me that winning isn't the only thing - although it's nice occasionally - and to my colleagues in Derby for unwittingly allowing me to carry on in the same vein! To Anne, Eleanor, Dave Healy and David Buck, my gratitude for not letting me take myself too seriously.

Finally, thanks to Jane, for patience over and above the call of duty.

## Chapter 1. Introduction

### 1.1 An Introduction to Cosmic Ray Astrophysics

The science of cosmic ray astronomy stems from the discovery of a flux of ionising radiation at the surface of the Earth, inferred from the reduction in the charge leakage from an electroscope when encased in a metal shield (Rutherford and Cooke, 1903). The initial hypothesis, that the radiation was terrestrial in origin, was disproved by numerous experiments that showed that the rate of charge leakage does not decrease with altitude (e.g. Goeckel, 1910; Hess, 1911). Furthermore, the radiation flux increased above a certain altitude. The sources of this cosmic radiation remain the subject of speculation to the present day.

The cosmic ray flux seen at the surface of the Earth is, apart from the solar component, isotropic. This is a result of the fact that the majority of the flux comprises charged particles, primarily protons. Interaction with the galactic magnetic field ( $10^{-6}$  G) causes charged particles to be deflected from a straight path, meaning that by the time they arrive at the Earth, all temporal and spatial information they carry about their progenitors is lost, resulting in the isotropy we see. The electrically neutral component of the cosmic ray flux is small (a few percent) but therefore important as this spatial information is retained. This component consists of neutrons, neutrinos and gamma rays. The lifetime of a neutron is too short for any significant flux to be detected over distances at the scale of galaxies and the interaction between neutrinos and matter is so weak that large scale projects are required to detect them in meaningful numbers (e.g. Halzen, 1998).

Thus, only gamma rays remain as a potentially useful component unaffected by magnetic fields. They are readily detectable over a wide range of energies and, at certain energies, have interaction lengths of intergalactic distances. The observation of gamma rays of astrophysical origin therefore allows for the potential association of astronomical objects with sources of cosmic radiation. As the photons all travel the same path to the observer with little speed variation due to changes in the refractive index of the interstellar medium, temporal information is also retained, allowing the identification of periodic and variable sources.

## 1.2 The Development of TeV Gamma-Ray Astronomy

Gamma-ray astronomy covers a wider energy range on the electromagnetic spectrum than any other branch of astronomy. It can be defined, somewhat arbitrarily, as ranging from 0.511 MeV (the rest mass of the electron), up to the highest energies observed, presently a few TeV. The field is subdivided according to the energy range of the primary gamma-rays and the different physical processes employed in their detection. In the low to high (LE/ME/HE) regimes ( $E < 30$  GeV), the gamma ray is absorbed high in the atmosphere and the energy propagated via an electromagnetic cascade, which does not survive to ground level. At these energies, observations can only be made above the atmosphere. The successes of satellite based observations such as *SAS-2*, *COS-B* and the *Compton Gamma Ray Observatory* has sustained a high level of interest in the field over the last 30 years (e.g. Pinkau, 1996, Mattox *et al.*, 1992). Detections at these energies are limited primarily by the size of instrument which can be deployed on a satellite and the lifetime of these experiments.

The very high energy (VHE) region covers gamma rays with energies from  $\sim 30$  GeV to  $\sim 50$  TeV. In this band, the electromagnetic cascade is still absorbed in the atmosphere, but contains particles which radiate Cherenkov light in measurable quantities. The mechanisms of the production and detection of Cherenkov light are discussed in chapter 2. This light is detectable at ground level and facilitates the detection of gamma-ray primaries of these energies by the correlation between primary energy and the amount of light in the Cherenkov shower.

At energies above 50 TeV, the electromagnetic cascade survives to ground level in sufficient quantity to be detected by, for example, scintillation counters. If such counters are arranged in an array, it is possible to reconstruct the arrival direction and energy of the primary (e.g. Yoshii *et al.*, 1996).

The subdivision of gamma-ray astronomy is summarised in table 1.1. This thesis describes work concerned with the utilisation of the atmospheric Cherenkov technique in the VHE gamma-ray region of the electromagnetic spectrum.

## 1.3 Candidate Gamma-Ray Sources and Interaction Mechanisms

Astronomical objects proposed as candidate sources of cosmic gamma-rays include the galactic centre, the galactic plane, active galactic nuclei (AGNs), supernova remnants, pulsars, cataclysmic variables, and primordial black holes. The differences in the fundamental natures of these objects makes it unlikely that the

Energy Range	Classification	Detection Technique
0.5 - 5 MeV	Low Energy (LE)	Scintillation Detector (Satellite)
5 - 30 MeV	Medium Energy (ME)	Compton Telescope (Satellite)
0.03 - 30 GeV	High Energy (HE)	Spark Chamber (Satellite)
0.03 - 50 TeV	Very High Energy (VHE)	Atmospheric Cherenkov Detector (Ground Based)
0.05 - $10^5$ PeV	Ultra High Energy (UHE)	e.g. Scintillation Detector Array (Ground Based)

*Table 1.1 The subdivision of the gamma-ray spectrum in terms of the instrumentation used for the detection of gamma-rays of differing primary energies (from Dickinson, 1995).*

same mechanism of gamma-ray production predominates in all of these environments. However, current models rely on only a few physical processes to account for the production of high energy gamma-rays. Generically, the production process involves the interaction between a relativistic electron or nucleon with other matter or a magnetic field. The particular processes considered of relevance at energies relating to the atmospheric Cherenkov technique are considered here, together with a brief discussion of detections of sources of cosmic gamma-rays.

### 1.3.1 Cosmic Gamma-Ray Sources

The EGRET experiment on board the *Compton Gamma Ray Observatory (CGRO)* has claimed detections for 200 objects at energies of 100 MeV and above (Thompson *et al.*, 1996 and references therein). Of these, only 5 have been observed at TeV energies up to 1997. The VHE gamma-ray source catalogue also includes a number of objects which have not been detected by EGRET. Table 1.2 shows those sources which have been detected by two or more observing groups or on more than one occasion.

Source	Object Type	Detection	Confirmation
Crab Nebula	plerion	Cawley et al., 1989	e.g. Konopelko et al., 1996
PSR B1706-44	plerion	Kifune et al., 1995	Chadwick et al., 1998a
Vela Pulsar	plerion	Yoshikoshi et al., 1997	Repeated Observations
Cen X-3	x-ray binary	Carramiñana et al., 1989	Raubenheimer, et al., 1989
Mrk421	AGN	Schubnell et al., 1996	Petry et al., 1996
Mrk501	AGN	Quinn et al., 1996	Bradbury et al., 1997
1ES2344+514	AGN	Catanese et al., 1998	None
AE Aquarii	cataclysmic variable	Bowden et al., 1992	Meintjes et al., 1992

*Table 1.2 Summary of VHE gamma-ray source detections. All except the last three are detected by the EGRET experiment.*

### 1.3.2 Gamma-Ray Production Mechanisms

VHE Gamma Rays may be produced by the decay of neutral pions, the interaction of charged particles with magnetic fields and the acceleration of low energy photons by the Inverse Compton Process. These processes are illustrated in figure 1.1.

Process	Mechanism
<b>Neutral Pion Decay</b>	
Accelerated Charged Particles <b>Bremsstrahlung Radiation</b>	
<b>Synchrotron Radiation</b>	
<b>Curvature Radiation</b>	
<b>Inverse Compton Acceleration of photons</b>	

*Figure 1.1 Gamma-ray production mechanisms pertinent to the energies observed using the atmospheric Cherenkov technique.*

Neutral pions are produced in nucleon-antinucleon annihilation and in inelastic collisions between cosmic ray protons or nuclei and interstellar matter or radiation. They decay into 2 gamma-rays, with a resulting energy spectrum that is a function of the proton cosmic ray energy spectrum and the matter density of the medium. The photon energy is typically 10% of the energy of the incident proton. The luminosity of the source region is merely the product of the proton flux and matter density if the gamma-ray optical depth is small. Neutral pions are also produced in

the decay of K mesons and hyperons which, in turn, are products of nucleon interactions.

The acceleration of a charged particle can also result in the production of a gamma-ray by one of the three methods shown.

Bremsstrahlung radiation is the product of a high energy electron being accelerated in the electrostatic field of a nucleus or other charged particle. The energy of the gamma-ray is dependent upon the amount by which the electron deviates from its original path and the energy of the incident electron. It can be as high as the energy of the incident electron. This is an important mechanism in regions where the matter density is high. The gamma ray luminosity is proportional to the product of matter density and electron flux.

Synchrotron radiation is the result of the interaction of a relativistic electron with the transverse component of a magnetic field. The electron acceleration is perpendicular to its instantaneous velocity and to the field. The photons emitted have energies several orders of magnitude lower than the electron. Therefore, the synchrotron process produces no gamma-rays of sufficient energy to be of direct interest to atmospheric Cherenkov astronomers although their detection at lower energies is indicative of the presence of relativistic electrons which can produce gamma-rays by other mechanisms.

Curvature radiation depends on the presence of a strong magnetic field ( $\sim 10^8$  T). Relativistic electrons are constrained to move along curved magnetic field lines. At the surface of a pulsar, the field is strong and the lines are highly curved so the gamma rays emitted can have energies almost as high as the radiating electron.

The final production mechanism for VHE gamma-rays involves the acceleration of a low energy photon via the inverse Compton process. The photon collides elastically with a relativistic electron and most of the electron energy is transferred to the photon. Considering the case where the energy of the incident electron ( $E_e$ ) is such that

$$E_e \gg (m_e c^2)^2 / h\nu$$

and  $h\nu$  is the energy of the incident photon, it is possible for the gamma-ray to emerge with energy approaching that of the incident electron.

### 1.3.3 Gamma-Ray Absorption Mechanisms

Cosmic gamma-rays with  $E > \sim 100$  KeV have a zero collision cross-section for pair production with atomic hydrogen. The mean free path for interactions is

$\sim 2.5 \times 10^6$  Mpc, assuming an intergalactic column density of  $< 10^{-5}$  g cm $^{-2}$  Mpc $^{-1}$ . This just leaves absorption due to photons and magnetic fields as an alternative mechanism.

Absorption of a gamma-ray by a photon is via electron-positron production resulting from interaction with the interstellar and intergalactic ambient photon flux. For pair production to occur thus

$$h\nu_1 + h\nu_2 \rightarrow e^+ + e^-$$

the combined energies of the photons must exceed  $(m_e c^2)^2$ . The cross section for interaction with starlight is therefore small and only significant at intergalactic distances. It is suggested that gamma-rays with energies in excess of 10 TeV may suffer interaction with the thermal microwave background (Gould and Schröder, 1966; Jelley, 1966). This mechanism also becomes an important consideration for observations of galactic sources at energies in excess of 50 TeV. At lower energies, most absorption due to pair production is the result of interactions with visible and IR background photons. The effect of this on observations of distant sources is discussed by, for example, Stecker, Salamon and de Jager (1992).

Absorption by magnetic fields is essentially the same process as described above. The gamma-ray interacts with a 'virtual photon' from the field. In the VHE regime, extreme magnetic fields ( $10^8$  T) are required, meaning that the mechanism is unimportant over galactic distances, but does place restrictions on the production sites of gamma-rays in neutron stars.

#### 1.4 Ground Based Gamma-Ray Astronomy

As detailed in section 1.2, ground based observations are practical for photons with primary energies greater than  $\sim 30$  GeV. As the primary energy increases, the flux of incident gamma-rays reduces significantly. Figure 1.3 shows the gamma-ray spectrum for the Crab Nebula, a well documented source, regarded as the standard candle against which northern hemisphere instruments and detections can be compared. As can be seen, the flux at 300 GeV is  $\sim 20$  times smaller than that at 100 GeV. As a result, ground based instruments must cover a sensitive area commensurately larger than satellite-based instruments to detect the same number of incident photons. Large ground-based gamma-ray telescopes typically have a sensitive area of the order of  $10^4$  m $^2$ .

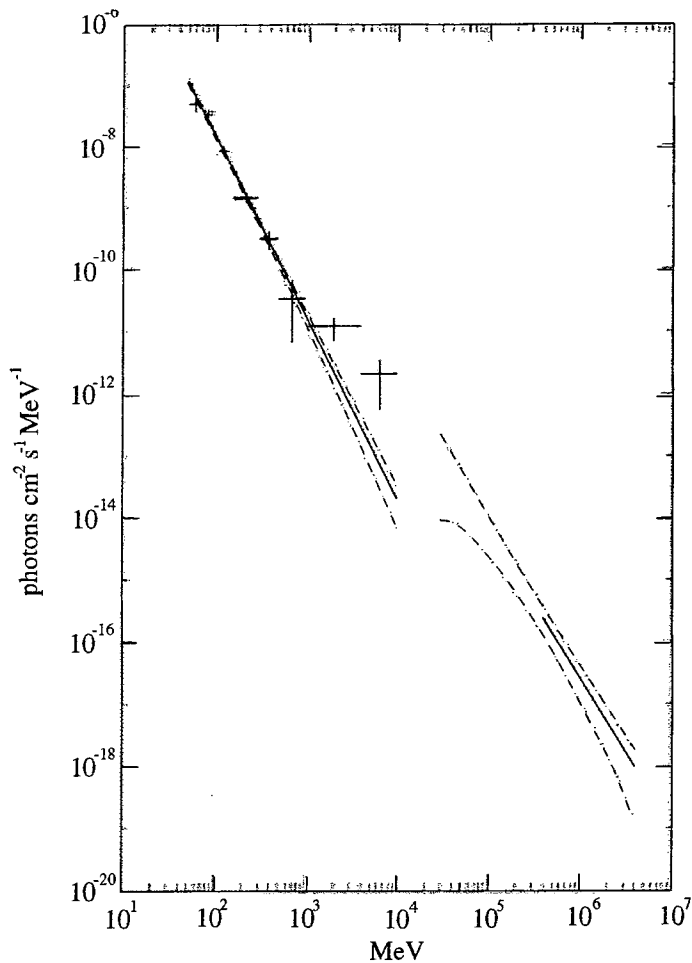


Figure 1.3 Differential spectrum of the unpulsed emission from the Crab Nebula (from Nolan et al., 1993).

### 1.5 Motivations for Observations at Lower Energies

This thesis describes the efforts made to reduce the energy threshold of the Durham Mark 6 atmospheric Cherenkov telescope. This aim is driven by four primary motives.

- A reduction in the energy threshold of an observation leads to a commensurate increase in the flux, with an improvement in counting statistics for an observation of given duration.
- It is hypothesized that the response of a Cherenkov telescope to the hadron induced background flux reduces at lower energies, while the gamma-ray flux continues to increase (Turver and Weekes, 1978).
- There is currently a gap between the upper energy bound of the sensitivity of satellite based experiments and the lower limit of ground based telescopes. A

full understanding of the emission and absorption processes can only be gained from observations over the complete energy range.

- Observations of objects made at energies below and above this gap currently suggest different values of the spectral index (the gradient of a plot of  $\log(\text{flux})$  against  $\log(\text{energy})$ ) for a number of objects. This suggests that there may be a step change in the gradient of such a plot although this phenomenon is yet to be observed.

## 1.6 Summary

Gamma-ray astronomy is the study of the highest energy quanta of light and has the potential to investigate the physical processes prevalent in some of the most extreme environments in the universe. The, as yet still unidentified, source of cosmic rays is but one area of interest in the field. Also of interest are the massive energy sources in active galactic nuclei, such as the EGRET detected source Markarian 421, X-ray binary systems, such as Cen X-3, discussed in chapter 6 and plerions such as PSR B 1706-44, which have been detected in the high energy regime of the gamma-ray spectrum.

The production and utilisation of the Cherenkov shower is discussed in chapter 2. Chapter 3 introduces the instruments used by the Durham group to observe Cherenkov light. Chapter 4 describes the progress made in understanding and controlling the factors which affect the operation of these instruments. Chapter 5 describes the work carried out to improve the performance of the telescope. Stereo techniques utilising the extra information on the height of origin of the light provided by a two telescope system are reviewed in chapter 6. Finally the current status of the Durham experiment is assessed and areas for future development are identified.

## Chapter 2. Ground Based Gamma-Ray Astronomy

### 2.1 Introduction

In this chapter, the production of Cherenkov light in the atmosphere will be introduced with an explanation of its utility in ground based gamma-ray astronomy. Methods of detecting the Cherenkov light from the ground and distinguishing between light produced by gamma-ray induced showers and those resulting from charged particles are also described.

### 2.2 Cherenkov Light

The production of light by a charged particle passing through a dielectric was first proposed by Heaviside (1892). The phenomenon was probably first recorded by Marie Curie around 1910, who observed a bluish glow from vessels containing a radium solution. Progress in investigating the effect was slow and the first detailed study was made by Mallet (1926, 1928 and 1929) who showed that the effect is distinct from fluorescence in that it displays a continuous spectrum. In apparent ignorance of the work of Mallet, Cherenkov conducted a series of experiments between 1934 and 1938 and showed that the site at which the radiation is produced is modified by the presence of a magnetic field (Cherenkov, 1937). Cherenkov's results were in excellent agreement with a contemporary theoretical treatment by Frank and Tamm (1937). Ginzberg subsequently added a quantum mechanical treatment and named the effect Cherenkov radiation.

#### 2.2.1 The Physical Basis of Cherenkov Radiation

Cherenkov radiation is a result of the passage of a charged particle through a dielectric medium at an ultrarelativistic speed. A charged particle will cause polarization of the electric fields of the atoms close to which it passes. For slow moving particles, the polarization field is symmetric, both about the path of the particle and perpendicular to the path. The result is that no net field is observed at distance from the particle. However, if the particle has a speed approaching that of light in the medium ( $c/n$ , where  $n$  is the refractive index of the medium), the polarization becomes asymmetric along the path. At any time, the resultant field can therefore be observed well away from the path. The asymmetry is demonstrated in figure 2.1.

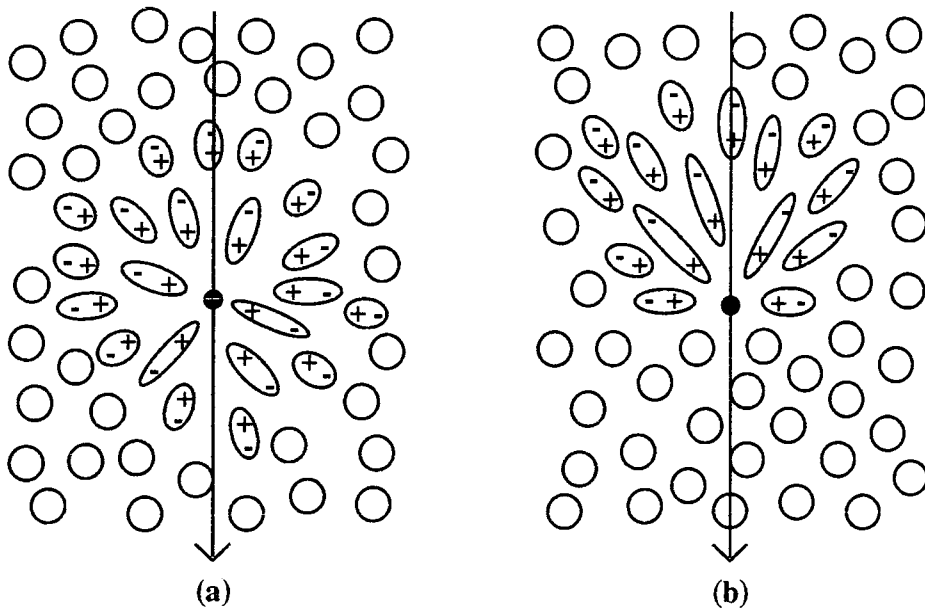


Figure 2.1 The polarizing effect of a charged particle passing through a dielectric at (a)  $v < c/n$  and (b)  $v > c/n$  (from Jelley, 1958).

A brief electromagnetic pulse, of the order of 10 ns duration, is emitted at each element on the path as a result of the field distortion. In general, the pulses interfere destructively with one another, with the result that the field intensity is still zero away from the local distortion. However, for the case where the particle is moving with a velocity greater than the phase velocity of light in the medium, there exists a conical surface, on which the 'wavelets' are coherent and in phase with one another, with the result that they interfere constructively and the radiation can be detected at distance from the path of the particle. The Huygens construction shown in figure 2.2 demonstrates that this condition exists only at one particular angle,  $\theta$ , from the particle path, defined by the Cherenkov relation

$$\cos(\theta) = \frac{1}{\beta n} \quad [2.1]$$

where  $\beta$  is the ratio of the speed at which the particle is moving to that of light in a vacuum ( $v/c$ ) and  $n$  is the refractive index of the medium. By writing  $n = 1 + \eta$ , with  $\eta$  being very small, the following relation can be obtained,

$$\theta_{max} = \sqrt{2\eta}. \quad [2.2]$$

It can be seen that no radiation is possible for particles moving with speeds such that  $\beta < 1/n$ . This radiation is most prominent in the visible and near-visible regions of the electromagnetic spectrum, for which  $n > 1$ .

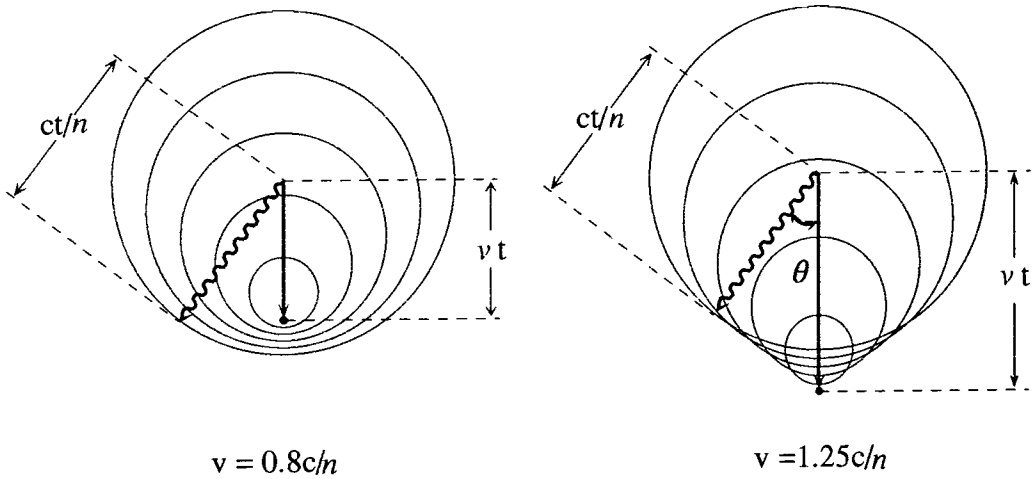


Figure 2.2 The constructive interference between wavefronts centred on different elements along the path of the charged particle for  $v > c$ , causing a plane wave at angle  $\theta$  to the direction of movement of the particle. No corresponding plane wave is seen for  $v < c$ .

The production of Cherenkov radiation requires that the particle track length is much greater than the wavelengths of the radiation produced and that the particle velocity remains constant, otherwise the constructive interference conditions are not met. It is important to understand that the emission of Cherenkov radiation occurs at macroscopic rather than microscopic levels and that the radiation is emitted by the medium rather than the traversing particle. The particle must be charged. Any Cherenkov radiation apparently caused by the passage of a neutral particle is due to charged secondary particles.

The energy emitted over a frequency range  $d\nu$  as the result of the passage of a particle of charge  $Ze$  through a path length  $dl$  is described by Frank and Tamm (1937) as follows

$$dE = \frac{4\pi^2 Z^2 e^2 \nu}{c^2} \left( 1 - \frac{1}{n^2 \beta^2} \right) dl d\nu. \quad [2.3]$$

This relationship can be written in terms of the number of photons  $N$  per unit path length

$$\frac{dN}{dl} = \frac{2\pi Z^2}{137c} \int_{\beta n > 1} \left( 1 - \frac{1}{n^2 \beta^2} \right) d\nu \quad [2.4]$$

where  $e^2 / hc \sim 1/137$  is the fine structure constant. Integrating this equation shows that the number of photons produced in a given wavelength range  $l_1 \rightarrow l_2$ , peaks in the ultraviolet region of the electromagnetic spectrum

$$N = \frac{2\pi l}{137} \left( \frac{1}{\lambda_1} - \frac{1}{\lambda_2} \right) \left( 1 - \frac{1}{n^2\beta^2} \right). \quad [2.5]$$

For a fuller description, the reader is referred to Jelley (1958) from which much of the above discussion is derived.

### 2.2.2 Cherenkov Radiation as an Astronomical Tool

In 1948, Blackett recognised that the atmosphere was a suitable medium for the production of Cherenkov light. The refractive index is 1.00029 at standard temperature and pressure (STP). It is therefore possible to detect the passage of ultrarelativistic charged particles through the atmosphere by observing the Cherenkov light radiated due to their passage. The small refractive index results in a higher Cherenkov energy threshold and smaller angle than is observed in other radiating media such as water and glass. The maximum possible angle can be derived from equation 2.1. and is seen to be  $1.3^\circ$  at sea level. This small Cherenkov angle, resulting in a high degree of beaming of the light produced, means that the Cherenkov light provides good information about the direction of travel of the primary particle responsible for its production.

It is also possible to use the limiting condition of equation 2.3 to define the minimum energy required of a particle to produce Cherenkov radiation as a function of its rest mass. The most important values at standard temperature and pressure in air are

- $E_{\min}$  (electron) = 21 MeV
- $E_{\min}$  (proton) = 39 GeV
- $E_{\min}$  (muon) = 4 GeV

Furthermore, it can be shown, from equation 2.3, that the number of photons emitted as a result of the passage of a particle of unit charge along a track length  $dl$  can be estimated by

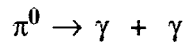
$$\frac{dN}{dl} \sim 780\eta \text{ photons cm}^{-1}$$

so an electron at sea level will produce  $\sim 22$  visible photons per metre.

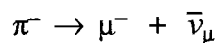
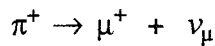
## 2.3 Extensive Air Showers

An extensive air shower (EAS) is the name given to the cascade of subatomic particles and electromagnetic radiation produced as a result of the impact of a high energy particle (usually a proton, generalized to a stripped atomic nucleus) or a gamma-ray on the top of the atmosphere. Primaries of the highest energies ( $E > 50 \text{ TeV}$ ) initiate showers in which a significant number of particles survive to ground level where they can be detected by particle detectors. Below this level, the cascade is absorbed in the atmosphere and cannot be directly detected at ground level.

An EAS induced by the collision of a primary charged cosmic ray with an air nucleus contains three components; hadronic, muonic and electromagnetic. The hadronic component consists of pions, kaons and potentially some energetic fragments of the nucleus into which the charged particle impacted. The pions are the most common daughter particles, with the three species,  $\pi^\pm$  and  $\pi^0$ , produced in almost equal numbers. It is the  $\pi^0$ s, which decay almost instantaneously to form two energetic photons, which go on to initiate the majority of the electromagnetic cascade.

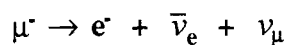
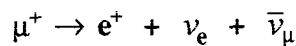


The charged pions either interact with further air nuclei or decay more slowly into muons and neutrinos.



The neutrinos produced by this decay have a small interaction cross-section and are assumed to play no further part in the development of the cascade. Kaons are produced at around 10 percent of the rate of pions. The four species of kaon may also further interact with air nuclei, or decay by various processes, producing further electrons, muons and pions.

The muons produced in the cascade lose energy, mainly through ionization losses, eventually decaying to electrons and neutrinos



The electromagnetic radiation produced in the EAS forms a cascade that propagates alongside the hadronic cascade. The high energy photons produce electrons via pair production

$$\gamma \longrightarrow e^+e^-$$

The deceleration of electrons and positrons in the nuclear fields of atmospheric atoms results in the emission of radiation via the Bremsstrahlung process. The Bremsstrahlung and pair production processes account for the majority of the electromagnetic cascade, the process continuing until the energy of the electron drops below some critical energy  $E_c$ . For an electron in air,  $E_c$  is  $\sim 85$  MeV. Below this energy, other mechanisms, principally ionization, dominate over Bremsstrahlung and the cascade quickly dies away.

The EAS generated by a primary gamma-ray behaves in a similar fashion to that resulting from a primary cosmic-ray. However, the much smaller photonuclear cross section means that the production of mesons will be much less frequent. The energy of the primary photon quickly degrades through Bremsstrahlung and pair production, as described previously, with the result that the shower is primarily electromagnetic in character. The simplest approach to cascade development was proposed by Rossi and Greissen in 1941 and is known as Approximation A. This treatment involves consideration only of the Bremsstrahlung and pair production components of the shower propagation. Both processes have similar interaction lengths and therefore at an atmospheric depth corresponding to  $n$  interaction lengths, each primary will have produced  $2^n$  secondary particles. This exponential growth continues until the average energy of the secondary particles is less than the critical energy  $E_c$ . Using  $E_c = E_0/2^n$ , it is possible to define the depth of shower maximum,  $x_{\max}$ , in terms of the primary energy  $E_0$ , interaction length  $x_0$  and the critical energy  $E_c$

$$x_{\max} = nx_r = x_0 \ln\left(\frac{E_0}{E_c}\right) \quad [2.6]$$

where  $x_r$  is defined as the distance in which half of the electrons emit Bremsstrahlung radiation or half the photons pair produce (Allan, 1971). This is derived from the interaction length  $x_0$  by the relationship

$$\exp\left(\frac{-x_r}{x_0}\right) = 0.5 \quad [2.7]$$

For a 300 GeV photon, the depth of maximum is found to be  $800 \text{ g cm}^{-2}$ . Despite being simplistic, the approximation reasonably accounts for the initial exponential growth of the shower, the relationships between primary energy and height of shower maximum and between primary energy and number of particles at shower maximum.

Some of the limitations of this treatment were addressed in Approximation B (Rossi, 1952). This incorporated ionization losses of  $\sim 80 \text{ MeV}$  per radiation length into the shower development. This was extended by Greissen (1956), allowing the particle number  $N_e$  to be expressed in terms of primary energy  $E_0$  and depth of observation,  $t$

$$N_e(E_0, t) = \frac{0.31}{\sqrt{t_{\max}}} \exp(t(1 - 1.5 \ln s)) \quad [2.8]$$

such that depths are expressed in radiation lengths and  $t_{\max}$  and  $s$  are defined thus

$$t_{\max} = \ln \left( \frac{E_0}{E_c} \right) \quad [2.9]$$

$$s = \frac{3t}{t + 2t_{\max}} \quad [2.10]$$

From equation 2.8, it can be seen that at shower maximum ( $t = t_{\max}$ ), a 300 GeV primary gamma ray produces  $\sim 380$  electrons.

The nature of the propagation of an EAS is such that the electromagnetic component has little transverse momentum in comparison with the muons and pions. In the case of a gamma-ray induced shower, where the electromagnetic component dominates, the shower is therefore confined tightly around the axis of the primary particle. It is this property that allows detection of the EAS to be used to determine the direction of travel and therefore the source of the primary gamma ray. In charged cosmic-ray induced showers, the production of muons and pions is much more prominent. Pions are created with significant transverse momenta (of the order of hundreds of  $\text{MeV}/c$ ). As a result, these particles may not decay until they have moved a significant distance from the shower core, producing photons and further particles over a greater area. This results in a more ragged shower development for a shower produced by a cosmic-ray primary. Figure 2.3 shows simulated shower developments for both (a) a 320 GeV gamma-ray primary and (b) a 1 TeV proton. These showers contain electromagnetic components which produce the same amount of Cherenkov light.

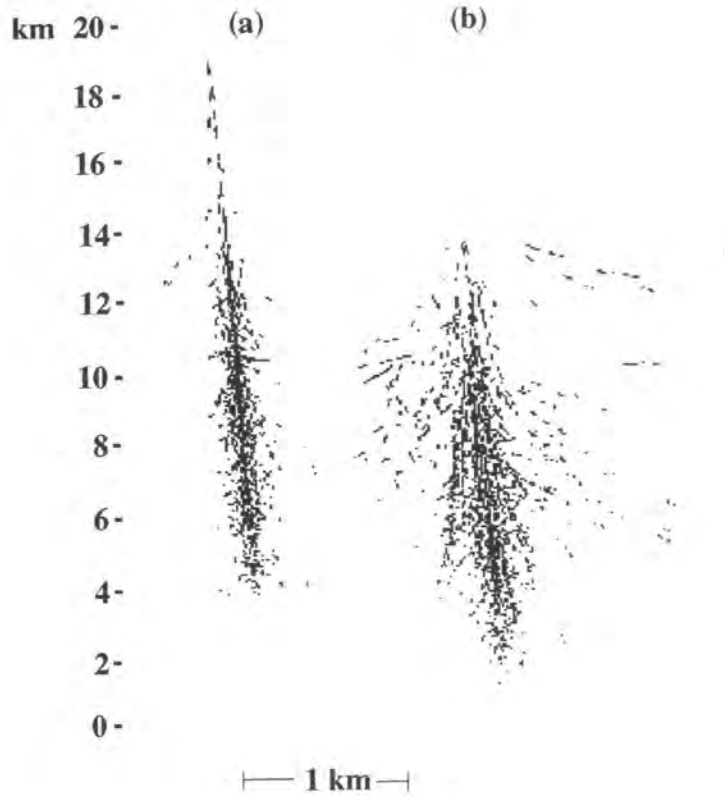


Figure 2.3 Simulated showers generated by (a) a 320 GeV gamma-ray and (b) a 1 TeV proton. The vertical scale shows altitude. The horizontal scale is exaggerated by a factor of 5. Each individual track is shown by a dashed line (from Hillas, 1996).

The density distribution of the atmosphere is approximately logarithmic with depth. This means that the shower develops rapidly in its initial phase, with the result that most of the secondary particles are constrained to lie in a thin disc, essentially forming a plane wave. The extent of this disc is defined by the Coulomb scattering which dominates the electromagnetic cascade. The relationship for multiple Coulomb scattering of an electron is

$$\langle \delta\theta^2 \rangle = \left( \frac{E_s}{E} \right)^2 \delta t$$

where  $E$  is the energy of the electron,  $E_s$  is approximately 21 MeV and  $\delta t$  is the distance travelled along the particle's path in  $\text{g cm}^{-2}$ .

### 2.3.1 Detection of EAS via the Atmospheric Cherenkov Technique

The energy threshold of ground based cosmic ray observations was reduced in the 1950s with the hypothesis of Galbraith and Jelley that EAS would produce Cherenkov light which could be detected by optical detectors at ground level (Galbraith and Jelley, 1953) and the subsequent detection of such radiation. Prior to this, only the charged particle component of EAS had been detected at ground level.

The charged particles in an EAS will emit Cherenkov light as they pass through the atmosphere. Due to the small refractive index of the atmosphere, this light is strongly beamed close to the paths of the particles. The result is that the Cherenkov light distribution as seen from the ground is similar to the disc-like distribution of the secondary particles. From equation 2.7, it is reasonable to assume that the particle distribution would be gaussian in section around the shower axis. However, the light associated with the shower is modified by the variation in Cherenkov angle with altitude, which increases as the particle approaches the Earth. The result is that much of the Cherenkov light produced high in the atmosphere (at altitudes between 10 km and 20 km) reaches the Earth in a ring of around 150 m radius around the shower axis. At lower altitudes, the atmospheric density (and therefore refractive index) varies less, so the Cherenkov angle at such altitudes remains approximately constant. The result is that the light is distributed evenly over the inner area of the light pool with an area of increased photon density around the circumference. Outside this ring, the light density falls off rapidly as  $r^{-2}$ .

The increased photon density around the circumference of the light pool is known as the Cherenkov shoulder (e.g. Hillas, 1996). The photon density as a function of radius is shown in figure 2.4. The shoulder has been observed for showers resulting from primaries of a wide range of energies, but is most prominent for low energy primaries, when most of the light is generated high in the atmosphere. It is seen only in gamma-ray induced showers. For a hadron-induced shower, the electromagnetic cascade around the shower axis persists to lower altitudes, as it is refreshed by the nucleonic component which develops close to the shower core.

The spatial distribution of the light from cosmic-ray and gamma-ray induced EAS have been simulated (see e.g. Hillas and Patterson, 1987). Photon densities from such simulations for showers initiated by a 320 GeV gamma-ray and a 1 TeV nucleon are shown in figure 2.5. The Cherenkov shoulder in the light distribution from the gamma-ray is clearly evident. The cosmic ray induced shower shows a

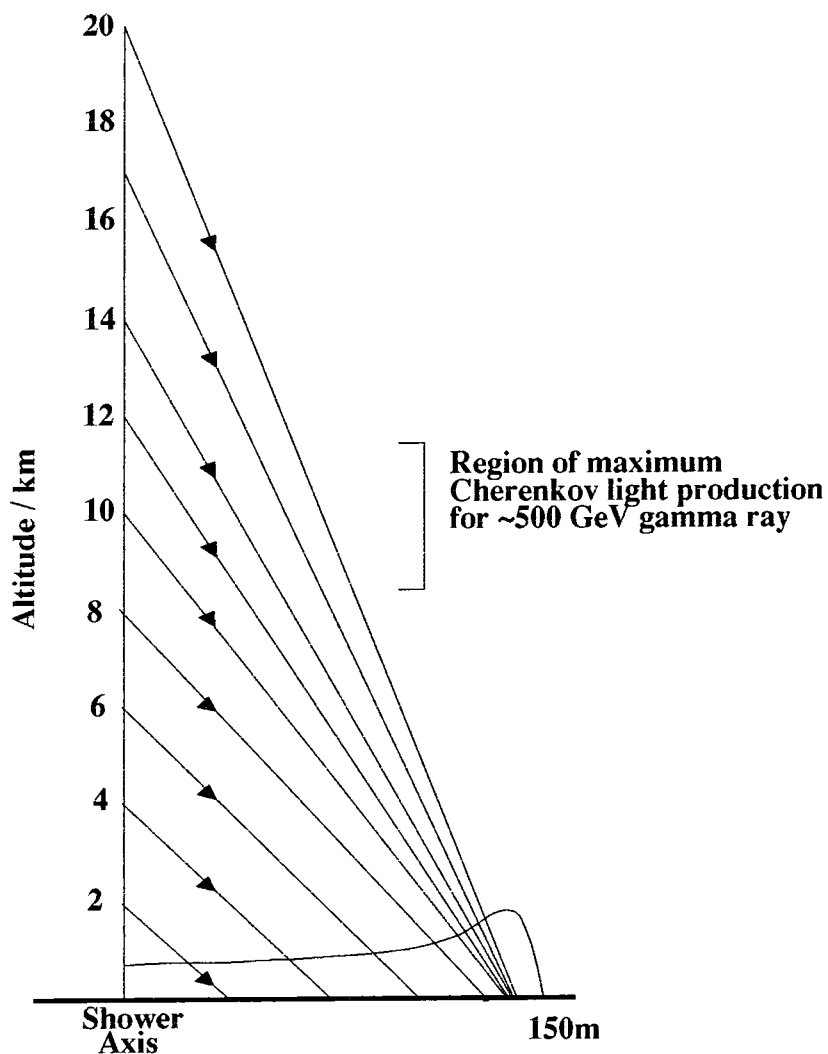


*Figure 2.4 The change in refractive index of the atmosphere with altitude causes a focussing effect on light produced high in the atmosphere. This results in the Cherenkov shoulder observed in the light pool produced in a gamma-ray induced EAS.*

more pronounced 'spike' at the shower axis due to the electromagnetic cascade propagating further towards ground level as a result of being replenished by the nucleonic component of the EAS. The small off-axis spikes seen in the cosmic ray induced distribution are due to local muons penetrating very close to the surface of the Earth or subshowers resulting from the decay of pions with large transverse momentum.

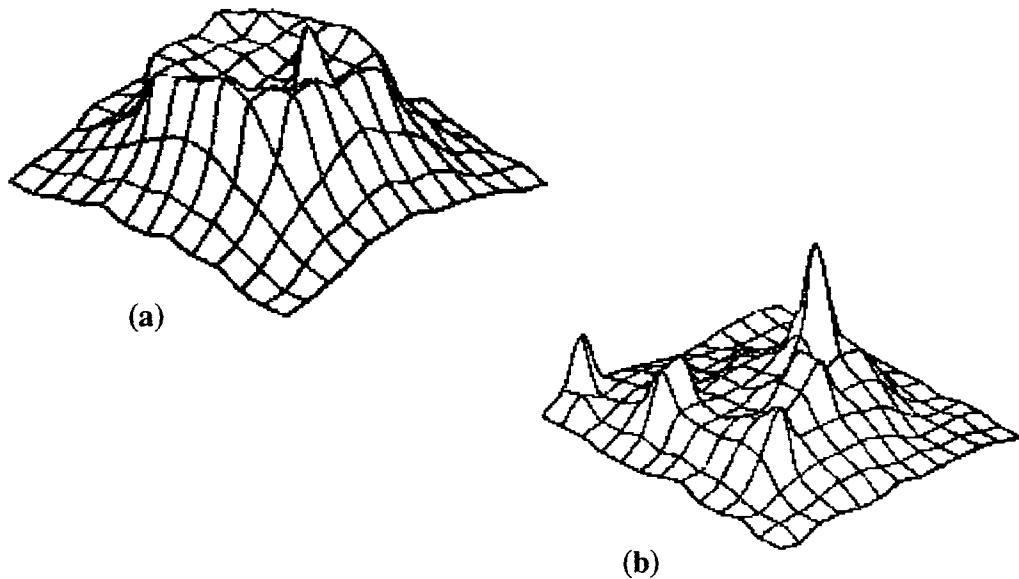


*Figure 2.5 Simulations of the photon densities of Cherenkov light on the ground resulting from EAS initiated by (a) a 320 GeV gamma-ray and (b) a 1 TeV nucleon. The Cherenkov shoulder is clearly visible in the gamma-ray initiated shower. The small spikes seen in the nucleon initiated shower may be due to local penetrating muons or the electromagnetic components of subshowers initiated by pions with large transverse momenta.*

Most of the Cherenkov light generated in a shower is produced in a short region of the longitudinal development around the shower maximum. This corresponds to the period when the number of particles in the shower is at a maximum. The region from which the Cherenkov light is emitted is consequently well defined when the shower is dominated by the bremsstrahlung/pair production processes involved in the electromagnetic cascades, as is the case for gamma ray induced showers. The region is less well defined for nucleon induced showers where the hadronic component dominates.

## 2.4 Atmospheric Cherenkov Telescopes

The design of an atmospheric Cherenkov telescope is influenced by a number of requirements; to detect the faint Cherenkov light from EAS while operating under conditions of background illumination due to the night sky; to distinguish between hadron and gamma-ray induced showers and to identify the direction of the source of any showers.

Although the Cherenkov angle is small, the dominant Coulomb scattering of the electrons in the cascade means that the Cherenkov light produced in an EAS is scattered over an area of approximately  $10^4 \text{ m}^2$  at ground level. It is therefore possible to increase the amount of Cherenkov light collected from an individual shower simply by increasing the size of the flux collectors. Construction considerations limit the size of the collectors used.

As the Cherenkov light produced in an EAS is extremely faint, the light detectors used in a VHE gamma-ray telescope must be of high sensitivity. High resolution of the image is not vital, although it can be useful, since the nature of the propagation of the Cherenkov light and Coulomb scattering in the shower means that there is a certain limiting (statistical) uncertainty in measurement of the position from which it originates. These requirements mean that photomultiplier (PM) tubes are very suitable. They have a fast response to incident light, which matches the short pulse width of the incident Cherenkov light. They can also be arranged in a matrix to provide resolution to  $\sim 0.1^\circ$  per pixel with reasonable optics. This satisfies the imaging requirements discussed in chapter 3, allowing the source direction to be identified. PM tubes are naturally blue-sensitive, matching the Cherenkov spectrum more closely than, for example, solid state detectors, which are maximally sensitive to red light.

The signal processing electronics must be capable of identifying Cherenkov light from EAS within the sky background. Simple coincidence requirements (that a number of pixels measure a signal greater than some threshold) allow sky noise triggers of individual PM tubes to be discarded. More complex coincidence logic can be employed to distinguish between images of gamma-ray and hadron induced showers. The electronics must also be of a suitably high bandwidth to be able to cope with the high rate of background (hadron induced) events.

## 2.5 Summary

The impact of a charged particle or gamma-ray on the top of the atmosphere will induce a cascade of particles and radiation known as an extensive air shower (EAS). The particles produced in a shower initiated by a high energy primary survive to ground level where they can be detected. Showers resulting from lower energy primaries die out in the atmosphere. The electromagnetic component propagates by Bremsstrahlung and pair production; the electrons causing the atmosphere to radiate Cherenkov light, which can be observed from the ground. The ability to detect Cherenkov light has therefore reduced the energy threshold

above which gamma rays can be detected at the surface of the Earth. Detection of gamma rays (and charged cosmic rays) by this method is known as the atmospheric Cherenkov technique and is the principle on which the Durham gamma ray telescopes operate.

## Chapter 3. The Durham Atmospheric Cherenkov Telescopes

### 3.1 Introduction

The Durham VHE Gamma-Ray Astronomy Group currently operates atmospheric Cherenkov telescopes (ACTs) at Bohna, near Narrabri, New South Wales, Australia. In this chapter, the three telescopes which were operational during 1994-1997 will be introduced, including an outline of the work leading to the construction and development of the latest instrument, the Mark 6 telescope.

#### 3.1.1 Historical Background

VHE gamma-ray observations by the Durham group began in Dugway, Utah, USA in 1981. The group relocated to Narrabri in 1986 in order to be able to observe the southern sky. Observations in Dugway suggested that X-ray binary systems had the highest luminosities of the sources observed and a large number of such systems are visible from the southern hemisphere, in addition to other sources of interest including the Galactic centre and the Large and Small Magellanic Clouds. Observations were also made, for 2 years, at a site on La Palma in the Canary Islands as a follow-up to the Dugway project.

##### *3.1.1.1 The Triple-Coincidence Technique*

Developments by the Durham group have been motivated throughout by the philosophy that the telescopes should be operated at maximal sensitivity and gain, thereby reducing the energy threshold of the telescope. This is of particular importance if the telescopes are to be operated near to sea level and lose the natural advantage of a reduced threshold which applies to mountain-altitude instruments.

As a result, all Durham telescopes have been constructed around a triple-dish design, with three light collectors and detector packages on a single mount and simultaneously exposed to the same area of the sky. All three detectors form part of the triggering mechanism and the central detector is used to measure the image of the Cherenkov light. The triple-coincidence triggering system requires that the signal exceeds some predetermined threshold in all three detectors within a short (10 ns) time interval in order to be recorded and that the light is observed in the same spatial position in each detector.

Such a system allows the individual photomultipliers to be operated at high gain/noise rates while retaining an acceptably low rate of accidental triggers. The rate of chance event triggers is defined by:

$$R = M!n^M t^{M-1}$$

where  $M$  is the required number of coincident elements,  $n$  is the noise rate of the individual photomultipliers and  $t$  is the gate time during which the coincidence must occur. The individual detector noise rate, and consequently gain, is therefore limited by the definition of an acceptable accidental event trigger rate  $R$ .

Increasing  $M$  allows a corresponding increase in acceptable noise/gain for each element, but at the expense of increased complexity in the telescope structure and electronics. Where overall instrument size is a limiting factor, increasing  $M$  may also necessitate a reduction in the size of the individual flux collectors, with a corresponding increase in energy threshold, as described in chapter 4.

For a predetermined total mirror area, a triple coincidence system has been shown to be an effective compromise between these conflicting requirements, showing significant improvements over a 2-dish instrument; the diminishing returns in moving from 3- to 4-fold coincidence make this the most cost effective and feasible option (Brazier *et al.*, 1991).

Within the framework of such a philosophy, the evolution of telescope design at Narrabri is the subject of this chapter.

### 3.1.2 The Bohena Observatory

The Bohena Observatory is located approximately 20 km southwest of Narrabri, New South Wales, Australia (site latitude 30°28'S, longitude 149°40'E, altitude 260 m above mean sea level (AMSL)). It is at a latitude suitable for observing most southern hemisphere galactic objects and, at the time of selection, had experienced many years of clear and stable weather conditions. Power and accomodation facilities were extant as the site was, until 1978, the location of SUGAR, the Sydney University Giant Airshower Recorder. Figure 3.1 shows a plan of the Bohena Observatory. The site is located in the Pilliga Scrub, a large forested region; the presence of surrounding trees reduces wind speeds across the site.

It should be noted that, unlike the Dugway and La Palma sites, the Bohena Observatory is not located at a significant altitude (260 m AMSL, compared to La Palma, 2500 m AMSL and Dugway, 1450 m AMSL). The effect of this is to

increase the energy threshold of a telescope, compared to that of an identical instrument operating at altitude. This is because the intensity of Cherenkov light produced in a shower of fixed energy reduces with distance travelled down through the atmosphere. In addition, lower energy showers are generated higher in the atmosphere and are therefore better sampled at a high altitude. A typical Cherenkov telescope operating at ~2500 metres AMSL will have a threshold energy about 50% of the value appropriate to operation at sea level.

### 3.2 The Durham Atmospheric Cherenkov Telescopes

Two telescopes are currently in operation at the Bohena Observatory. The Mark 5A telescope was deployed, with limited imaging capability, in 1992. Construction of the Mark 6 telescope was carried out in the austral winter of 1994. An earlier instrument, the Mark 3A telescope was decommissioned in 1998. All three telescopes are located on an approximately east-west baseline as indicated in figure 3.1. In addition, the Mark 4 telescope was moved to Narrabri in April 1990 from a temporary site in La Palma. The Mark 3 and Mark 4 telescopes provided valuable experience in operating multiple telescopes. The Mark 4 telescope has not been used since October 1993 and numerous parts have been incorporated into the other telescopes.

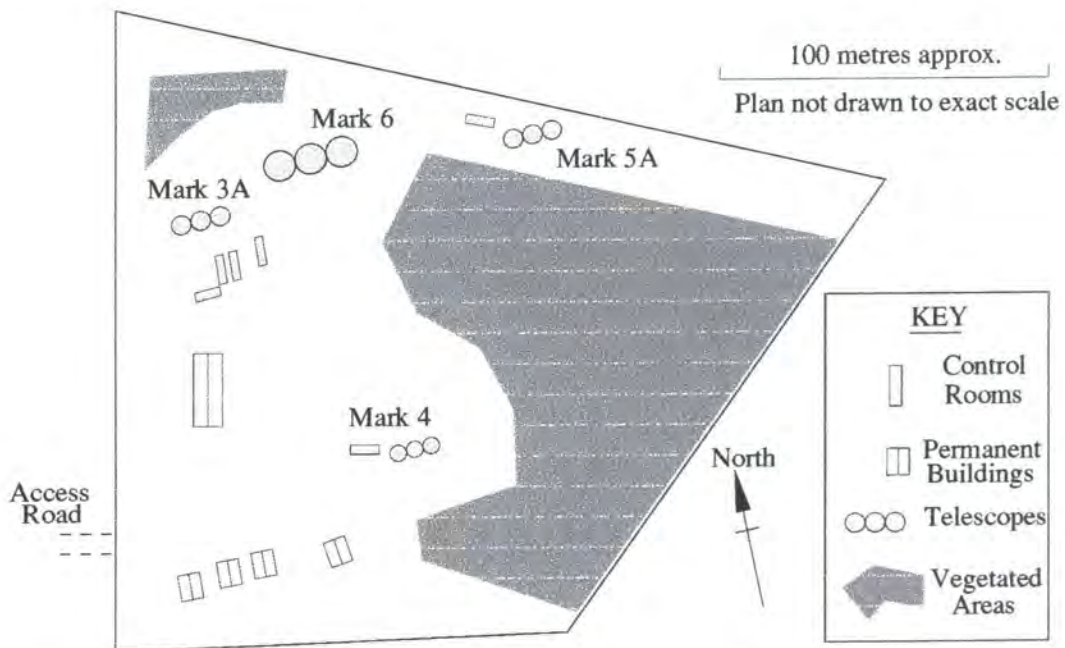
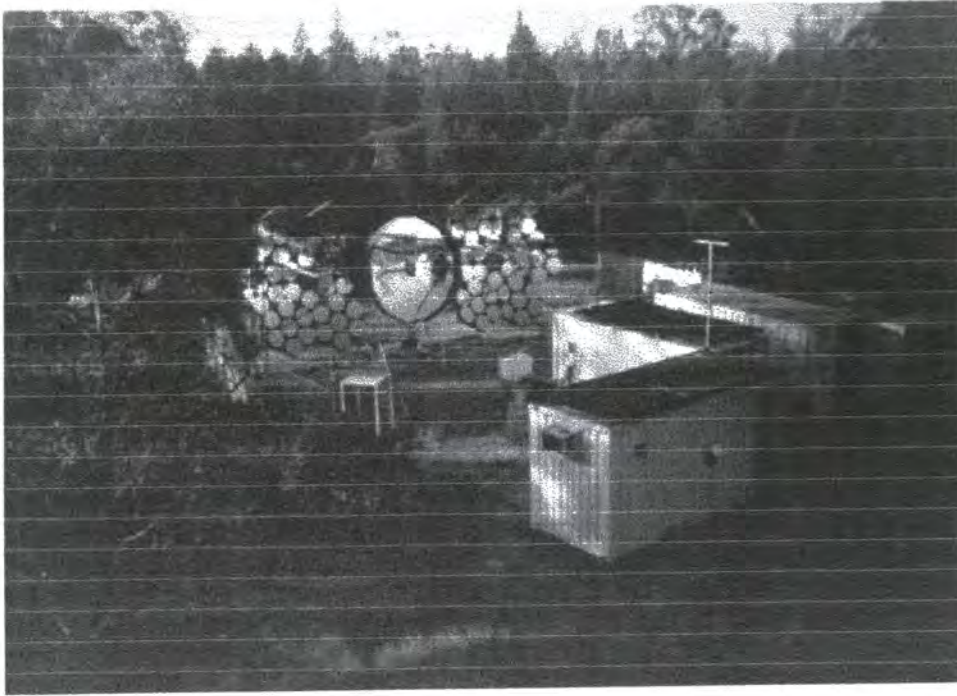


Figure 3.1 The Bohena VHE Gamma-Ray Observatory, Narrabri, Australia.

### 3.2.1 The Mark 3A Telescope

The Mark 3 telescope was the first instrument used by the group in southern hemisphere observations. The design was an evolution of that of the Utah telescopes, with increased mirror size and improved optics. Three mirrors of focal length 2.5 m and parabolic section, each comprising arrays of circular mirrors were used to focus light onto the photomultiplier packages. These originally consisted of three packages, each comprising 4 PM tubes, providing four triple coincidence channels. The central channel was used to observe the source, while the remainder were originally conceived as monitors of off-source background regions, arranged at  $120^\circ$  intervals around the central tube, viewing the sky  $2^\circ$  from the source. Three further PM tubes were added to each detector package to provide continuous coverage at  $60^\circ$  intervals around the source direction. The surrounding tubes were subsequently employed to provide a simple method of rejecting background events. The selection of events in which the on-axis PM tubes responded, but none of the surrounding 'guard ring' tubes did, provided an improvement in gamma-ray signal to proton background of a factor of about 2. The guard ring PM tubes were subsequently moved to  $1.5^\circ$  from the central PM tube to optimise the efficiency of this rejection following the results of simulations and observational experience.

In April 1993, the central flux collector of the Mark 3 telescope was replaced by a sectored design of f-number 1.0 and focal length 3.3 m, as shown in figure 3.2. The 12 mirror sections constitute a composite parabolic flux detector. At the same time, the PM tubes in the detector packages were upgraded. The PM tubes in the central detector were replaced by an array of 31 smaller PM tubes to provide a medium resolution imaging capability. The inner 19 tubes are Burle S83062E 25 mm diameter PM tubes and form a close packed array with a 30 mm pitch between tubes, with a total field of view of  $2.5^\circ$ . These are surrounded by 12 Burle C7151Q 38 mm diameter tubes. The PM tubes of the left and right detectors were replaced by close packed arrays of C7151Q PM tubes. These tubes have poorer gain/noise characteristics than the alternative (the 50 mm RCA 8575 PM tube) but allow the trigger packages to have fields of view which match the field of view of the central detector. This aperture matching was sacrificed in 1995, when the tubes in these detectors were replaced by Philips XP3422 56 mm hexagonal tubes with low noise and high gain characteristics, following their successful implementation in the triggering system of the Mark 6 telescope. Full details of these PM tubes can be found in section 5.3.1. This upgrade, since which the telescope has been designated the Mark 3A, increased the sensitivity of the instrument to be comparable to that of the Mark 5A telescope.



*Figure 3.2 The Mark 3A Telescope*

Following developments on the Mark 6 telescope, a CCD camera has also been installed on the Mark 3 telescope, mounted paraxially with the optic axes of the flux collectors, to improve knowledge of the telescope attitude and a facility exists to perform laser calibration of the gains of PM tubes to ensure uniform response to light.

A fuller discussion of the Mark 3A telescope has been given by Holder (1997). The telescope was decommissioned, as an economy measure, in January, 1998.

### 3.2.2 The Mark 5A Telescope

The Mark 5 telescope was constructed in Durham in 1991 and was deployed on site at Narrabri in 1992. It is located approximately 100 m due east of the Mark 3 telescope. It was intended to fulfil two purposes. It served as a half-scale prototype for the Mark 6 telescope and allowed a number of design concepts to be tested. It also acted as a stereo counterpart to the Mark 3 telescope and allowed the development of a system for sampling the Cherenkov light from a single shower at two points on the ground as a basis for stereoscopic studies of the cascades.

The three standard flux collectors are 3.5 m in diameter, f1.0 and of the same sectored design as the modified central mirror on the Mark 3A telescope. The central mirror focuses light onto a camera consisting of 19 25 mm diameter PM tubes surrounded by 12 38 mm diameter tubes; the outer mirrors focus light onto

two trigger packages of 7 PM tubes each, which cover the same region of sky as the central package. The trigger is a simple coincidence system requiring corresponding left and right channels and any one of the 19 central PM tubes to measure signals above a fixed threshold. The outer ring tubes in the central package are not incorporated into the trigger. A fuller discussion of this trigger method can be found in section 3.3.3.2.

For the imaging section of the camera, 19 Burle S83062E 25 mm diameter PM tubes are used. The outer ring was constructed from Burle C7151Q PM tubes because of the comparable performance with the S83062E. The PM tube packages in the outer detectors originally contained Burle 8575 50 mm diameter PM tubes. These were replaced by 56 mm hexagonal Philips XP3422-SG4 PM tubes in March 1995 following the successful use of these PM tubes in the Mark 6 trigger system.

A fourth dish was incorporated into the Mark 5A design. This is of the same focal length but smaller than the other three (area 6 m<sup>2</sup>) and focusses light onto a single 12.5cm diameter RCA4522 PM tube, which is consequently exposed to an aperture of little more than 2°. This fast PM tube forms no part of the trigger, but its response to any event triggering the telescope can be recorded. This system was included to allow sampling of the pulse profile of the Cherenkov flash as an additional method of background rejection, but is not routinely used. This 'timing dish' is mounted above the central flux collector, as shown in figure 3.3.

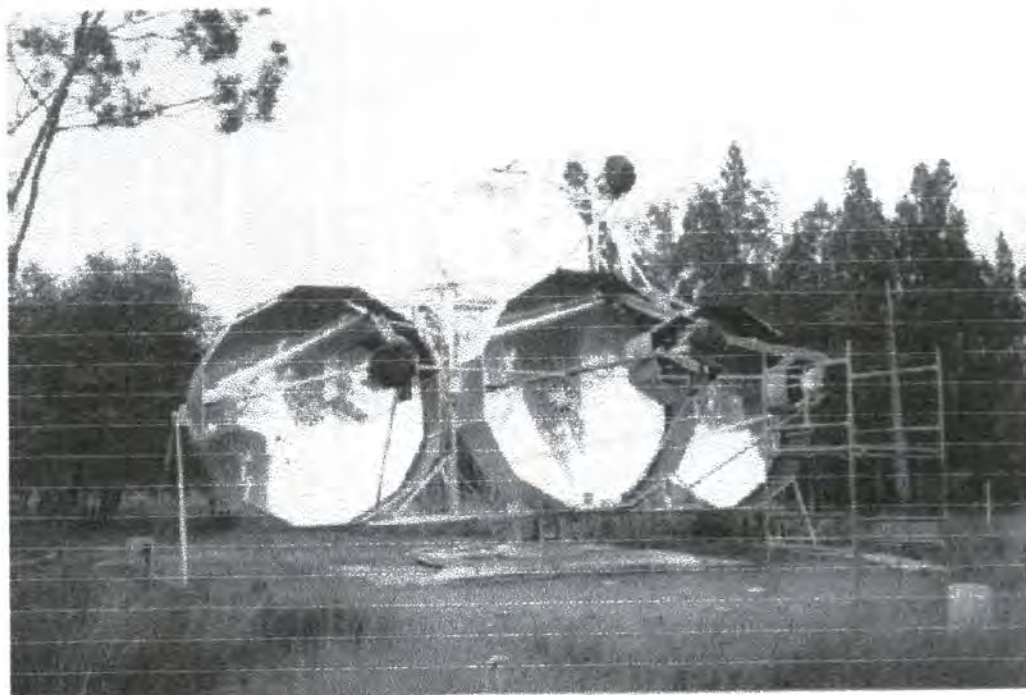


*Figure 3.3 The Mark 5A Telescope*

As a precursor to the Mark 6 telescope, the Mark 5A telescope was the first medium resolution imaging system constructed by the Durham group and offered a significant improvement in sensitivity and threshold over the Mark 3 telescope. The limited imaging capability has provided valuable experience in imaging techniques and event parameterization and consequent rejection criteria to discard events obviously due to the hadronic background. It is, therefore, a viable scientific instrument in its own right. A detailed discussion of the performance of the Mark 5A telescope has been given by Dickinson (1995). The Mark 5A telescope was placed on a care and maintenance basis as an economy measure in January 1998.

### 3.3 The Mark 6 Telescope

The most recent telescope at Bohena was constructed in Durham between April 1993 and May 1994 and assembled on site in the austral winter of 1994. The Mark 6 telescope was designed with the intention of providing a low energy threshold telescope of high sensitivity and imaging capabilities, with a view to reducing the gap between energy ranges studied using ground-based and satellite-borne gamma ray experiments. Existing ground-based telescopes were operating at energies down to  $\sim 500$  GeV, while the upper sensitivity limit of the EGRET experiment is  $\sim 30$  GeV, as outlined in chapter 1. Exploiting this decade of the electromagnetic spectrum is an area of significant interest as it will hopefully shed light on a number of astrophysical processes involved in the production of gamma-rays in different source environments.

#### 3.3.1 Overview

Construction of the Mark 6 telescope drew on the lessons learned from the Mark 5 telescope project. In particular, the aim of reducing the energy threshold was pursued in a fivefold manner.

- optimization of signal collection (reduction of signal loss combined with an increase in mirror area),
- suppression of background light induced noise,
- matching of telescope response to the Cherenkov flash,
- Use of a stable, high bandwidth system with large data handling capacity and
- employment of effective event selection.

The construction of the telescope and the means by which these targets were met are discussed in this chapter. During two years of initial operation, further improvements in the operation of the telescope have been made. These are discussed in chapters 4 and 5. The Mark 6 telescope is shown in figure 3.4.

### 3.3.2 Flux Collectors

The flux collectors are all 7 m diameter (area 42 m<sup>2</sup>, f1.0) of sectored design in order to maximise the light collection within a given area. Each dish consists of 24 sectors, of width 96 cm at the mirror edge.

The mirror surfaces are constructed from anodised aluminium (Alanod 410G). The reflectivity of the material is high, >83% in the wavelength range from 300 nm - 500 nm (Weekes, private communication, Vickers, private communication). It has previously been used to surface the mirrors of the Marks 3A, 4 and 5A telescopes. The reflectivity does not deteriorate over long timescales (10 years). The surface is mounted on an aluminium honeycomb structure, providing lightweight and rigid support.

The adoption of a parabolic section for the mirrors means that there are no on-axis spherical aberrations and the light collection is isochronous. This is optimal for the telescope triggering mechanism since it avoids temporal smearing of the signal and loss of sensitivity.

The design of the mirrors with f-number 1.0 avoids serious imaging aberrations and allows effective use of light collecting cones. The image scale in the focal plane produced by the mirrors is 0.078° cm<sup>-1</sup>. The combination of mirror size, focal length and pixel size (0.25°) ensures that the image of a Cherenkov flash will not be distorted by the finite depth-of-field.

### 3.3.3 Light Detecting Packages

The light detectors have been designed to provide a high resolution imaging camera of 91 pixels facing the central flux collector, with triggering packages of 19 elements each facing the left and right collectors and covering the same area of sky.

#### 3.3.3.1 *The Imaging Camera*

The camera consists of a total of 109 PM tubes. Of these, 91 are in a close packed array to form a high resolution (0.25°) image of the shower. The remaining 18 are arranged around the outside of the camera to form a guard ring. The arrangement is shown in figure 3.5.

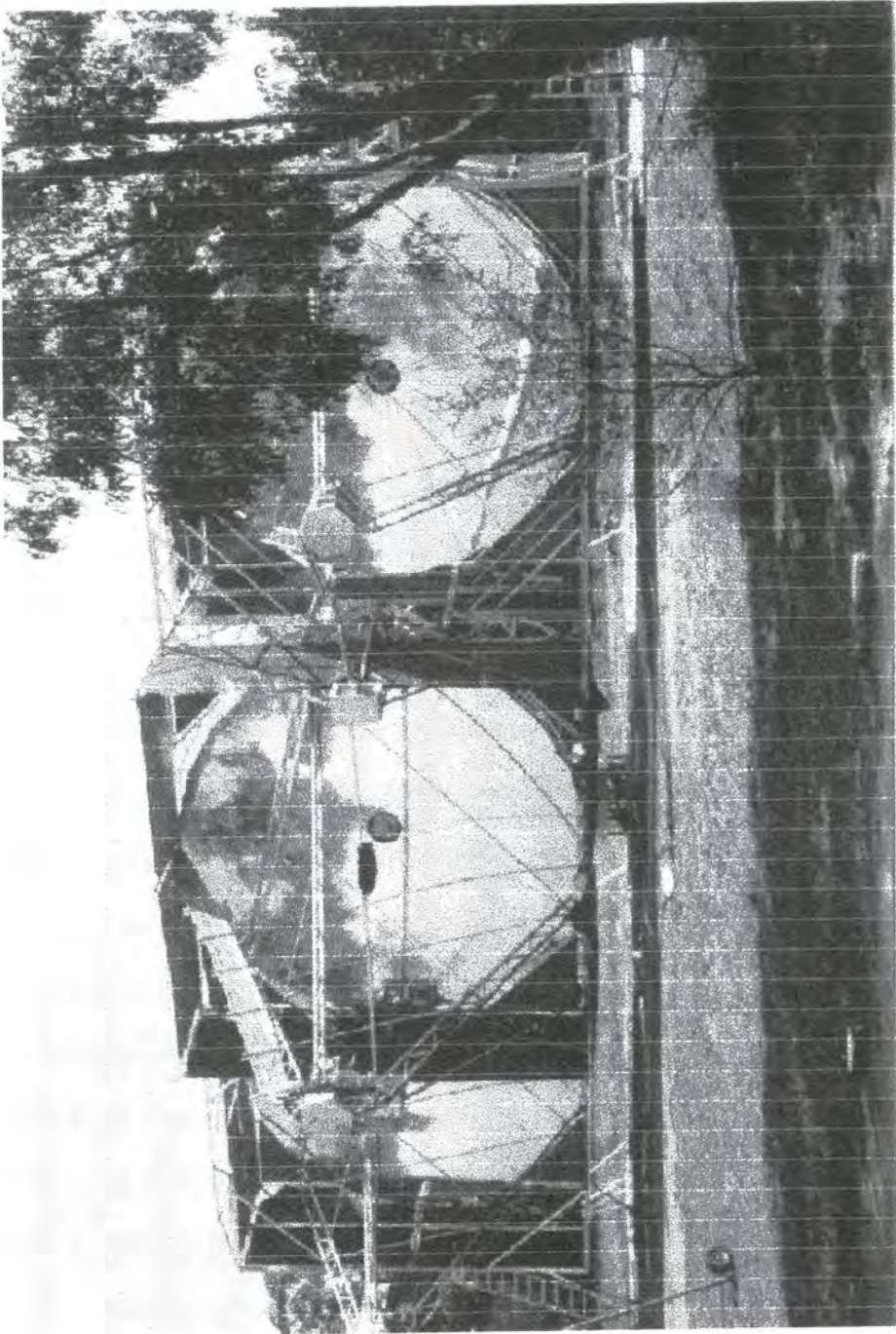


*Figure 3.4 The Mark 6 Telescope*

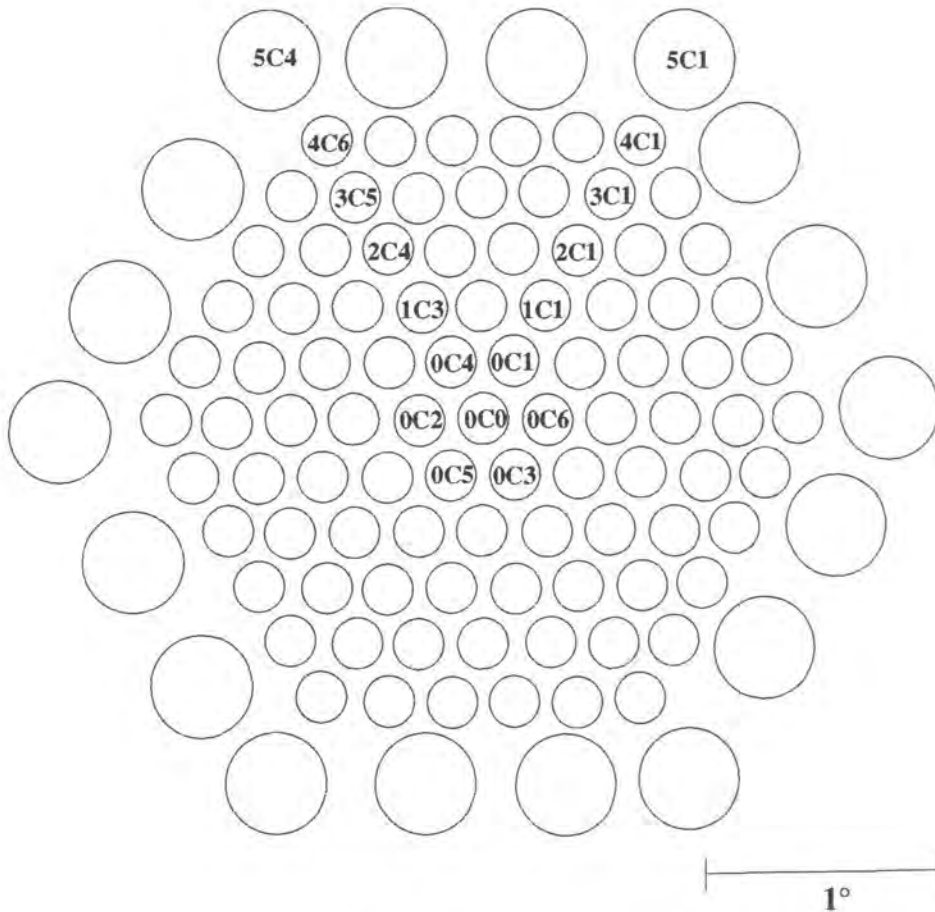


*Figure 3.5 Arrangement of PM tubes in the imaging camera of the Mark 6 telescope, as seen looking at the front of the camera. Each ring of tubes numbers anticlockwise, except for the 0Cx ring which is numbered alternately for compatibility with the convention used in the earlier Durham telescopes.*

The close packed array consists of Hamamatsu R1924 25 mm diameter PM tubes. The photocathode is 21 mm in diameter. The 30% dead area between the photocathodes is minimized by the use of light collecting cones to reflect light onto the active parts of the PM tubes, as described in chapter 5.

The R1924 is a fast response PM tube, with a pulse rise time of  $<2.0$  ns and a transit time of 19.0 ns. It is sensitive to light of wavelengths 300-650 nm, covering the range from green light down into the ultraviolet, with a peak sensitivity at 420 nm.

The guard ring consists of 18 Burle 8575 55 mm diameter PM tubes. These provide information about the images of showers which are detected towards the edges of the camera.

### 3.3.3.2 The Triggering System

The left and right detector packages, which form part of the coincidence system outlined in section 3.3.1, consist of 19 PM tubes in close packed arrays at the prime foci of the collectors. Originally, the PM tubes incorporated in the trigger packages were 55 mm diameter circular Burle 8575 units. In 1995, these were replaced by Philips XP3422-SG4 PM tubes of higher specification. The reasons behind this change, and the benefits gained as a result, will be discussed in chapter 5.

The  $19 \times 0.5^\circ$  pixels arrays in the left/right trigger system are exposed to the same area of sky as the 91 times  $0.25^\circ$  pixels which comprise the central camera. Each event trigger channel comprises a PM tube in each of the left and right detectors and a corresponding group of 7 PM tubes in the camera. A number of the camera tubes contribute to 2 triggering groups, as shown in figure 3.6.

The original trigger system required that a signal exceeds a predefined threshold in the same  $0.5^\circ$  channel of the left and right detectors and any *one of the seven* corresponding  $0.25^\circ$  camera PM tubes, within a coincidence gate time of 10 ns. This was modified in 1995 to require a 4-fold temporal coincidence between left, right and *two adjacent tubes* in the corresponding set of seven in the central camera. This any-two-of-seven coincidence is intended to allow an increase in gain of the camera PM tubes, without an unacceptable increase in the noise rate, by relying on the fact that the image of a Cherenkov flash normally extends over two (adjacent)  $0.25^\circ$  pixels. For gamma-ray events, this requirement may enhance the detection probability; the mechanisms causing this difference are described in chapter 2.

### 3.3.4 Electronics

The performance monitoring and data logging systems, which comprise the telescope electronics, utilise local area networks (LANs) of distributed computers, each performing a specific control/monitoring task. Data transfer is via a high bandwidth (ethernet) LAN. The performance monitoring systems operate over a medium bandwidth (econet) LAN. The signal processing, which is applied to every PM tube signal, is shown schematically in figure 3.7.

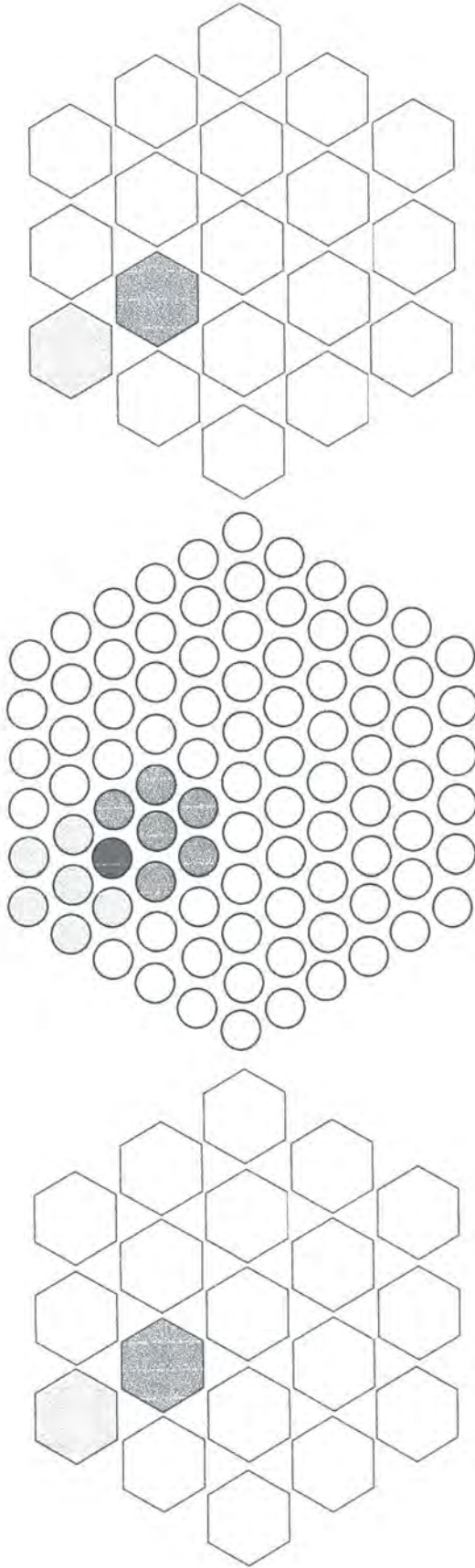


Figure 3.6 A map showing the scale of the trigger channels and the central imaging camera. Each pair of left/right PM tubes is matched with all of the camera tubes it overlaps. The shadings represent two individual triggering channels. The telescope will record an event if the indicated left and right and any 2 adjacent corresponding camera tubes produce signals which exceed a threshold, within 10 ns. The camera tube shaded dark grey is part of both of the triggering channels shown.

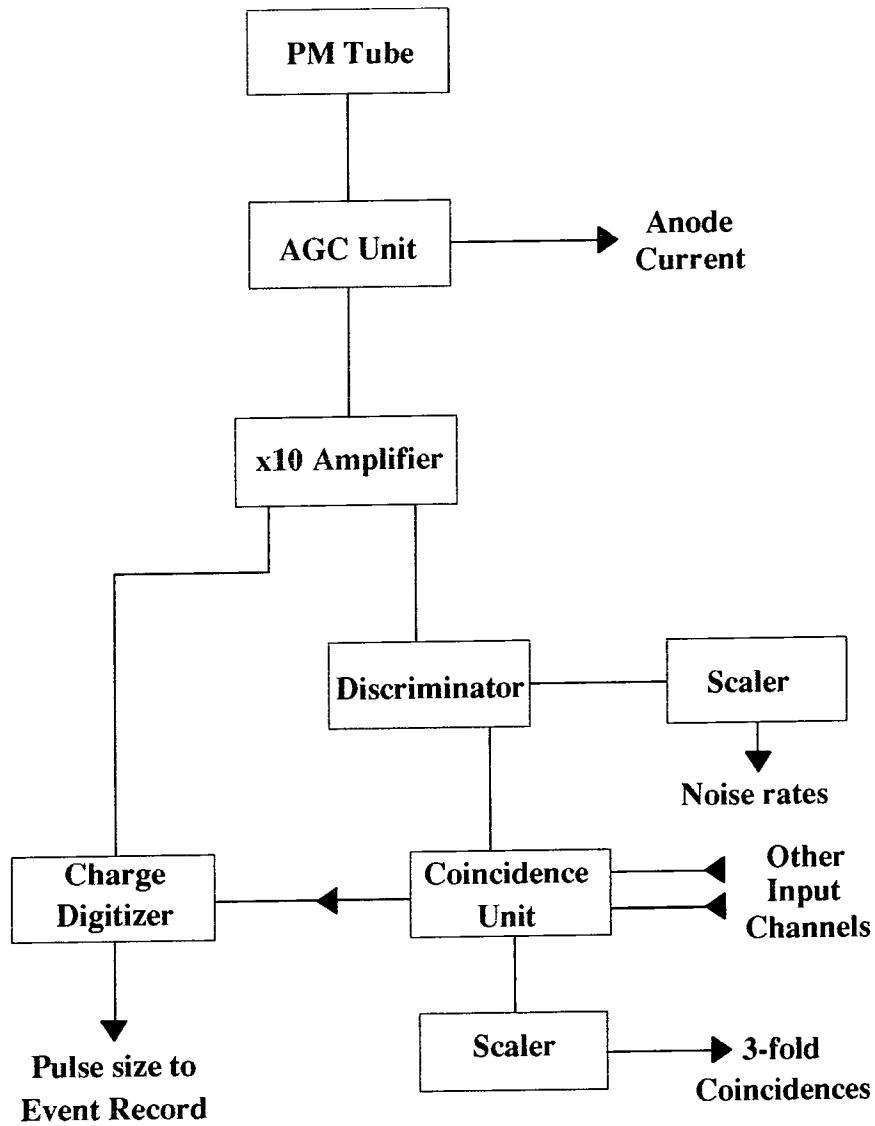


Figure 3.7 A single channel of signal processing in the telescope electronics.

The signal from the PM tube is fed via high quality  $75\Omega$  cable into an automatic gain control (AGC) unit, which has four functions:-

- it couples the  $75\Omega$  cables from the PM tubes to the  $50\Omega$  cables employed in the subsequent electronics,
- it provides an output voltage which corresponds to the anode current being generated in the tube,
- it provides a LED driver voltage suitable for hardware padding (if in use) and
- it removes the DC component from the signal voltage, providing an AC coupled signal for processing.

The AC coupled,  $50\Omega$  output is then passed to a  $10\times$  amplifier (LeCroy Model 612A), the output of which is passed in parallel to a QT (charge-time converter) unit (LeCroy Model 2249A) and a voltage discriminator (LeCroy Model 4413). The discriminator detects the input signals which exceed a threshold of 50 mV resulting in the output of an ECL pulse of 10 ns duration. This signal is used in the coincidence logic, where processing speed is important, and in the scalers, which monitor noise rates. The scalers count the number of times the signal from each PM tube exceeds threshold and operate at frequencies up to 10 MHz.

The coincidence system is a two stage process. Both stages rely on the fast processing of pulses from PM tubes in the three detector packages. This means that ECL standard logic is used, rated at frequencies of up to  $\sim 300$  MHz and with pulse widths as narrow as a few nanoseconds (Horowitz and Hill, 1989). There are 19 circuits which provide the complex logic requirements to generate the 2-of-7 camera coincidence. The output from these units, together with the left and right signals are passed to 3-fold AND gates. Lengths of delay cable are used in order to account for the time differences arising from the processing of the '2-of-7' coincidence signals in the camera.

If the coincidence requirement is satisfied, an event trigger is generated and the signals passing to the charge digitizer QT units are measured. These units are CAMAC fast ADCs (analogue-to-digital converters, LeCroy Model 2249). These units measure the charge due to the current flowing from, and hence the amount of light falling on, each PM tube in a user-defined time. This gate time must be matched to the duration of a Cherenkov flash in order to maximize the signal-to-noise. It was originally set at 40 ns and has recently been reduced to  $\sim 25$  ns.

The Master Trigger unit is responsible for sending the request to measure signals and other routine measurements when the coincidence conditions are met or when a random event is introduced, as discussed in section 3.8.

Figure 3.8 is a block diagram of the electronics for the Mark 6 telescope. The megahertz bus, shown in grey, forms the backbone of a high bandwidth data transfer network. The LAN carrying performance monitoring data is shown as a broken grey line.

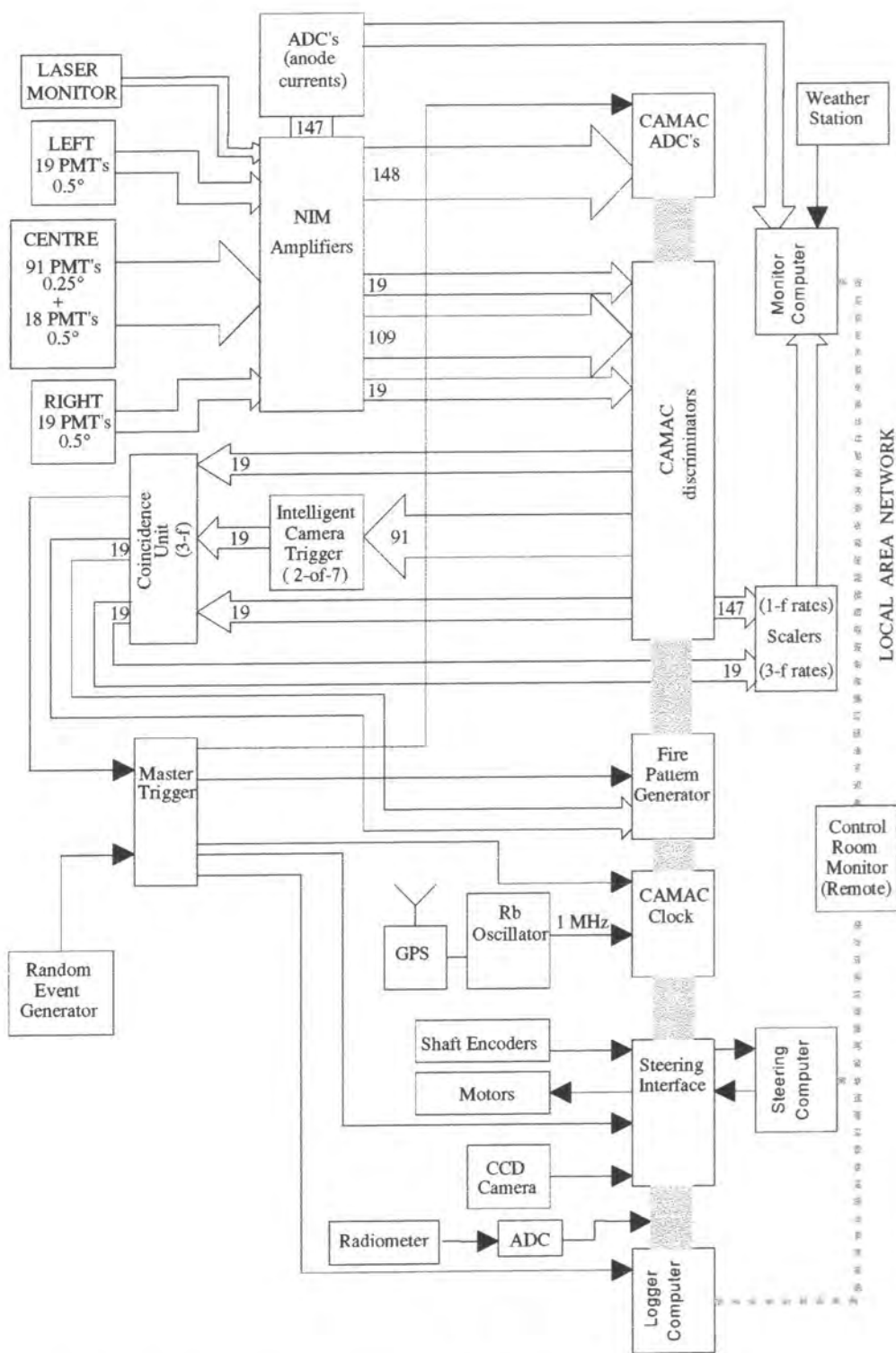


Figure 3.8 Schematic representation of the Mark 6 telescope electronics. The MHz and CAMAC buses are shown in grey. The LAN connecting the computers is shown as a broken grey line (Modified from Dickinson, 1995).

### 3.3.5 Data Logging

Events are logged to the disk of a dedicated computer on the local network. Data from the telescopes are collected onto a single disc for subsequent archival to digital tape and transport to Durham. This is done after observing has completed, to minimize the 'dead-time', the time when the logger computer cannot record data. Performance monitoring data, as discussed below, are also collected and archived in the same way.

### 3.3.6 Routine Monitoring

Separate computers record environmental data, performance data, steering and CCD camera information. These computers also broadcast summaries of this information over a network to a computer designated as the 'Monitor', which also receives information concerning the operation of the telescope electronics, as shown in figure 3.8. The Monitor incorporates a number of user-definable alarms which are triggered by indications that the telescope is operating outside normal conditions.

### 3.3.7 Steering

In common with previous Durham telescopes, the Mark 6 telescope is built on an alt-azimuth mount. It is free to move through zenith angles from  $90^\circ$  to within  $1^\circ$  of the zenith and through all azimuth angles. In practice, the rapid telescope movement required to follow a source close to the zenith means that data are not normally taken at zenith angles less than  $\sim 3^\circ$ , although the spatial angle containing the source is accurately followed.

Accurate positioning information is provided by absolute shaft encoders which measure the attitude of the telescope around both axes. Both encoders provide 14-bit resolution over a full  $360^\circ$ , resulting in the measurement of the position to  $0.02^\circ$ . However, only the most significant 12 bits are returned to the steering computer, which consequently steers to an accuracy of  $0.1^\circ$ , in common with the Mark 3A and Mark 5A telescopes. Encoder data are, however, recorded, with full 14-bit positioning information for each event.

#### 3.3.7.1 CCD Camera

A CCD camera is mounted paraxially with the optic axes of the flux collectors, exposed to an area of sky  $2^\circ$  around the source. A full frame exposure is recorded

for each source observation. Subsequently, for each event, the location and intensity of the brightest CCD pixel (and hence a star within the field) are recorded. During data processing, the position of the guide star can be used to make accurate corrections to the pointing measurement of the telescope. This method is discussed in section 3.8. In addition, measurement of the amplitude of the brightest pixel provides a potential method for monitoring the clarity of the sky.

### 3.4 The Control Room

When the Mark 5A telescope was constructed, it was decided to centralise the telescope supervision systems for the Marks 3A, 4 and 5A telescopes in a single central control room. From this room, the operation of all three telescopes can be monitored and key actions performed (PM tube high voltages and steering switched off). Provision was also made for the future incorporation of the Mark 6 telescope.

Data recorded by the local monitoring system of each telescope, as described in section 3.3.6 are passed via a sitewide LAN to remote monitor computers in the control room. Information on telescope steering, CCD sky camera field, logger computer performance and event rate information for each telescope are also passed via video links to the control room.

It was deemed important that active control of the telescopes be confined to the local control room adjacent to each telescope for reasons of safety and operational integrity. As a result, only emergency cutouts for the PM tube high voltages and motor power can be operated, via hardware switches, from the control room. All other operations, including the start and end of runs and source changes, must be performed from the relevant telescope control room.

### 3.5 Methods Of Observation

Two methods of data acquisition are in common use, depending on the nature of the source under observation. 'Tracking' involves following a source, in the centre of the camera for the duration of an observation. 'Chopping' mode involves spending an equal amount of time observing a control area of sky in order to obtain a reliable measure of the background. A third method, the 'drift scan', involves holding the telescope at a fixed attitude and allowing an area of sky to pass through the field of view.

### 3.5.1 Tracking Mode

Tracking the source continually provides the maximum amount of on-source data for a given exposure. It is a method well suited to observing pulsed sources where periodic variations in signal strength may be expected and exploited.

It is also possible to detect a DC source with this method, providing that an established set of imaging cuts is applied, as described in section 3.9, which has been shown to preferentially retain gamma-ray induced events over the background. An excess of such selected events over the expected number provides the evidence for a DC source.

### 3.5.2 Chopping Modes

For an unconfirmed or weak source, a 'chopping' mode can be used to incorporate a background dataset, against which the data from the field containing the source can be directly compared. The background field is offset from the source by a fixed step in right ascension which is equal to the duration of each on/off source observation in minutes. This is so that the telescope tracks through the same range of azimuth and zenith angles during both source and background observations. The background is therefore recorded under identical operating conditions to the target field. The background field is selected to be similar in brightness to the source field. Given the  $2^\circ$  field of the camera, a 15 minute interval is close to the minimum that avoids overlap between the two fields. Either the trailing or leading offset field can be used as the background. If both are used and observed alternately with the source region, the effect of any first order secular variations in the behaviour of the telescope on the dataset can be removed.

### 3.5.3 Drift Scans

A drift scan involves maintaining the telescope at a constant attitude throughout an observation, while the potential source transits through the field of view. It relies on the detection of an excess of Cherenkov showers coincident with the source position. It is typical to observe off source for equal times before and after the passage of the source. The method is simple in execution, but remains susceptible to changes in atmospheric and instrumental conditions.

### 3.6 Timekeeping

Site-wide timekeeping is provided by a rubidium atomic oscillator (Efratom Model FRK-L) which supplies a 10 MHz output signal. A battery back-up power supply allows for an interruption in the mains supply of up to 10 days, as such oscillators are known to be prone to changes in drift rate when reset after interruptions. Internal batteries also allow the oscillator to be transported for comparison against time standards, necessary prior to the adoption of the Global Positioning System (GPS) time marker. A second, standby oscillator is available.

This atomic clock is very stable. Broadcast time signals are used to measure the small and constant drift rate of the oscillator. Originally, an Australian Government radio station (VNG) time signal was used. This was superseded in 1992 by a PC-based GPS timing system. The drift rate of the Rb oscillator relative to Coordinated Universal Time (UTC) received from the GPS system is shown in figure 3.9. The drift rate over a 2 year period is seen to be  $0.05287 \pm 0.00005$  ms per day. A 1 MHz signal is provided by the Rb oscillator to each telescope and forms the basis of the telescope event timing system. This telescope clock allows the relative time of events to be recorded to microsecond accuracy; the absolute time of an event is known to an accuracy of  $\leq 10 \mu\text{s}$ . This has been the case since 1986.

### 3.7 Data Recording

An event is recorded for a particular telescope when the spatial and temporal coincidence requirements discussed previously are satisfied. A gate input to the QT units causes the accumulation and measurement of the charge passing from each PM tube for a period of 25 ns (previously 40 ns) after the arrival of a pulse at the unit gate. Event records are slightly different for the three telescopes, but are fundamentally similar. In addition to the data from the PM tubes, events are stamped with a time to microsecond accuracy and include measurements of telescope attitude and drive and the source position. Some housekeeping data, to enable quality checks to be made, are also recorded. These include the observing (chop) mode, CCD pointing information, anode currents and an event count. Full details can be found in Holder (1997).

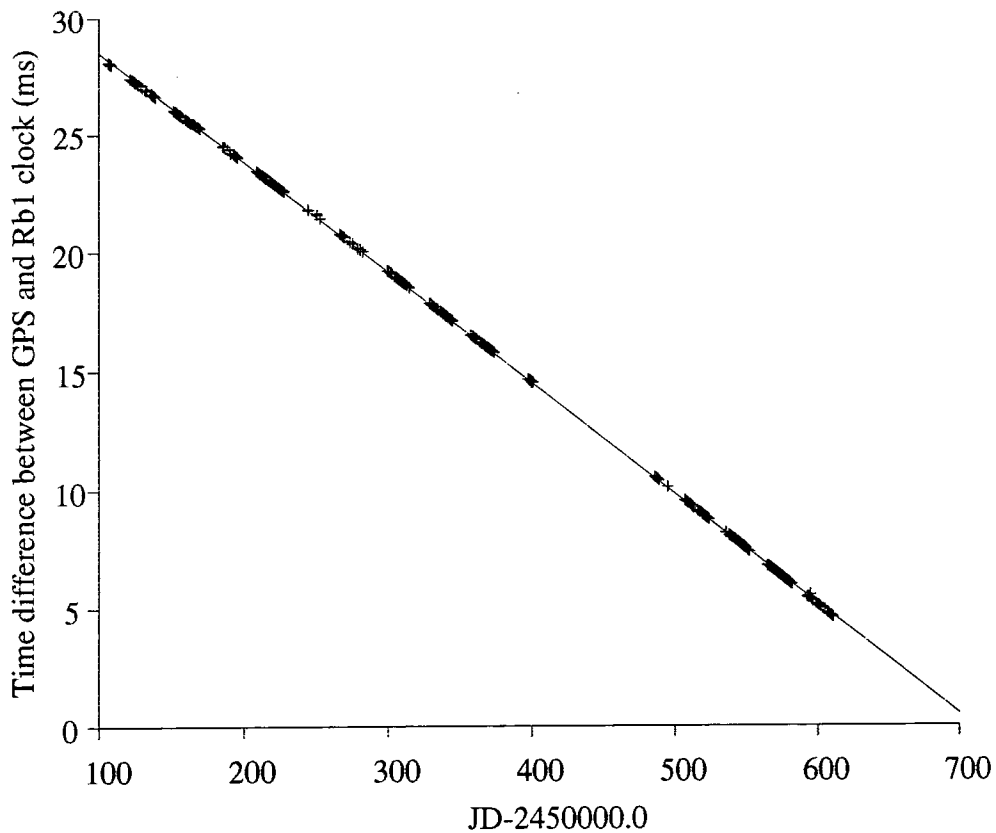


*Figure 3.9 Difference between time measured by Rubidium oscillator no. 1 and the GPS time standard between January 1996 and June 1997.*

### 3.8 Data Calibration

Data must be calibrated before they can be analysed. Calibration is a two or three stage process, dependent upon the nature of the object being observed. In all cases, it is necessary to determine the relationship between the electrical signal recorded from individual PM tubes and the amount of light to which they were exposed. Secondly, information from the CCD camera system is used to determine the telescope attitude relative to the celestial sphere. These calibrations are discussed further in section 3.8.2. In searches for periodic emission, a third stage of calibration is required to adjust event times to the solar system barycentre to account for the motion of the Earth around the Sun and of the motion of the source if it lies in a binary system.

#### 3.8.1 PM Tube Response Calibration

This calibration requires knowledge of three parameters used to describe the operation of the PM tubes and electronics. These are the digitizer pedestal, system

noise and PM tube gain. The digitizer pedestal is the DC offset - the digitizer output corresponding to zero input. The digitizer records strictly negative inputs. A negative offset is therefore applied at the amplifier stage to ensure that positive-going noise fluctuations can be recorded. The PM tube noise is defined as the standard deviation of the resulting distribution and is a measure of the quality and operating stability of the PM tube, noise in the associated amplifier and variations in sky brightness. PM tube gain is the ratio of the corrected electrical output to the amount of incident light. It is therefore a measure of the sensitivity of the PM tube and associated electronics.

Values for pedestal and PM tube noise are determined from an analysis of the PM tube behaviour under normal conditions during an observation. The PM tube gain is measured by using a standard light source, also throughout an observation.

The digitizer pedestal and PM tube noise are measured by analysing a dataset comprising artificial events. These 'null' events are generated at an average rate of  $50 \text{ min}^{-1}$  throughout an observation. They are initiated by the master trigger unit in response to signals generated at random time intervals by a dedicated microcomputer. They are recorded in the datastream, identified for extraction and analysis by a 'null event' bit in the fire pattern. These events trigger the telescope in the same way as genuine events, except that they contain no Cherenkov light and are therefore a measure only of the digitizer characteristics and PM tube noise. The PM tube output will be due to electronic and, predominantly, sky noise. Analysis of such events throughout an observation allows the construction of a noise spectrum for the PM tube, an example of which is shown in figure 3.10. This distribution is approximately Gaussian in shape. The pedestal is defined as the mean of the distribution and the tube noise is the standard deviation.

Tube gain is defined as the ratio of the increase in signal size to the increase in the amount of light observed. The EHT supplies to the tubes are set such that the output from each tube is similar when exposed to the same light, but this approach is limited by restrictions on PM tube performance such as acceptable values of noise rate. Tube noise rate, the frequency at which an individual PM tube produces spurious output pulses not resulting from incident Cherenkov flashes, provides a restriction on gain by limiting the EHT which can be applied to a PM tube. The result of this is that it is not possible to produce a totally flat field (uniform sensitivity across the camera) in any of the detector packages. It is necessary to measure the relative gains of the PM tubes during observations in order to produce a fully flat field response.

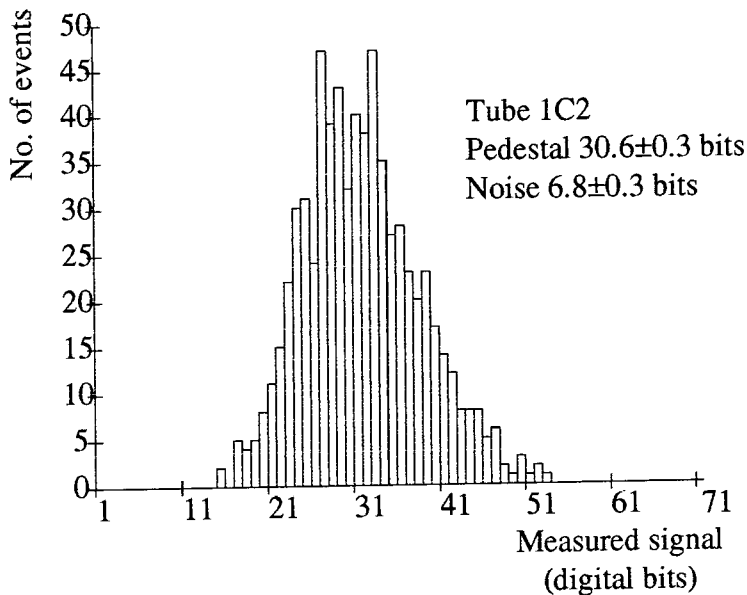


*Figure 3.10 Pulse Height Distribution of null events for a single tube for one 15 minute observation (650 events). The digitizer pedestal is the mean and the detector noise is the standard deviation of the distribution.*

To perform this flatfielding operation, it is necessary to uniformly illuminate each PM tube in the telescope with a short flash of light, of duration similar to that of a Cherenkov flash ( $\sim 10$  ns). Initially, this was carried out by using a radioactive source distributed in a scintillator, producing a constant light flux. This light pulser was exposed to each PM tube in turn, while the telescope was parked and the detectors were shielded from all other light sources. To measure light in this way, it is necessary to reduce the coincidence requirement from 3- or 4-fold to 1-fold, allowing the telescope to record events in which only one PM tube is illuminated. The mean pulse height, after allowing for the digitizer pedestal, can be used to determine the absolute gains of the PM tubes. There are, however, a number of limitations with this method. The light source is in contact with the photocathode and so can only illuminate part of the photocathode surface and the results do not account for sensitivity variations across this surface. This method does not replicate the effects of the sky background on the PM tube gain since the effect of the sky background must be removed if the small signal is to be measured. The procedure is also very time consuming. It is practical only to make one set of measurements per month which must be applied to all data from that period. It does, however, provide a measure of absolute gain, which is necessary to determine the energy threshold of the telescope, as discussed in chapter 5.

An improved method of calibration of relative gains utilises a pulsed light source to provide a flash of light similar in intensity, duration and spectral distribution to a Cherenkov flash. A pulsed nitrogen laser/scintillator arrangement mounted on the telescope is used. The laser is a 337 nm 70 kW nitrogen pulse laser and the scintillator reradiates light with a spectrum similar to that of Cherenkov radiation. The laser and scintillator are mounted in a lightproof box. Light from the scintillator is fed to an opal diffuser at the centre of each mirror via a fibre-optic cable. All tubes are therefore illuminated simultaneously and uniformly across each detector package. This method is used both as a more efficient replacement for the above procedure, and to allow calibration events to be injected into the datastream during an observation. This allows gain measurements to be made under normal operating conditions. The telescope triggers normally, as the laser is set such that enough light is produced that all channels satisfy the coincidence requirement. An extra PM tube, collimated so that it is exposed to the laser light from the diffuser but not to that from the mirror or sky, is used to identify and monitor laser induced events.

A backup method of gain calibration uses the response to cosmic-ray induced events to determine gain. This procedure requires the assumption that the distribution of events is uniform across all of the tubes. It follows that the illumination of all PM tubes due to cosmic-rays will also be isotropic. An integral signal distribution for all events is generated, as shown in figure 3.11. The range of signal size (in digitizer bits) over which the integral signal falls from 30% to 5% of the total, PHA530, provides a measure by which the relative gains of individual tubes can be compared. The use of 5% and 30% count rates avoids the effects of the smallest flashes where triggering biases are critical. The procedure is based on a study by Punch (1993).

### 3.8.2 Accurate Measurement of the Telescope Attitude

Data specifying the attitude of the telescope are recorded from the shaft encoders, as described in section 3.3.5. The shaft encoders on the Mark 6 telescope measure to 14-bit accuracy (12 bits on the Mark 3/5 telescopes) over a full 360°, corresponding to  $0.02^\circ \text{ bit}^{-1}$  ( $0.09^\circ \text{ bit}^{-1}$  on the Mark 3/5 telescopes). However, the absolute offset between the shaft encoder readings and the actual pointing position on the celestial sphere is not known accurately for all regions of the sky.

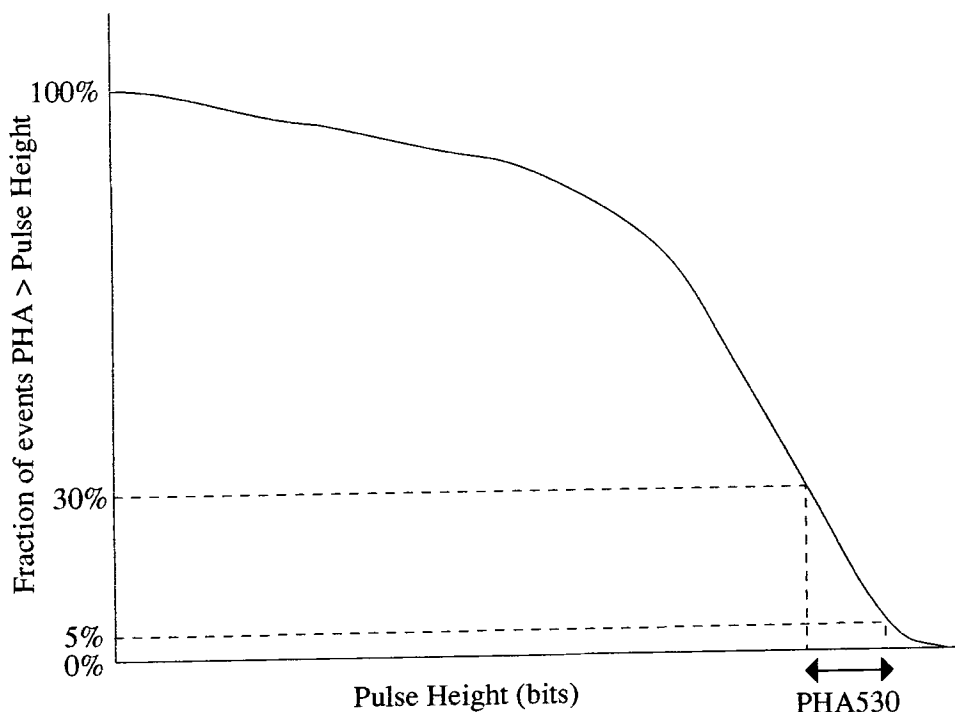


*Figure 3.11 The integral pulse height distribution for an individual PM tube detecting cosmic ray induced Cherenkov events. The interval between 5% and 30% of events, measured in digital counts, is used to calibrate relative gains.*

A full description of the procedures previously used to determine the absolute pointing of the telescope can be found in Dickinson (1995). The use of an SBIG ST4 CCD camera, aligned with the optic axis of the telescope allows a much improved 'inflight' attitude measurement. At the beginning of each observation, a full image of the CCD field is taken. The 5 second exposure allows 8<sup>th</sup> magnitude stars to be resolved. The CCD then takes a continuous stream of 3 second exposures during an observation and, for each event, the location and brightness of the brightest pixel within the CCD field of view from the exposure is included. Off-line, the full frame image is compared to a database of stars to determine the orientation of the CCD chip relative to the celestial sphere. For each event, the brightest pixel in the CCD image is associated with a database star. The deviation between the positions of the brightest pixel and the star is used to calculate the shaft encoder offsets. These offsets are applied to the shaft encoder readings to locate the source position in the field of view. The  $x,y$  coordinates of the true source location are written to the event record and Cherenkov images are parameterized relative to this position for the source. This CCD based procedure improves the knowledge of the absolute source position within the field of view of the telescope to better than  $0.03^\circ$ . Figure 3.12 shows typical CCD data composed

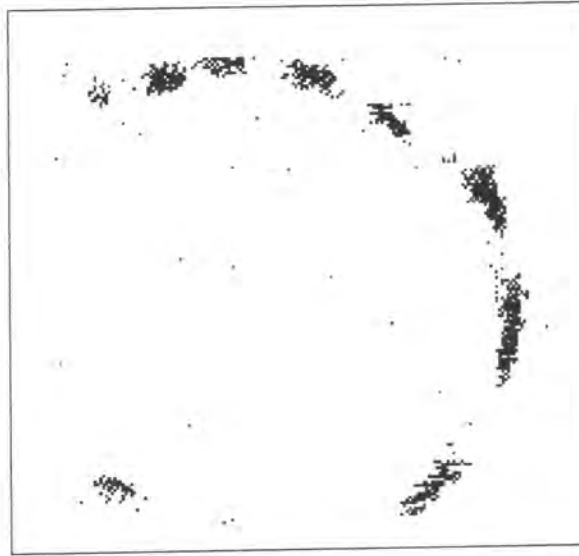


*Figure 3.12 The locus of the stellar image through the field of PKS 2005-489, during a long observation. The box is  $2^\circ$  square. Each dot corresponds to the brightest pixel in an individual exposure. The gaps in the track correspond to periods spent observing the background field.*

of the locus of the brightest pixel from each exposure taken throughout an observation. Figure 3.13 shows the corrections which are used to improve the measurement of the telescope attitude.

### 3.8.3 Adjustment of Event Times to the Centre of the Solar System

In analyses where event times are important, such as searches for periodic emission, it is necessary to measure the arrival time of pulses at a fixed point in space, to account for effects due to the movement of the telescope on the Earth. To do this, a three stage correction must be applied;

- translation of the event times to the centre of the Earth,
- translation of the event times to the centre of gravity of the solar system (barycentre) and
- application of relativistic corrections.

The first stage removes the Doppler effect introduced by the rotation of the surface of the Earth. This also corrects for the absolute position of the observatory on the surface of the Earth. These corrections can alter pulse arrival times by up to 21 ms, the time taken for light to travel a distance equal to the radius of the Earth.

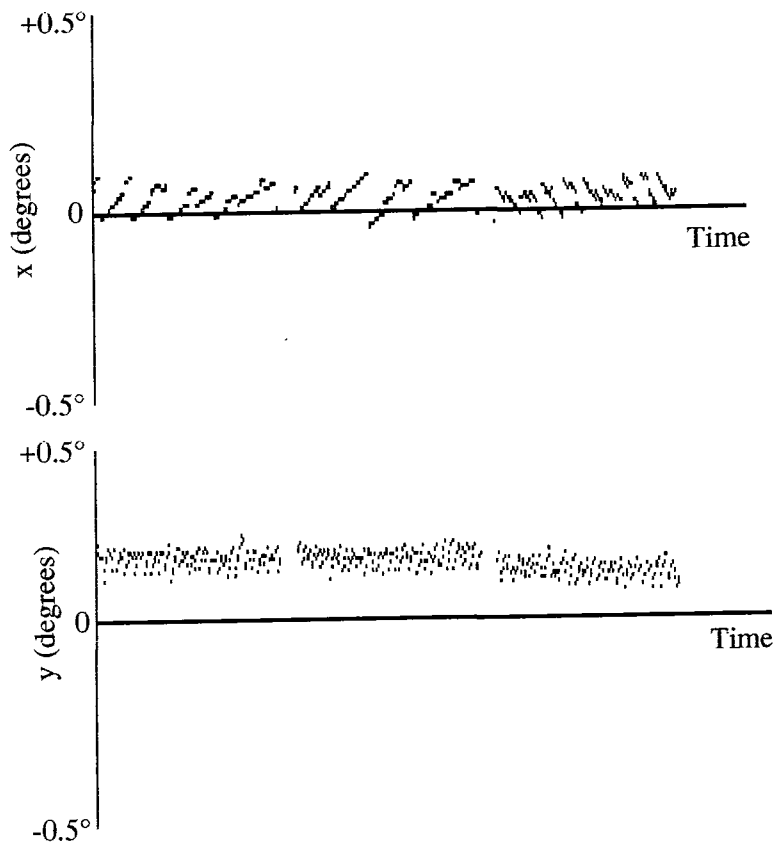


*Figure 3.13 Measurements of the telescope position with respect to the source as determined with the Shaft Encoders and CCD information.*

Translation to the solar system barycentre accounts for the same effect due to the motion of the Earth about the sun and about the Earth/Moon barycentre. Corrections are based on the JPL DE200 Earth ephemeris (Standish, 1982) and can be up to 500 s. The relativistic correction is necessitated by the motion of the Earth and the different gravitational environments at the surface of the Earth and the solar system barycentre. It can be as large as 3 ms (Mannings, 1990).

#### 3.8.4 Adjustment of Event Times for an Object in a Binary System

For a candidate source in a binary system, it is necessary to compensate for the orbital motion of the system. Angular velocities in binary systems can be very large, resulting in significant Doppler effects due to high velocities of candidate sources along the line of sight. Corrections to times are made based on an orbital ephemeris obtained from observations of the object at another wavelength and assume that the site of any VHE gamma-ray emission is coincident with the emission at other wavelengths. The procedure is well established and full details can be found in Carramiñana (1991).

### 3.9 Analysis of Data from Individual Telescopes

The purpose of data analysis is to identify any population of gamma-ray induced events within the hadronic background. Distinctions between the two can be made either on the geometric properties of the image of the Cherenkov light (imaging analysis) or by investigation of the time profile of the data (timing analysis).

#### 3.9.1 Imaging Analysis

Analysis techniques based on geometric differences between images of gamma-rays and hadrons require that the images are treated as ellipses. Hillas (1985) defined the ellipse which describes a Cherenkov image in terms of 6 basic parameters, which can be used to provide some degree of distinction between images of gamma-rays and hadrons. Five of these parameters relate to the orientation of the image relative to the source and are shown in figure 3.14. The descriptions of the 'Hillas Parameters' are given in table 3.1. Furthermore, derived parameters have been developed, such as  $\alpha = \sin^{-1}(\text{miss}/\text{distance})$ .

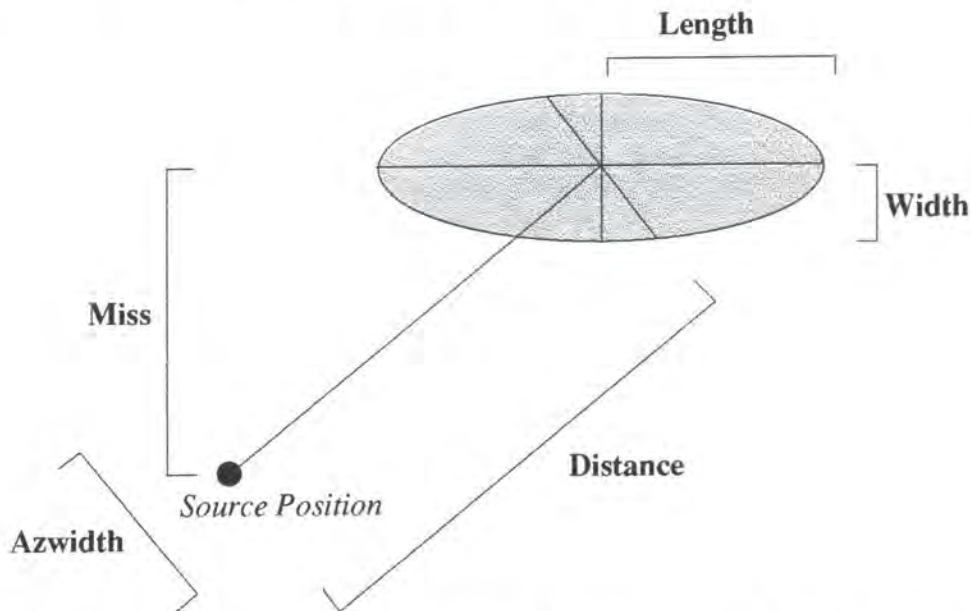


Figure 3.14 An illustration of the Hillas Parameters for parameterization of images of Cherenkov showers.

The ellipse is defined by calculating the lower order moments (0<sup>th</sup>, 1<sup>st</sup> and 2<sup>nd</sup>) of the image. This involves determining which PM tubes form part of the image. The definition of image and border tubes is based on one of two methods, which treat the signal in units of RMS noise. A PM tube may be considered as part of the image if the calibrated signal is greater than some multiple of the tube noise. Each

PM tube is labelled as an 'image tube' if this criterion is met. A tube is set as part of the 'border' if the signal is greater than some smaller multiple of the tube noise ( $\sigma$ ) and it is adjacent to an image tube. Alternatively, a fraction of the peak signal may be used to define the image and border thresholds. Typically signal values of 37.5% and 17.5% of the largest calibrated signal in any pixel are used to determine image and border respectively (Armstrong *et al.*, 1999).

Width	The RMS length of the semi-minor axis of the image. Sensitive to the lateral spread of the shower.
Length	The RMS length of the semi-major axis of the shower. Sensitive to the longitudinal development of the shower.
Miss	The perpendicular distance between the major axis and the centre of the field of view. This is a measure of image orientation, and is sensitive to the arrival direction of the primary particle.
Distance	The distance between the centre of the field of view and the centroid of the image.
Azwidth	Abbreviation of azimuthal width. Defined as the RMS width of the image perpendicular to the line joining the image centroid and centre of the field of view. Azwidth is dependent on both width and orientation of the image.
Frac(2)	The ratio of the two largest tube signals to the total tube signals.

*Table 3.1 Definitions for parameterization of shower images recorded by imaging atmospheric Cherenkov telescopes - proposed by Hillas (1985).*

The Durham group has developed a method of defining the image and border tubes which is a hybrid of the two approaches. The tube with the largest corrected pulse size ( $QT_{\max}$ ) is identified. A tube is then treated as an 'image' tube if it produces a signal greater than 37.5% of  $QT_{\max}$  and  $> 4.25\sigma$ . Similarly, a tube is treated as a 'border' tube if the signal is greater than 17.5% of  $QT_{\max}$  and  $> 2.25\sigma$ . This is based on work showing that the point spread function of an image is not represented by a single Gaussian distribution, but has a distinct 'tail'. Full details are given by Holder (1997).

Having defined the PM tubes which constitute the image, the moments are calculated thus

$$\begin{aligned} \text{sum} &= \sum_{i=1}^n s_i & \langle x \rangle &= \frac{\sum_{i=1}^n s_i x_i}{\sum_{i=1}^n s_i} & \langle y \rangle &= \frac{\sum_{i=1}^n s_i y_i}{\sum_{i=1}^n s_i} \\ \langle x^2 \rangle &= \frac{\sum_{i=1}^n s_i x_i^2}{\sum_{i=1}^n s_i} & \langle y^2 \rangle &= \frac{\sum_{i=1}^n s_i y_i^2}{\sum_{i=1}^n s_i} & \langle xy \rangle &= \frac{\sum_{i=1}^n s_i x_i y_i}{\sum_{i=1}^n s_i} \end{aligned}$$

where the image includes  $n$  tubes,  $x_i$  and  $y_i$  are the coordinates of the  $i^{\text{th}}$  PM tube and  $s_i$  is the calibrated signal from that PM tube. From these, the variances can be calculated as follows.

$$V(x) = \langle x^2 \rangle - \langle x \rangle^2 \quad V(y) = \langle y^2 \rangle - \langle y \rangle^2 \quad V(xy) = \langle xy \rangle - \langle x \rangle \langle y \rangle$$

Using  $d = V(x) - V(y)$  and  $z = (d^2 + 4V(xy))^{1/2}$ , the major axis of the ellipse is defined by the straight line  $y = ax + b$ , where

$$a = \frac{d + z}{2V(xy)} \quad b = \langle y \rangle - a \langle x \rangle$$

These identities can then be used to determine the Hillas parameters of the image. Simulations have shown differences between gamma and hadron induced showers in terms of these parameters. It is therefore possible to use the Hillas parameters to reject events which experience, whether based on simulations or otherwise, shows to be probable hadron induced showers, with the result that a gamma-ray signal may be enhanced. The best single discriminant in early works was the *azwidth*

parameter. Gamma-rays are expected to produce images with small values of *azwidth*, pointing towards a common source direction, while the hadronic background shows no preferred source direction. Rejection methods such as these are known as cuts. The efficiency of a set of cuts is defined by the quality factor,  $Q$ , thus:

$$Q = \frac{\eta^\gamma}{\sqrt{\eta^N}}$$

where  $\eta^\gamma$  and  $\eta^N$  are the fractions of gamma-ray and hadron induced events retained by the cuts respectively (Fegan, 1992).

The use of background rejection techniques based on image parameters has allowed the development of VHE gamma-ray astronomy to progress. A simulation-based *azwidth* cut allowed the Whipple group to reject 99% of background events and detect VHE emission from the Crab nebula (Weekes *et al.*, 1989) at the  $9\sigma$  level from 82 hours of on-source data. A multiparameter cut, known as 'supercuts' developed by the Whipple group is estimated to reject 99.7% of background events while retaining 50% of gamma-rays, a  $Q$ -factor of greater than 9 (Fegan, 1996). The parameters were optimized on data from observations of the Crab nebula and can now be applied *a priori* to new data taken under similar circumstances, retaining the full significance of any detection. Other methods of background rejection have been attempted, including the use of neural networks (Reynolds, 1991) and genetic algorithms (Lang, 1995), but nothing has been found to be as efficient as the 'supercuts' and related techniques.

The parameter distribution of a number of events is dependent not only on the shower development, but also on the characteristics of the telescope. A low resolution imaging system will be unable to determine shape parameters as well as a high resolution system, although the total amount of light measured may be the same. Furthermore, spreading of an image due to blurring by the optics may cause uncertainties in the determination of the image dimensions.

Simulated gamma-ray and hadron initiated EAS have been generated by Holder (1997) using the MOCCA Monte Carlo program (Hillas, 1982). Results, presented in figure 3.15, show the predicted distinction between hadron and gamma-ray images for 3 of the Hillas parameters (*width*, *length* and *distance*) plus the derived parameter *alpha*. Holder further shows that the simulated hadron induced events are a reasonable representation of the cosmic-ray background in the telescope.

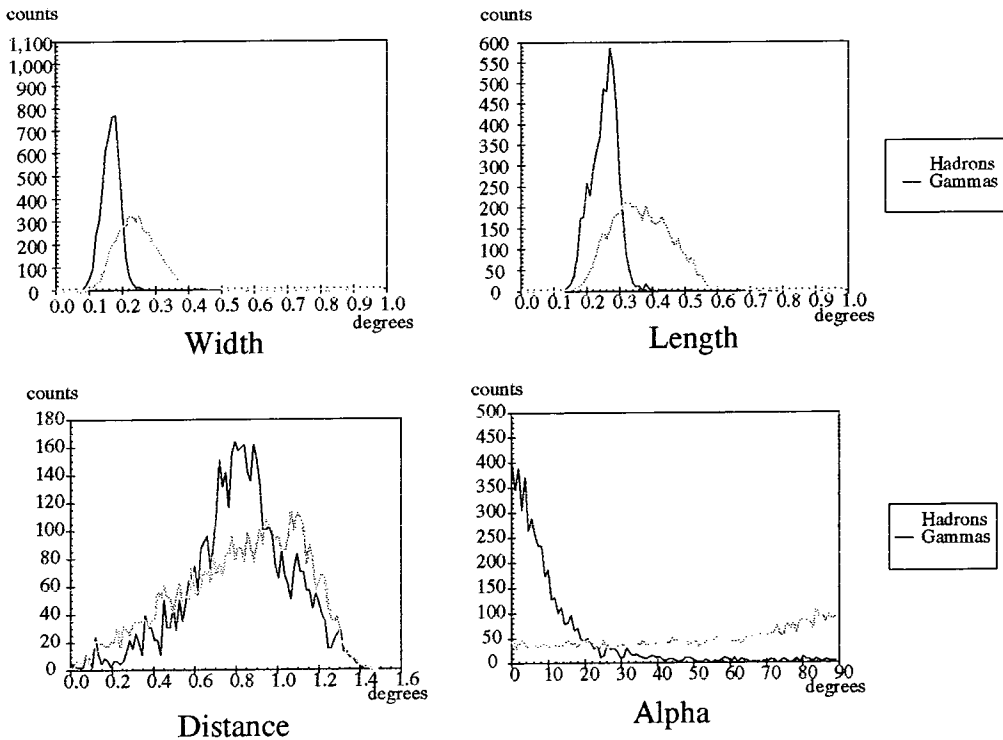


Figure 3.15 Parameter distributions for simulated hadron and gamma ray images (from Holder, 1997).

From such simulations, and from observations of a gamma-ray source, it is possible to optimize the effectiveness of a set of cuts. Gamma-ray images are, for example, seen to have shorter *length* and *width* than images of hadron induced showers. A distribution showing an excess of events at small values of *alpha* is often used as evidence of gamma-ray emission. Hadrons produce a relatively flat *alpha* distribution. The increase in number of events often seen at around  $90^\circ$  is due to the effects of truncation of events falling close to the edge of a camera of finite size. This results in the apparent 'turning' of such events to lie along the edge of the camera. As this will also apply to gamma-ray induced events, it is prudent to reject events with a *distance* greater than some value in order to ensure that sufficient light from retained events is contained within the camera and provides a true indication of the orientation of the image.

Imaging analysis is well suited to observations of candidate DC (steady) gamma-ray sources. The detection of a DC source involves the demonstration of the existence of an excess number of gamma-ray like events in the direction of the source compared to the number of similar events in a control dataset taken under similar operating conditions. Identical cuts must be applied to data from both on- and off-source fields to provide effective background rejection, with the result that any signal will be enhanced. If all systematic effects, such as differences due to

zenith angle or sky clarity effects, are accounted for, then any excess events must be due to gamma-ray emission. The significance of any excess is given by:

$$Significance(\sigma) = \frac{N_{on} - N_{off}}{\sqrt{N_{tot}}}$$

where  $N_{on}$  and  $N_{off}$  are the number of on source and off-source (background) events retained after any set of cuts and  $N_{tot} = N_{on} + N_{off}$  (Gibson *et al.*, 1982).

### 3.9.2 Timing Analysis for Pulsed Sources

To search for periodic emission from a candidate source, event times must first be adjusted for the motion of source and observer, as discussed in section 3.8. Subsequently, two analysis techniques can be used, depending on the accuracy to which the periodicity at other wavelengths and shape of the light curve of the object are known.

For sources where stable observations are available at other wavelengths, epoch folding techniques can be used. Where such information is not regularly available and where emission may be variable in terms of intensity, periodicity and light curve shape, more general tests are required (e.g. Charles and Seward, 1995).

Epoch folding involves assigning a relative phase to each event, based on arrival time and compiling a light curve from the number of events in each phase bin. By using Pearson's  $\chi^2$  test, a comparison can be made between the observed light curve and the expected uniform distribution (Leahy *et al.*, 1983). If the light curve is known, then the size and position of the peak in the phase bins can be determined *a priori*. This maximises the significance of the signal. Where the light curve is less well known, a narrow phase peak may be split over more than one bin. Re-binning will increase the number of degrees of freedom, with a reduction in the significance of the signal.

The arbitrary binning decisions unavoidable in epoch folding when the light curve is poorly measured can be avoided by the use of circular statistics. The arrival time of each event can be represented as a radial vector on a circle with phase angle  $\phi_i$ , relative to some arbitrary phase. These vectors can be summed to provide a resultant, which, if large, is indicative of an excess of events around a particular phase. The Rayleigh test (Rayleigh, 1894, Batschelet, 1981) was introduced to VHE gamma ray astronomy by Gibson *et al.* (1982) and is a widely used statistic in this field. This test is most sensitive to broad sinusoidal light curves. It cannot, for

example, be used directly, with a source with a double-peaked light curve with peaks  $180^\circ$  apart, where the peaks cancel each other out. A test carried out at the half-period would however, respond to such a light curve.

### 3.9.3 Compensations for Differences Between On- and Off-Source Fields

The behaviour of the PM tubes varies with the level of background illumination. In particular, the size and rate of noise pulses increases with brightness. As the response of a PM tube to noise increases, so does the likelihood that negative fluctuations in the random noise will cancel out the Cherenkov signal. Therefore, in bright fields, the presence of large noise will cause the signal from a number of PM tubes to be reduced. Some of these will be reduced below the threshold for definition as a 'border' tube and will not be treated as part of the image. This results in a reduction in the number of tubes forming the image, with a corresponding reduction in the *width* and *length* of the ellipse. For observations made in a 'chopped' mode, this may lead to systematic differences between the number of events retained after any set of cuts in the on- and off-source data.

Cawley (1993) suggested that adding randomly generated noise, based on the brightest field, to the signals from the PM tubes when exposed to the dark field would equalise the noise levels. This technique is known as 'software padding' is appropriate for *a posteriori* correction of signal differences due to differences in sky brightness. It is analogous to the use of hardware padding lamps used to maintain constant illumination of PM tubes in earlier experiments. It is routinely applied to the data reported here.

## 3.10 Quality Control

To be considered as suitable for analysis, data must satisfy the following criteria;

- difference in numbers of events between corresponding ON and OFF source scans prior to any selection must be  $\leq 2.5\sigma$  and
- event count rates must vary smoothly with no evidence of poor weather, atmospheric conditions or freezing.

The behaviour of gamma-ray images at large zenith angles ( $> \sim 60^\circ$ ) is less well understood, due to the effects of, for example, the increased path length. Data taken in this regime may be analysed, and is likely to respond to the same treatment as applied to events recorded at smaller zenith angles with changes in selection criteria.

### 3.11 Observing Campaigns for 1994-1997

Observations in these three years concentrated on 3 types of objects; active galactic nuclei (AGNs), X-ray binaries (XRBs) and plerions.

The detection of 60 AGNs at EGRET energies (Thompson *et al.*, 1995) and three, Mrk 421 and Mrk 501 (Punch *et al.*, 1992 and Quinn *et al.*, 1996) and 1ES 2344+514 (Catanese *et al.*, 1998), at VHE energies makes these objects attractive candidates for searches for TeV emission. In particular, close (low redshift) X-ray selected BL Lacs have been identified as potential sources (Stecker *et al.*, 1996). These are AGNs of low luminosity, which are characterized by the absence of emission lines in the spectrum and where the jet is believed to be pointing towards the Earth. It is suggested that TeV photons are produced by Comptonization of the particle flow in the jet. Absorption of the gamma-ray flux by the infrared background means that distant objects are unlikely to be seen in this regime (Stecker and de Jager, 1996). Mrk 421 and Mrk 501 are at redshifts of 0.031 and 0.034 respectively, being the closest X-ray selected BL Lacs. Candidate southern hemisphere sources that have been observed are shown in table 3.2. Unfortunately, it can be seen that the four prime candidates are all at considerably larger redshifts than Mrk 421 and Mrk 501.

Object	Redshift
PKS 0548-322	0.069
PKS 1514-241	0.049
PKS 2005-489	0.071
PKS 2155-304	0.117
(Mrk 421)	0.031

*Table 3.2 BL Lac objects observed with the Durham Mark 6 telescope. (Mrk 421 has not been observed, but is included for comparison, as the first BL Lac object to be detected using the atmospheric Cherenkov technique.)*

TeV emission from XRBs has been reported by the Durham group using earlier telescopes (e.g. Carramiñana *et al.*, 1989). TeV emission from Cen X-3 and Vela X-1 have also been detected by the Potchefstroom group (e.g. Raubenheimer *et al.*, 1989, 1994). The Mark 6 telescope project has provided the opportunity to re-examine these objects at increased sensitivity. Results of observations of Cen X-3 will be presented later (Chadwick *et al.*, 1998b and summarised in chapter 6).

A plerion is a supernova remnant, which has no clear shell structure. Synchrotron radiation from inside the shell is much brighter than any that may be emitted by a shell. A pulsar would account for the continuous stream of relativistic electrons required for the emission. The non-detection of a pulsar in a plerion may be a result of the orientation of the pulsar relative to the Earth. Radiation from the pulsar is reradiated following interaction with the nebula, resulting in diffuse emission. Examples include PSR 1706-44 and the Vela and Crab pulsars. PSR 1105-61 is also believed to be a plerion. PSR 1706-44 has now been detected at TeV energies by two groups (Kifune *et al.*, 1995, Chadwick *et al.*, 1998a).

Other objects which have been the subjects of observing time in these years include SN1006, PSR 1509-58 and PSR1055-52. SN1006 is a supernova remnant which has been predicted to be a source of TeV photons (Pohl, 1996) and has been observed by the CANGAROO collaboration (Tanimori *et al.*, 1998). PSR 1509-58 has been detected using the BATSE and OSSE experiments on the Compton Gamma Ray Observatory, but has not been detected at EGRET energies (Brazier *et al.*, 1994) and has also been observed by the CANGAROO collaboration (Tanimori *et al.*, 1997). PSR 1055-52 is also an EGRET detected pulsar (Fierro *et al.*, 1993) Results of Durham observations of these objects will be presented elsewhere.

### 3.12 Summary

In this chapter, the instruments operated by the Durham group have been introduced, with a discussion of the practices involved in operation and data analysis. Particular attention has been paid to the newest instrument in operation, the Mark 6 telescope. The types of sources observed with the Mark 6 telescope have been discussed.

## Chapter 4. The Stability and Operation of Atmospheric Cherenkov Telescopes

### 4.1 Introduction

The detection of gamma-rays using the atmospheric Cherenkov technique involves the identification of a signal against a background, induced by hadrons, which may be up to 4 orders of magnitude more populous. In order to improve this signal to noise ratio, it is necessary to be able to identify the parameters which distinguish gamma-rays from the background. This can be done either using the telescope hardware, in selection of Cherenkov light flashes, or later during analysis. A complete identification relies on the reproducible and distinguishable behaviour of the light production in the showers that form the signal and those which constitute the background noise. As shown in chapter 3, there is, however, no neatly defined set of parameters that can be measured with a single telescope which define gamma-rays to the total exclusion of the background noise; rejection of >99% of background events is seen to be possible while retaining >50% of the signal.

The Cherenkov radiation is produced by cascade processes in the atmosphere, as described in chapter 2. These processes are assumed to arise in a constant, ideal atmosphere. Such an assumption breaks down under the real atmospheric conditions where there can be changes in the atmosphere and the presence of obscurants can cause variations in the amount of detected light. Furthermore, the features of the Cherenkov radiation which form the basis of the background identification may also change with variations in the atmosphere.

The behaviour of the telescope used to record the Cherenkov light may also deviate from the ideal with, for example, a small change in detector gain, both during and between observations. Such variations may result in changes in the appearance of similar light signatures at different times, reducing the efficiency of the measures intended to identify the background.

The operational stability of an atmospheric Cherenkov telescope and an understanding of the radiative properties of the atmosphere are therefore fundamental to the successful interpretation of data recorded in a series of observations. In this chapter, those elements of the Durham Mark 6 telescope which can affect operational stability are identified and studied. The problems inherent in using the atmosphere as the Cherenkov radiator and of using sensitive

electronics in a less than ideal environment are discussed. Investigations have been carried out to determine the responses of the Mark 6 telescope to changes in environmental and operating conditions. Systems have been installed on the telescope to monitor changes in the environment and to record the operating conditions. Where such investigations, together with subsequent laboratory work, indicate that such variations may be sufficient to have significant effects on the data recorded, control measures have been implemented.

## 4.2 Nominal Performance of the Mark 6 Telescope

The successful operation of an atmospheric Cherenkov telescope depends on a number of functions. These include telescope steering, light collection and detection, signal processing and data recording. The components involved in each of these processes should maintain a constant performance throughout an observation and also ideally between successive observations. The rate at which the telescope records background Cherenkov flashes is often regarded as the ultimate measure of the stability of the optical and electronic components of the instrument. It would be expected that the count rate recorded by the telescope would vary in a predictable manner during the course of an observation of a single object, due to changes in zenith angle; a similar performance during further observations of the same object would be expected.

The rate of detection of Cherenkov flashes is expected to vary primarily with zenith angle ( $\theta$ ) of the telescope. As the zenith angle increases, so does the atmospheric path length, with increased distance to the point of Cherenkov emission, subsequent attenuation of the Cherenkov light and a corresponding reduction in count rate. The light pool of the shower is also dispersed over a larger area on the ground; showers with smaller primary energies will trigger the telescope with reduced probability, causing a further reduction in the count rate and an increase in the energy threshold of the telescope for large zenith angles.

In a simple model, the path length increases as  $\sec(\theta)$  and the area of the light pool increases as the square of the path length, due to the near-constant angle of propagation of the Cherenkov flash. The expectation is that count rate should vary as  $\cos^n \theta$ , with  $n \sim 2$  for many telescopes. However, the precise value of  $n$  is dependent upon many aspects of the telescope operation, including event selection requirements and the light detection threshold. Figure 4.1 shows typical plots of count rate versus time and zenith angle for observations with the Mark 6 telescope. For this data, the count rate variation is as  $\cos^n \theta$  with  $n \sim 1.2$ . Count rate variations

due to zenith angle changes are reproducible to a sufficient accuracy that it is possible to account for the effects of the change. Any deviation from this behaviour is taken as an indication of some variation in the behaviour of the instrument or atmosphere.

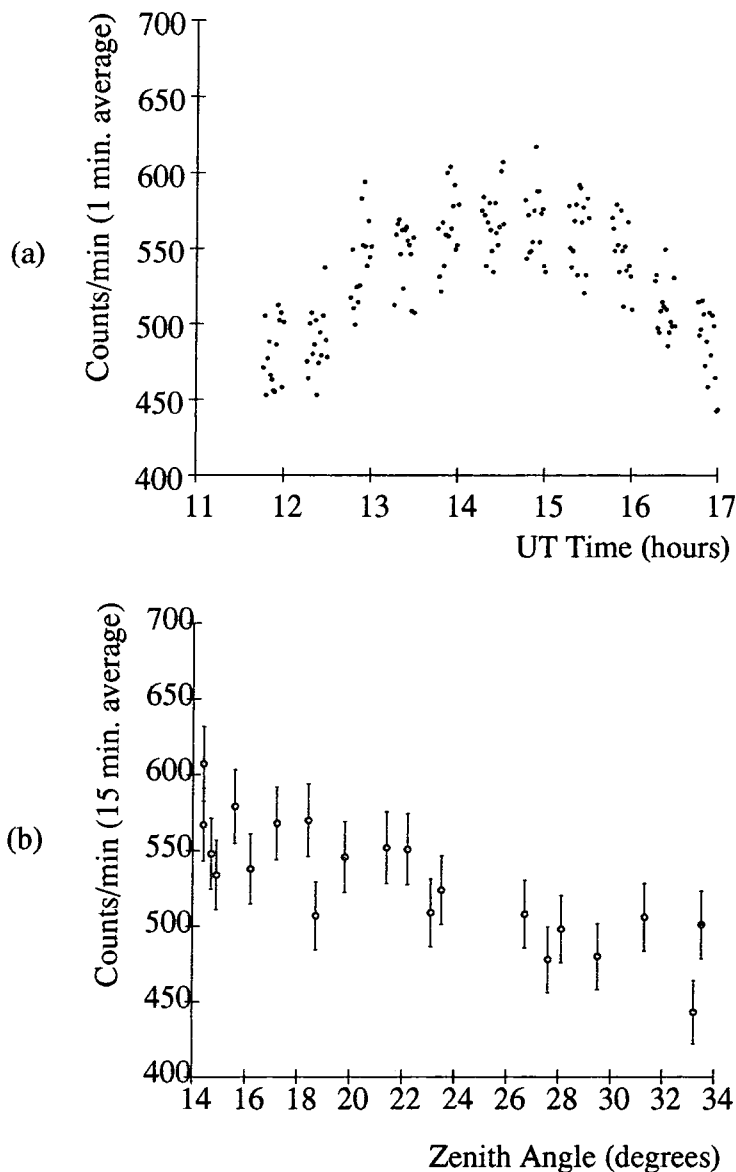


*Figure 4.1 Mark 6 Telescope Count Rate as functions of (a) time and (b) zenith angle during an observation of PSR 1706-44.*

The values of the anode currents of individual PMTs in the telescope light detectors also provide an indication of the clarity of the atmosphere coupled with the behaviour of individual channels within the detector/electronics packages. A change in the anode current from a PM tube is indicative either of a change in the brightness of the area of sky to which it is exposed, the atmospheric transparency

or of a change in the gain of the tube. In general, a change over a relatively short time scale is likely to be the result of a change in the atmospheric transparency, while gain changes are more likely to be evident as a drift over a longer period of time. A change in the gain of PM tubes will affect the threshold of the telescope and will have significant effects on the acceptance and parameterization of smaller events around threshold. Figure 4.2 shows a typical anode current history for an observation where a star moves through the field of view of a number of PM tubes in an observation of PSR 1706-44. The gaps in the data are due to the nature of the observation which is made with interspersed off-source observations to measure the background (chopped mode). The positions of the PM tubes in the imaging camera through which the image of the star passes can be seen in figure 3.5.

### 4.3 Factors Influencing the Performance of Atmospheric Cherenkov Telescopes

In this section, the factors which define the telescope performance are identified as the mirrors, the light detectors, the accuracy with which telescope pointing is known and the quality of the control and signal processing electronics. The effect of variations in the operating conditions of each of these factors is investigated. Particular attention is paid to the operation of the PM tubes used in the light detecting packages.

The effects of changes in the telescope environment on data quality are also discussed; the effects of variations in ambient temperature, background illumination and strength of the magnetic field are explored.

The atmospheric Cherenkov technique is an example of an unusual approach to astronomy in which the atmosphere is an integral part of the detection system. It serves as the radiating medium in which the Cherenkov light is generated and propagated. Although there have been few attempts to date, it is desirable that some attempt is made to understand the effects of changes in sky clarity and weather conditions on the data recorded.

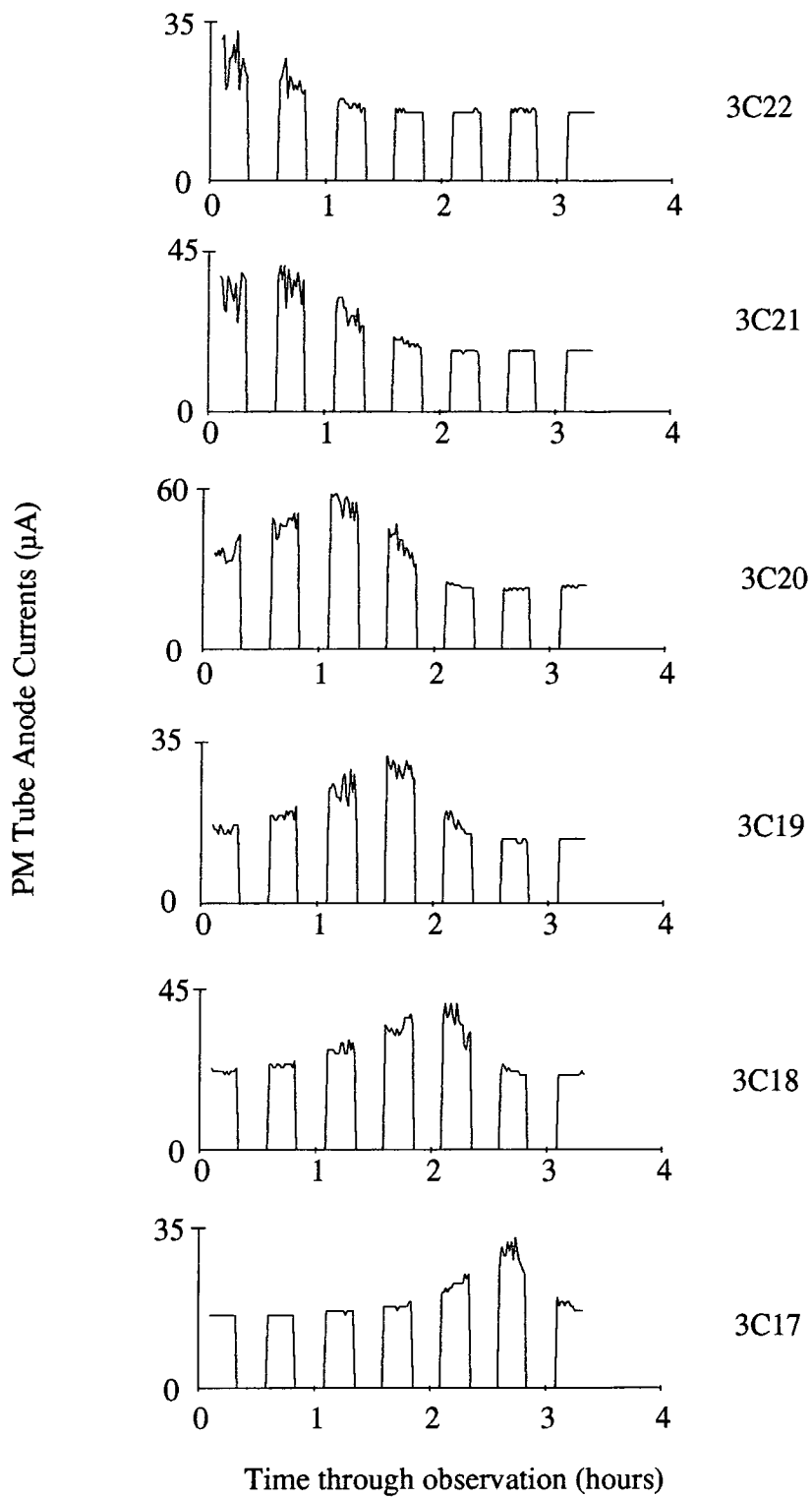


*Figure 4.2 Anode current measurements showing the passage of a star in the field of PSR 1706-44 through a number of PM tubes in the 3rd ring (3C) of the camera.*

### 4.3.1 Telescope Design and Operation

Data recorded by the telescope are affected by four areas of the instrument's performance, shown schematically in figure 4.3. Changes in any of these functions will have an effect on the recorded data in terms of quality and/or quantity.

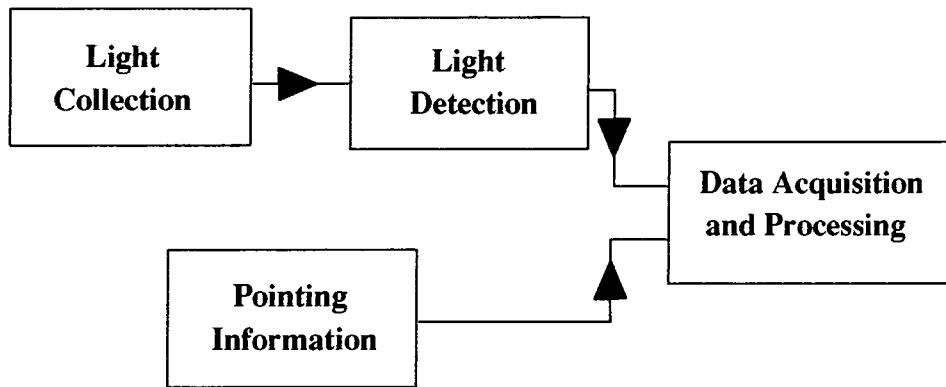


*Figure 4.3 Factors defining the performance of an atmospheric Cherenkov telescope.*

Measurements of variations in these functions required the emulation of the operation of the telescope, particularly the electronic components. In order to investigate and quantify any variations, a dark laboratory was set up to measure and monitor PM tube operating behaviour. Background illumination, to simulate the night sky as required, was provided by using a green light emitting diode driven by a variable current to allow changes in the brightness of the background. A Cherenkov flash was simulated by exposing a sample of plastic scintillator to a 337 nm 70 kW nitrogen laser pulse. The scintillator reradiates light at wavelengths comparable to those of Cherenkov light. The pulse duration (4 ns) is also similar to a Cherenkov flash. The light from the laser, situated in an adjacent room, was passed into the dark laboratory via a fibre-optic link. The PM tube signal was passed to the signal processing electronics representative of a single channel in the Mark 6 telescope in Narrabri. The signal cable used was the same length (50 metres) and had the same bandwidth (cable type CT100) as that in the telescope. The signal processing electronics were also located in an adjacent room for monitoring purposes. An oscilloscope (LeCroy Model 9350A) and scaler unit were used to investigate the size and shape of the signal pulses and to monitor the background noise rate.

#### 4.3.1.1 Mirror Characteristics

The flux collectors contribute to the determination of the energy threshold of a telescope and the quality of the Cherenkov light image; factors involved are size, shape and surface condition.

The size of the mirror area can be increased to collect more signal light, up to a theoretical maximum of the size of the light pool from the Cherenkov flash on the ground. However, since this is typically  $\sim 10^5 \text{ m}^2$ , construction limitations provide more reasonable restrictions on mirror area, unless large existing solar concentrators are to be used, such as STACEE (e.g. Ong *et al.*, 1996). Different groups favour different mirror arrangements. Many (e.g. Whipple (Cawley *et al.*, 1990), HEGRA (Kohnle *et al.*, 1996) and early Durham telescopes (Chadwick, 1987)) favour a flux collector comprising a matrix of small spherical mirrors. Recent Durham telescopes have utilised a segmented design, forming a single continuous reflecting parabolic surface in order to minimize the gaps in the reflecting surface and therefore to maximise the light collection in a given area.

The choice of the shape of the light collector is a compromise between minimizing aberrations (maintaining image quality) and minimizing the temporal spread of the signal. The former is achieved by using, for example, a Davis-Cotton design (Carter, 1990). Temporal spreading of a signal is reduced by the use of a parabolic mirror. The energy threshold is dictated by the ability to concentrate light over a small area (good optics) in a short time (isochronous collection).

Size and shape are defined during construction and remain constant throughout the lifetime of the telescope. The form of the mirror is influential in determining the light collection efficiency of the telescope. Deviations from a parabolic form will cause an image to be blurred. This is demonstrated in the blur spot measurements shown in figure 4.4. These are images of stars, point sources, in the focal plane of the central flux collector, recorded using a CCD camera. The left hand image shows the blur spot as measured at the time of construction (from Dickinson, 1995). On the right is the image as recorded in September 1996, just over 2 years later. In both cases, the blur spot is seen to be  $0.18^\circ$  (RMS) wide. A recent (May 1997) measurement made using a solid state photodiode produced an RMS width value of the blur spot of  $0.15^\circ$ . The constancy indicates that the surface quality of the mirror has remained unchanged over three years since construction.

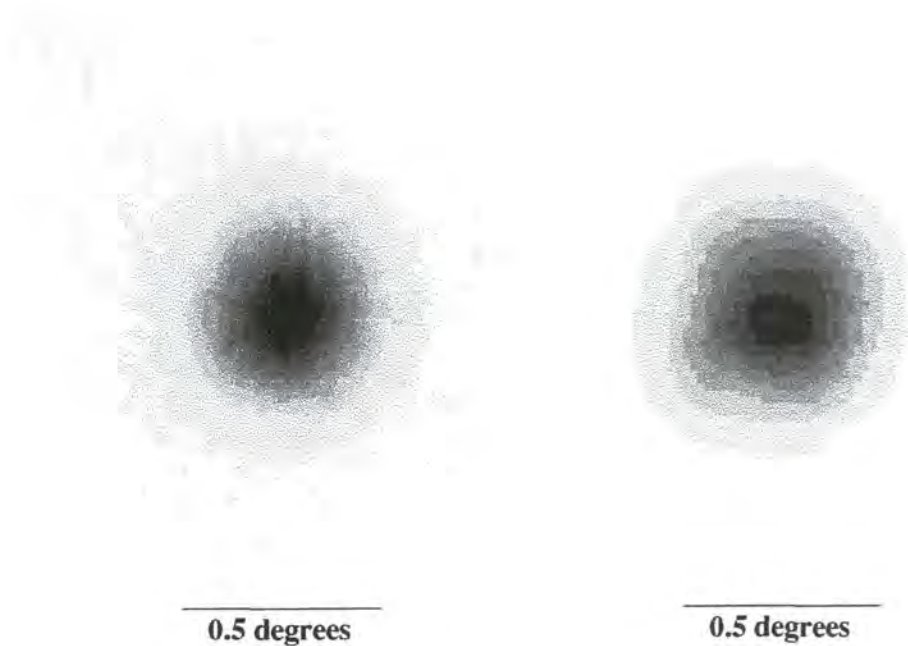


*Figure 4.4 Representations of images of stars formed in the focal plane of the central flux collector of the Mark 6 telescope (left) at construction in August 1994 (from Dickinson, 1995) and (right) in September 1996. Each image is background subtracted and shown in greyscale. The half maximum is the boundary between the fourth and fifth grey shades.*

The reflectivity of the mirror surface may vary with time due to its exposure to the weather since most atmospheric Cherenkov telescopes are not housed in buildings. However, the same material, anodised aluminium, had been used during the construction of mirrors for the Mark 3 telescope in 1985. The constant reflectivity of the mirrors on this telescope over a period of >10 years indicates that the surface quality does not degrade significantly with time. There is therefore no need for re-aluminising mirrors manufactured in this way.

#### *4.3.1.2 Telescope Pointing Accuracy*

The attitude of the telescope mount is measured directly by two shaft encoders, which return positional values to 14-bit accuracy over a 360° range, accurate to 0.02°. This pointing measurement is absolutely calibrated off-line by using data from a paraxially mounted CCD camera, as discussed in section 3.3.5. With this correction it is possible to calculate the telescope's absolute attitude in azimuth and zenith to within 0.02°. Whilst the attitude of the mount may be well measured, the location of the prime focus detectors may alter, e.g. due to gravitational bending. This effect may be different at different zenith angles.

Measurements have been made of the position of the optic axis of the telescope (defined by the centre of the imaging camera) by using a paraxially mounted CCD sky camera and the light measured using a stopped down central PM tube. The detector package is seen to move relative to the mirror system as the zenith angle of the telescope changes. Values of this small offset (in x and y directions) have been measured and are used to correct the attitude measurements of the telescope. The offset in the x-direction is constant for all zenith angles. In the y-direction, a second order relationship exists; the offset is seen to change at a rate of  $3 \times 10^{-3}$  degrees per degree change in zenith angle.

The effects of the successful treatment of small errors in source position measurements are best demonstrated by a false source analysis. This is a process in which the excess (ON - OFF) number of events having a small value of  $\alpha$  ( $< 30^\circ$ ) relative to each point in a matrix around the purported source location. The results from such an analysis can be represented graphically, by showing the significance of the excess corresponding to each position in the matrix, as shown in figure 4.5. This plot was produced from data taken during observations of PSR 1706-44 during May and July 1996. This shows that the most significant number of small  $\alpha$  events (prime gamma ray candidates) corresponds to the source being at the centre of the field of view, where the signal is significant at the  $6\sigma$  level. The significance reduces to  $\sim 3\sigma$  at a distance of  $\sim 0.2^\circ$  away from the source direction.

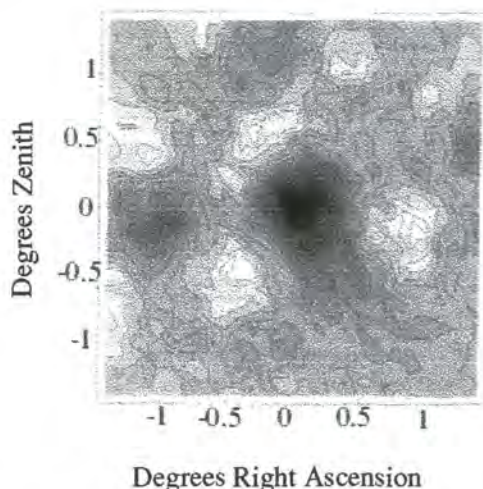


*Figure 4.5 Results of a false source analysis performed on data taken on PSR 1706-44. The colour scheme denotes the significance of the excess signal after background rejection cuts, including an  $\alpha < 30^\circ$  cut, had been applied, for a source at that location. The putative source is located at the origin, corresponding to the most significant signal.*

#### *4.3.1.3 Electronics Stability*

Electronic components are susceptible to variations in operating conditions due to fluctuations in supply voltages, temperature changes etc. Electronic circuitry may contribute to changes in its own environment when resistive heating is significant.

In attempts to minimize these effects, the signal processing electronics are switched on up to two hours prior to the start of an observation. This means that any changes in temperature due to resistive heating effects have levelled out by the time the observation starts. Further changes in the ambient temperature within the control room are minimized by the use of a thermostatically controlled air conditioning system.

The processing electronics are powered from stabilised DC supplies, operated, in turn, off regulated AC supplies, to ensure that voltage variations are kept within small tolerances.

The signal processing electronics connected to each photomultiplier may limit the performance of the system if the PM tube has a higher bandwidth than the electronics. According to manufacturer's specifications, the LeCroy 10× amplifier only maintains linearity up to input voltages of 500 mV with a bandwidth of 200MHz (LeCroy 612A amplifier). Deviations from linear operation by the amplifier would have the same result as changes in the gain of the PM tube. The result would be a non-uniform response to light across the surface of the imaging camera.

In order to test this, a Philips XP3422 PM tube was exposed to a light flash produced using a laser/scintillator light source. The amount of light to which the PM tube was exposed was progressively increased. The amplitude of the output signal pulse from the PM tube was measured pre- and post-amplifier. The results are shown in figure 4.6, with the raw signal scaled by a factor of 10 for comparison. It is seen that the amplifier does not produce linear amplification for input pulses greater than  $400 \pm 30$  mV.

Figure 4.7 shows pulse shapes for two amplified pulses. The first shows the amplifier operating within limits, while the second shows the effects of saturation of the system. The pulse broadens in time as a result of conservation of charge, as the maximum output voltage has been reached. This means that there is no reduction in pulse area.

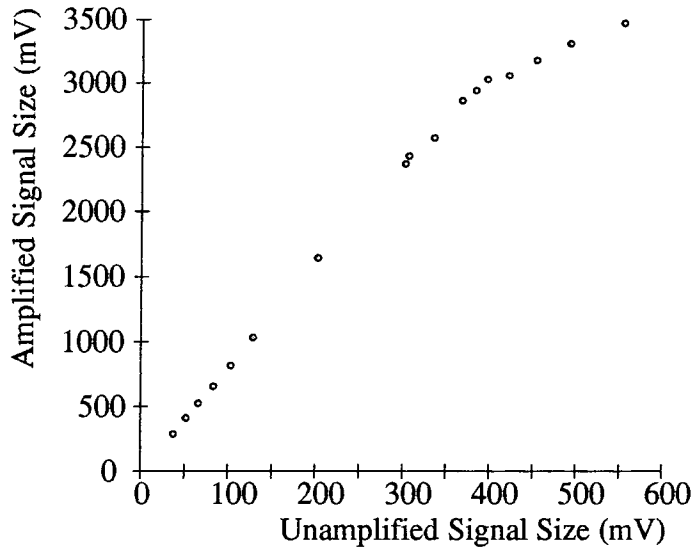
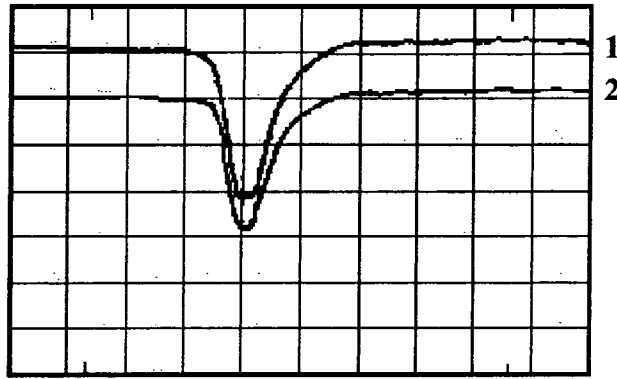


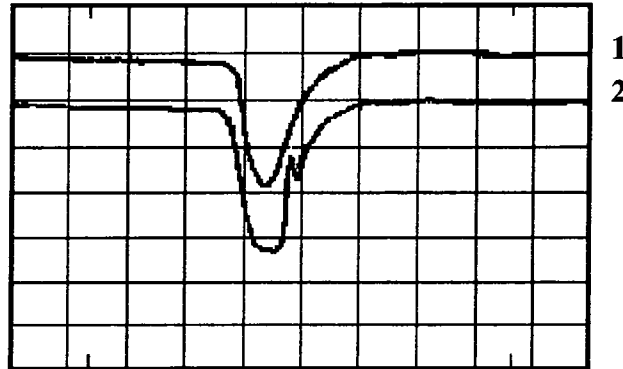
*Figure 4.6 Amplifier Output Voltage as a function of Input Voltage showing limit of linear operating range. The amplifier operates reliably at input voltages below ~400 mV. This is not a limitation on the operation of the PM tubes under normal circumstances.*

#### 4.3.1.4 Variation in Laser Calibration

The calibration systems used on the telescope are subject to the same variations in operating environment as the instrument itself. As such, an understanding of the stability of the calibration systems is important to give credibility to the results they provide. Laser flashes are generated automatically throughout all observing runs, triggering the telescope and are recorded in the datastream of genuine events. It is assumed that the average amount of light generated in the scintillator is constant during an observation and that variations observed in the recorded laser events indicate systematic changes in the operation of the PM tubes/electronics. To test this hypothesis, the laser was set up adjacent to the dark laboratory and the scintillator light transmitted via fibre-optic into the dark room. Investigations were carried out to investigate any variation in laser/scintillator performance. A Hamamatsu R1924 PM tube, under near constant environmental conditions was used to monitor laser output.



Amplitude (1)    580mV  
 Amplitude (2)    680mV



Amplitude (1)    5.46V  
 Amplitude (2)    6.2V

*Figure 4.7 Measurements of PM tube output pulse size as recorded on an oscilloscope (top) before and (bottom) after x10 amplification in a LeCroy amplifying unit. The pre-amplified signal is scaled by the oscilloscope for comparative purposes. The deformation of the amplified trace compared to the sharp preamplifier signal shows that the LeCroy amplifier has a lower maximum useful operating level than the PM tube to which it is connected. The trace 2 baseline is offset from that for trace 1.*

Figure 4.8 shows the amplitude of the laser pulse as a function of time since switch on under conditions of constant temperature. This suggests a rapid increase in pulse size of ~10% during a 'warm-up' period of approximately 30-40 minutes, which is longer if no external heat source is provided. The heat source used to obtain the second series is a high power dissipation resistor mounted in the laser box on the telescope.

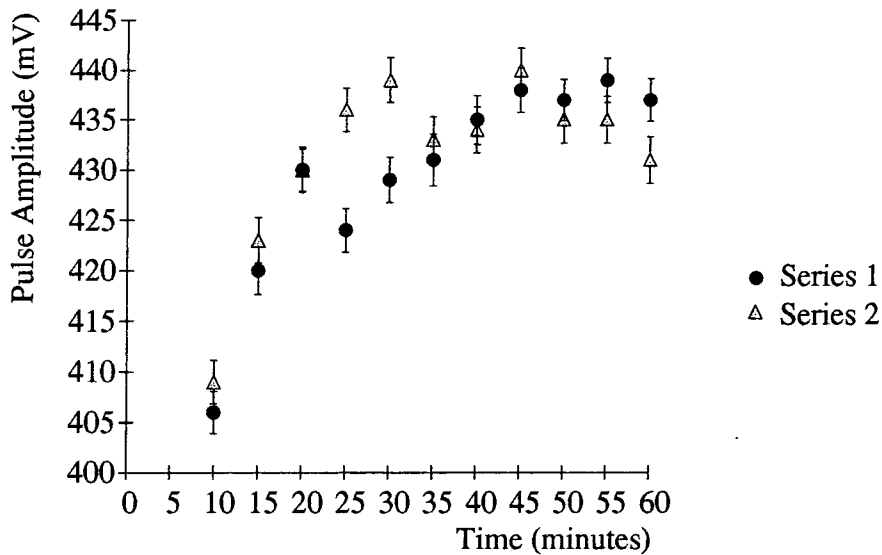


Figure 4.8 Laser output size increases with time for approximately 1 hour after switch on. Pulse size is measured using a PM tube allowed to stabilize prior to the experiment. Series 1 was recorded while the laser was heated only by internal effects. For series 2, an external source of heat was located in the laser box.

#### 4.3.2 Photomultiplier Tube Performance

The principles of operation of a PM tube and the operating characteristics of the types of tube used in the detector packages of the Mark 6 telescope are described in chapter 3.

During telescope operation, PM tube operating conditions are defined by the singlefold noise rate, the rate of noise pulses from individual tubes (greater than a fixed discrimination level after amplification), together with the anode current which, under constant illumination, is a measure of the gain. PM tubes are used in atmospheric Cherenkov telescopes under conditions of high illumination due to the sky. This is not the type of environment for which they are intended, as most applications require that PM tubes operate in near total darkness, so tube behaviour must be monitored closely.

Two types of PM tube were initially used in the Mark 6 telescope; Hamamatsu R1924 25 mm diameter circular tubes in the imaging camera and Burle 8575 50 mm diameter circular tubes in the guard ring of the camera and the triggering detectors. The PM tubes in the triggering detectors have subsequently been replaced by Philips XP3422 55 mm hexagonal-shaped tubes. The motivation for this change is discussed in chapter 5.

Quantum efficiency and spectral sensitivity are combined to define the overall sensitivity of the PM tube to incident light. Both are functions of the wavelength of the light and are well defined by the manufacturer for new tubes. Spectral sensitivities for the tubes used in the Mark 6 telescope are shown in figure 4.9. The similarity between the curves for the two tubes is due to the use of tubes with the same bialkali photocathode material. It is important that the sensitivity curve matches the Cherenkov spectrum in order to maximise detection efficiency and the choice of tube is made to ensure the closest match. The Cherenkov spectrum peaks in intensity at around 300 nm and reduces as  $\lambda^{-2}$ . However, the photosensitive material used in the photocathode may degrade over time, with exposure to adverse conditions, including bright light. As a result, it is expected that the sensitivity of PM tubes may deteriorate slowly over a period of years.

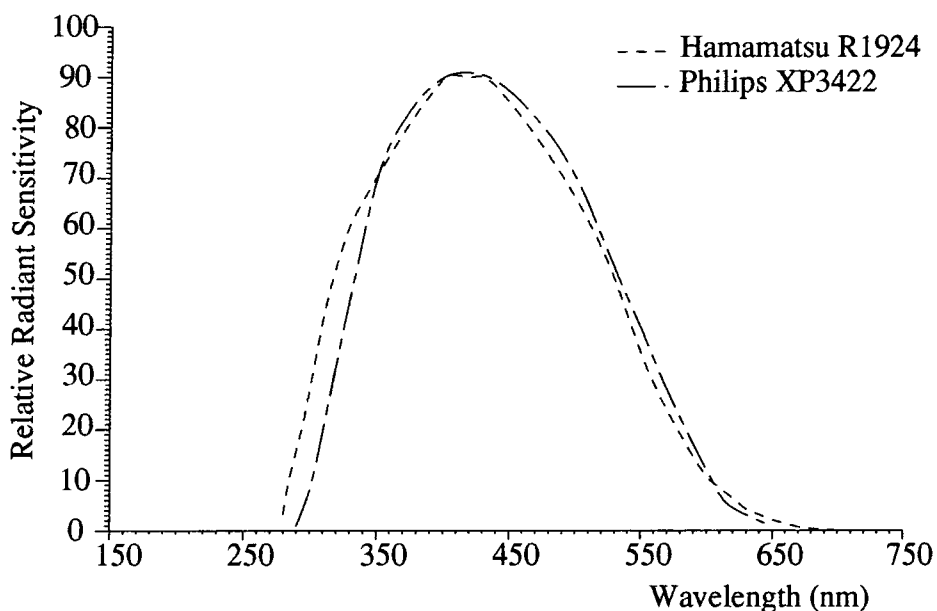


*Figure 4.9 The PM tubes used in the Mark 6 telescope are maximally sensitive in the 350-500 nm range. This is a function of the materials comprising the photocathode and tube windows. The Cherenkov spectrum peaks in intensity around 300 nm. The PM tubes used are chosen to maximise sensitivity to this region. They are not sensitive to light at the red ( $\lambda = 500-700$  nm) end of the visible spectrum.*

Direct measurements of the quantum efficiency and spectral sensitivity are not vital to understanding the operation of the PM tubes *in situ* in the telescope. It is sufficient to have some understanding of the overall response of the tube to incident light. In particular, it is important to know how the gain and time response

of the tube changes for light falling at all positions on the photocathode. This is particularly important for the XP3422 tubes which have comparatively large hexagonal shaped photocathodes, with significant scope for variation in response.

#### *4.3.2.1 Performance Variations across the Photocathode of an XP3422 PM tube*

With the tube operating under typical conditions of noise and anode current, the 24 cm<sup>2</sup> photocathode of the XP3422 hexagonal PM tube was masked down so that only 1 cm<sup>2</sup> was exposed at any time. The tube was illuminated by the background light LED for the typical Narrabri level and the flashes from the laser/scintillator. The oscilloscope was configured at a trigger level such that it recorded >95% of laser pulses and <1% of the recorded pulses were due to noise background (i.e. non-laser induced). Pulse amplitude was measured as a function of the location of the exposed part of the photocathode. The results demonstrate radial symmetry about the photomultiplier axis and are shown in figure 4.10. This figure clearly shows that sensitivity/gain is reduced at the edge of the photocathode, by as much as 50% compared to the centre; the sensitivity decrease with distance from the central axis is approximately quadratic in form. The fit shown is obtained from the following expression for amplitude ( $A$ ) as a function of distance from the central axis of the PM tube ( $r$ )

$$A = 118 - 0.045r^2$$

with amplitude measured in mV and radial distance in mm.

The transit time of the XP3422 PM tube was determined using a similar system. In addition, a Hamamatsu R1924 25 mm diameter tube was exposed to the same light pulses and used to provide a time reference, against which the change in transit time of the hexagonal tube for light incident on different parts of the photocathode area could be measured. Although the transit time of the XP3422 PM tube cannot be measured directly by this method, it can be inferred by using the manufacturer's specification for the 25 mm tube and measuring the difference between the pulse arrival times for the 2 tubes. More importantly, any variations in propagation times across the photocathode surface of the XP3422 tube are immediately obvious. The time delay represents the difference between the amplitude peak of the signal from the R1924 and the peak for the XP3422 and is ~12 ns when the total photocathode is illuminated. Figure 4.11 shows the variation in transit time as a function of position of the exposed part of the hexagonal photocathode, when a 1 cm<sup>2</sup> area is exposed. The variation in transit time between the centre and the edge of the

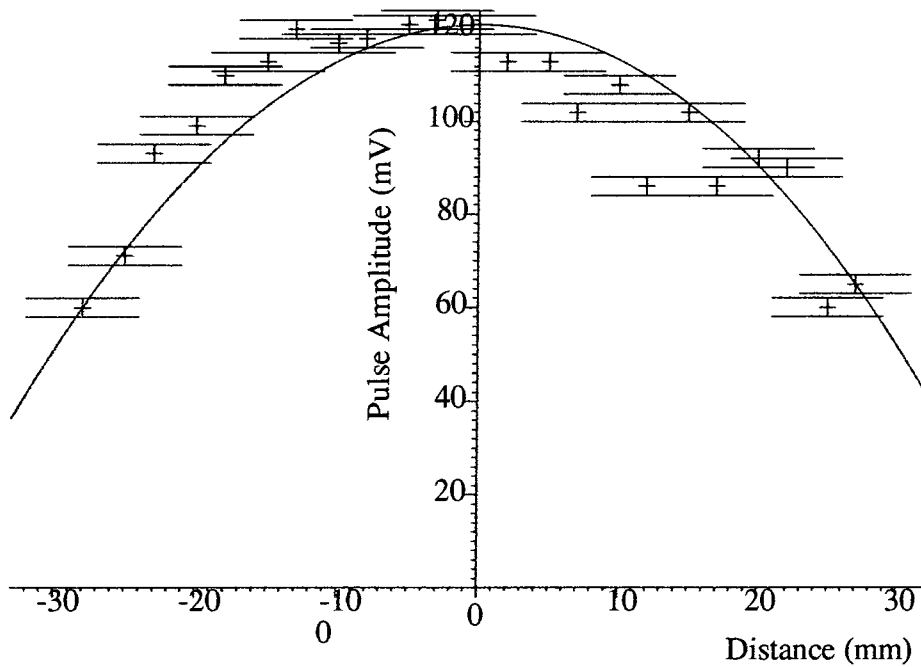


Figure 4.10 Output pulse amplitude measured in response to a standard input light pulse as measured across one axis of the photocathode of a Philips XP3422-SG4 PM tube. A quadratic fit to the data is also shown.

photocathode contributes to an increase in pulse rise time ( $t_{10-90\%}$ ); this is measured as  $8.0 \pm 1.0$  ns when the whole photocathode is exposed and is reduced to  $6.0 \pm 1.0$  ns when only the central  $1 \text{ cm}^2$  of the photocathode is exposed. The minimum time difference between the signals from the two tubes is  $\sim 12$  ns and increases approximately quadratically with distance from the tube axis. The difference is  $\sim 9$  ns between the transit times at the axis and edge of the XP3422 PM tube. The fit is represented by the following expression

$$t = 11.8 + 0.035r^2$$

where  $r$  is the distance from the central axis in mm and  $t$  is the transit time in ns.

This degradation in time response has an undesirable effect on the performance of the triggering system which employs XP3422 PM tubes. The total amount of light (and hence charge from the PM tube) is proportional to the energy of the gamma-ray. The peak amplitude, which governs the triggering probability based on voltage discrimination, depends upon the temporal performance of the PM tube. Peak amplitude is reduced if the tube response causes the pulse to be spread over a longer period of time. The lowest energy threshold is attained for fast response PM tubes which produce pulses of optimal amplitude for a given signal size.

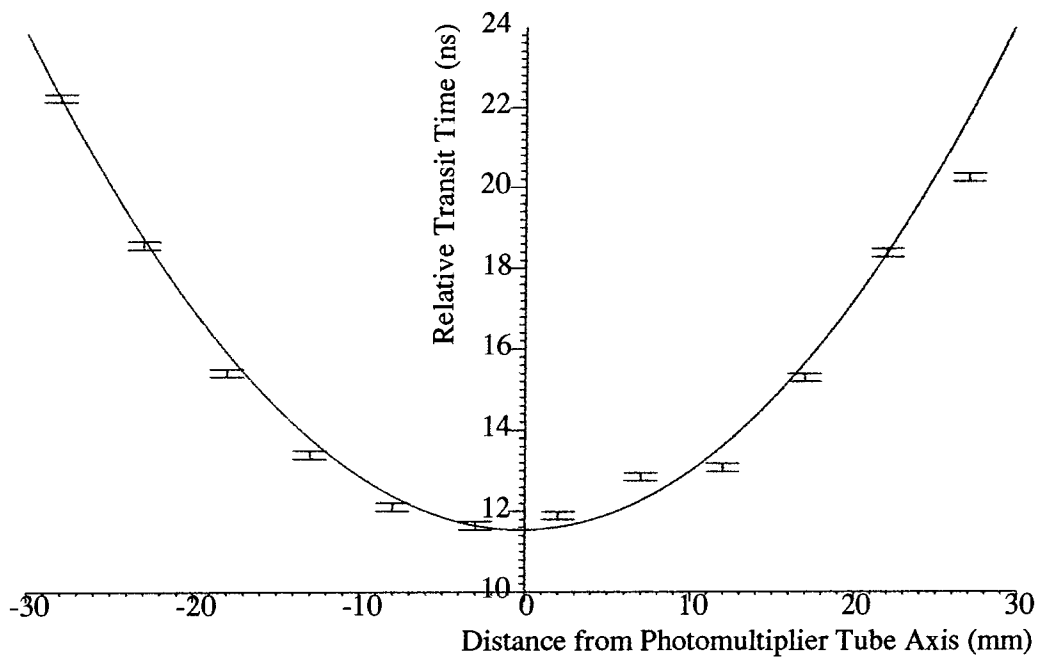


*Figure 4.11 Transit time of a Philips XP3422-SG4 PM tube measured for light incident on different parts of the photocathode. Time is measured relative to a Hamamatsu R1924 PM tube triggered from the same light flash.*

The value of the anode current defines the limitations on the operating conditions of a PM tube when installed in the telescope. PM tubes are not, in general, designed to be exposed to the background illuminations seen in Cherenkov telescope observations for extended periods of time. The maximum anode current specified by the manufacturer must not be exceeded; as a safety factor, a limit ~25% of this is applied. For continual operation, the R1924 tube is not run at currents exceeding 30  $\mu\text{A}$  and the XP3422 should not exceed 60  $\mu\text{A}$ .

#### 4.3.2.2 Summary

Photomultiplier tubes are selected on the basis of their spectral characteristics compared to the spectrum of Cherenkov light, their noise-gain characteristics and their stability over time when operated under conditions of high illumination. Both the XP3422 and R1924 PM tubes have bi-alkali photocathodes, providing good spectral coverage of Cherenkov light. The XP3422 operates in a high gain, low noise regime suitable for effective use in the trigger detectors. Some temporal and sensitivity variation is seen in the operation of the XP3422 PM tube. The centre of the tube is seen to be both faster in response and more sensitive than the edges to incident light. This is discussed further in chapter 5.

### 4.3.3 Effects of Changes in the Telescope Environment

The telescope operates in an environment in which conditions (e.g. temperature) can vary markedly during the course of a night ( $>10^{\circ}\text{C}$ ) or between nights in different seasons (approximately  $20^{\circ}\text{C}$ ). In this section, the effects of changes in temperature and background illumination, orientation of the telescope relative to the Earth's magnetic field and excitation of PM tubes by exposure to sunlight/ultraviolet light are discussed.

#### 4.3.3.1 Ambient Temperature

Diurnal variations in the temperature at Narrabri can be of the order of  $20^{\circ}\text{C}$ ; in the course of a full night's observation, the temperature may drop by more than  $10^{\circ}\text{C}$ . The effect of this ambient temperature variation on the temperatures of various components is modified by, for example, resistive heating in the laser system, PM tube system and electronics. This means that temperature variations can be different in different components of the telescope.

Laboratory measurements were made to investigate the effects of ambient temperature changes on the performance of the PM tubes and laser calibration system. The laboratory used was underground and had a thick (0.5 m) concrete roof, was insulated from outside climate changes and did not quickly lose heat energy. Thermostatically controlled heaters allow the temperature of the room to be set between  $\sim 12^{\circ}\text{C}$  and  $30^{\circ}\text{C}$ ; the use of small portable heaters allowed higher localised temperatures to be provided. Temperatures were measured using 16 thermistors placed around the room and attached to the elements being tested.

The effect of variations in ambient temperature on PM tube performance was investigated for XP3422 and R1924 tubes. Each tube was exposed to the light flash from a pulser, consisting of a source of alpha radiation ( $^{241}\text{Am}$ ) distributed through a scintillator. This pulser is specified by the manufacturer to provide some 700 disintegrations per second, each of  $\sim 300$  photons. It has been measured to produce  $\sim 70$  pe per pulse.

An R1924 PM tube and the associated electronics were switched on prior to the measurements in order to allow them to stabilise. The environment of the PM tube was heated and gain (measured as the total charge of the  $^{241}\text{Am}$  pulse signal) and temperature recorded as functions of time. When the upper temperature limit was reached, the heaters were switched off and the environment allowed to cool. Measurements continued throughout this period. The experiment was repeated for

the XP3422 PM tube. Figure 4.12 shows the variations in pulse amplitude with temperature for both tubes.

These results suggest that the change of gain of the R1924 camera PM tubes with temperature is of the order of  $-(0.5 \pm 0.25)\%/^{\circ}\text{C}$ . This is consistent with the manufacturer's specification for light of wavelength 300-400 nm as shown in figure 4.13 (from Hamamatsu data sheet). The XP3422 tube shows a more significant variation, with a temperature coefficient of gain change of  $-(1.0 \pm 0.5)\%/^{\circ}\text{C}$ .

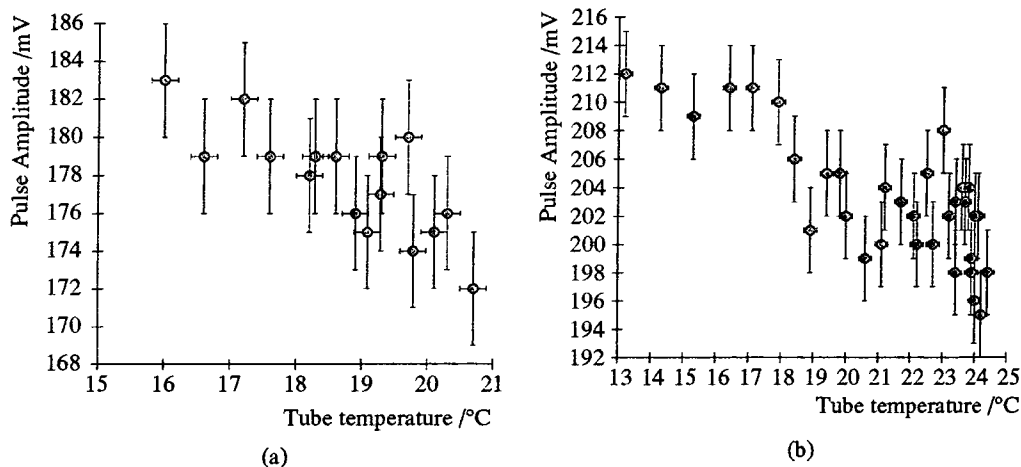


*Figure 4.12 Variation in measured output pulse amplitude with ambient operating temperature for (a) a hexagonal Philips XP3422-SG4 PM tube and (b) a Hamamatsu R1924 circular PM tube. Input pulses of constant amplitude were produced by a laser/scintillator arrangement.*

The effect of variations in the ambient operating temperature of the laser have also been investigated. An R1924 PM tube, chosen for its relative stability, was used to monitor laser pulse size. The tube was exposed to the flashes induced in the scintillator by the laser. Two measurements were made; with heating due only to the operation of the laser itself and with external heating supplied. In both cases, the PM tube and electronics ambient temperatures varied by  $<2^{\circ}\text{C}$  during the experiment. The results, shown in figure 4.14, suggest that there may be a small negative correlation between temperature and pulse amplitude, of the order of  $<1\%/^{\circ}\text{C}$  under typical operating conditions. However, there is also evidence that at high operating temperatures, the temperature coefficient becomes greater. Figure 4.14b shows that a change of the order of  $2.5\%/^{\circ}\text{C}$  may occur at temperatures above  $\sim 27^{\circ}\text{C}$ .

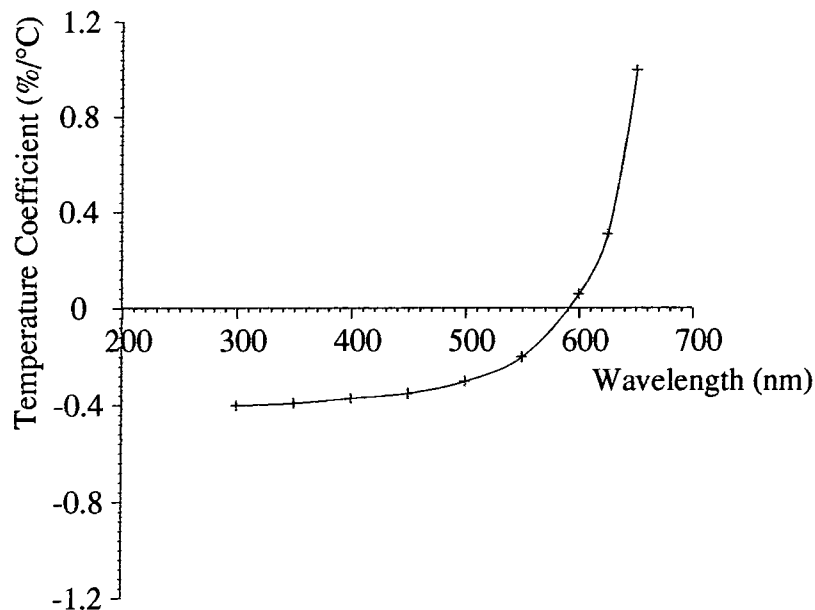
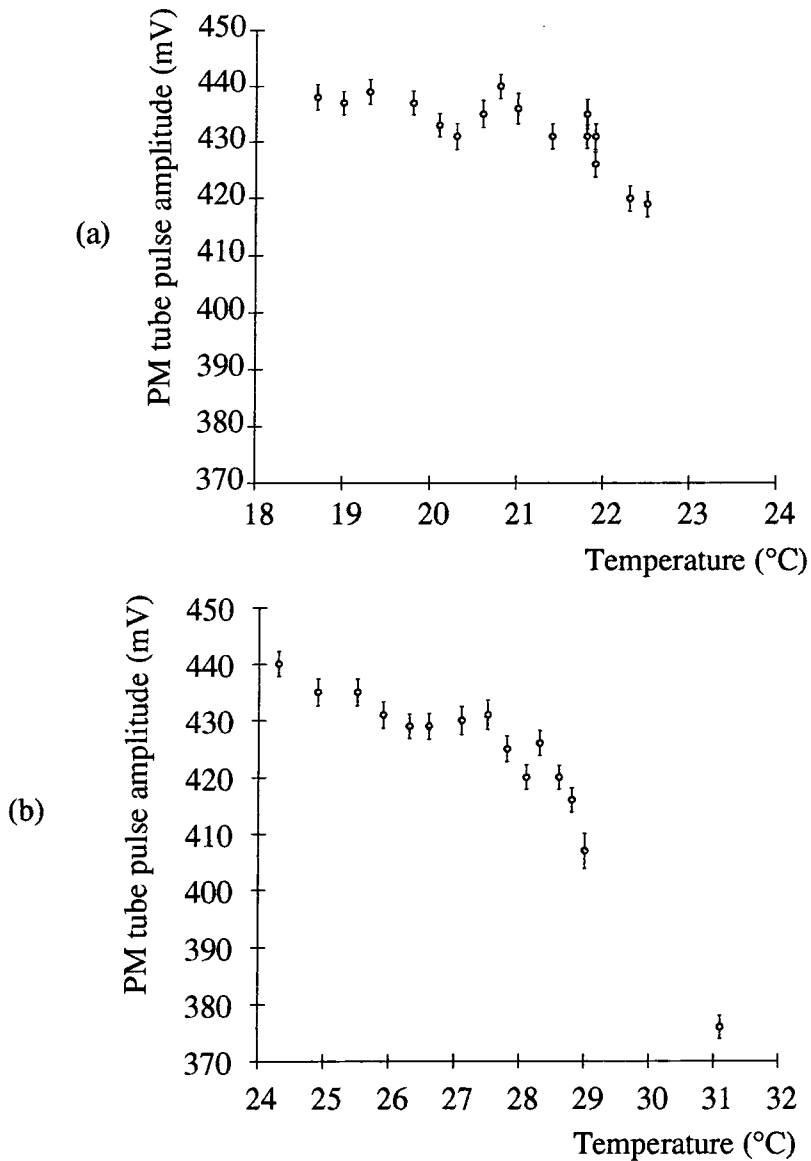


Figure 4.13 Typical Temperature Coefficient of Anode Sensitivity for Hamamatsu R1924 PM tube (from Hamamatsu data sheet).

#### 4.3.3.2 Background Illumination

The amount of background light falling on the PM tubes is the limiting factor in telescope operation as it causes a steady level of illumination which dominates the anode current and noise produced in the PM tubes.

Background illumination originates from a number of distinct sources. Albedo is the component of light reflected back off the ground and surroundings onto the photomultipliers. It is a significant source of light, particularly when the telescope is operating close to the zenith. Zodiacal light is produced by backscattering of light near to the ecliptic around dawn and dusk. It is only a problem when using the telescope at very large zenith angles and will not be discussed further here. Reflected stray/starlight, caused by stars lying within the field of view of the telescope, is an important consideration for some sources; candidate sources lying in the galactic plane will often be situated in fields which contain a number of stars which contribute to the background illumination. In some cases, such as the starfield of PSR1706-44, a single bright star, which is bright enough ( $\epsilon$ -Sco,  $m_v \sim 3.3$ ) to register in a PM tube, is involved. This has the effect of significantly increasing the anode current and noise produced in one channel of the camera at a time. The change in PM tube gain which may result would cause this tube to behave significantly differently to its neighbours.



*Figure 4.14 Measurement of laser pulse size for various ambient temperatures of the laser environment. The first plot (a) shows the laser heating only due to internal effects. For the second dataset (b), a source of heat was introduced to the laser box. Measurements were made using a Hamamatsu R1924 PM tube. In both cases, data from an initial 45 minute 'warm up' period have been omitted.*

Background light is more spectrally diffuse than that produced by Cherenkov radiation; it is redder than Cherenkov light (Mirzoyan and Lorenz, 1994). Little can be done to avoid background starlight from the field containing the potential source. The possibility of using wavelength shifting filters to increase the sensitivity of the PM tube at low wavelengths (Bradbury *et al.*, 1995) has been rejected as has the possibility of using filters to reject light of wavelengths at which the Cherenkov contribution is low (due to problems with identifying a suitable

filter which did not also significantly reduce the blue light and which can be satisfactorily bonded to the surfaces of the PM tubes).

Under comparable illumination, the Philips PM tube typically operates at lower noise rates than the older Burle 8575 PM tubes, as discussed in the next chapter. The Philips XP3422 PM tubes are typically operated at around 10-15 kHz noise rate, while the R1924 tubes usually operate at noise rates up to 1 MHz, in order to satisfy the maximum acceptable accidental coincidence rate.

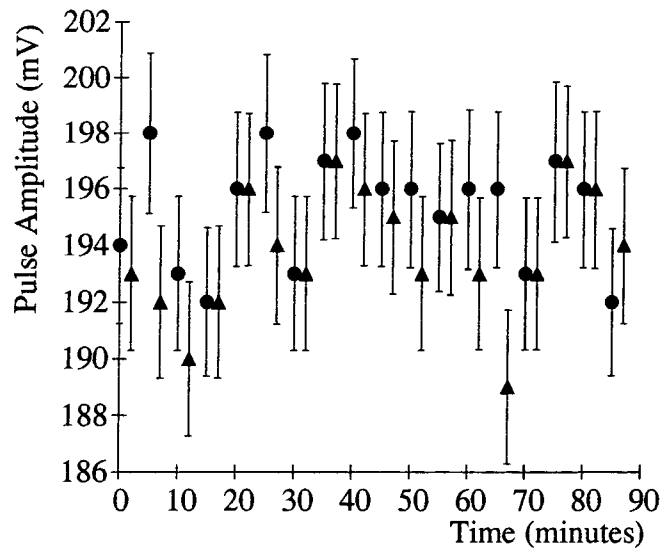
#### *4.3.3.3 Photomultiplier Tube Orientation Relative to the Earth's Magnetic Field*

There are at least two consequences for the operation of a telescope at different orientations to the geomagnetic field. The development of the  $e^{+/-}$  cascade in the atmosphere in a direction perpendicular to the field will become elliptical rather than circular in shape. At the same time, the gain of the PM tube may alter as the effect of the geomagnetic field on the electron cascading/focussing sections of the PM tube changes.

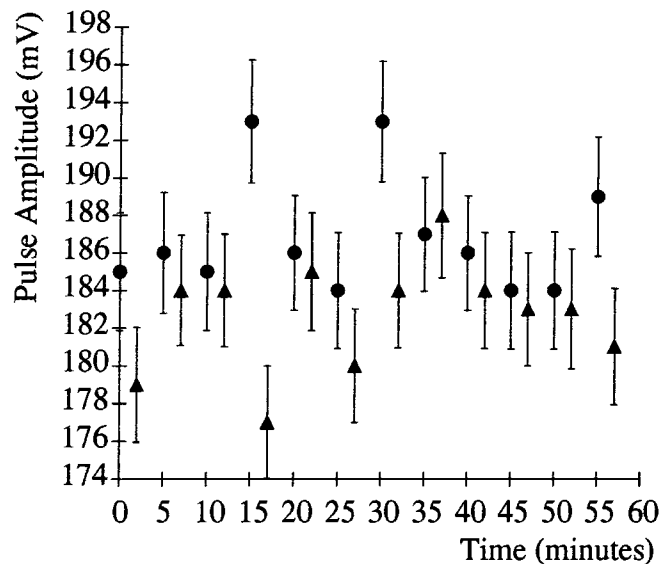
The effects of the terrestrial magnetic field on the cascade development and its consequences for the imaging capabilities of ground based gamma-ray telescopes have been discussed previously (Bowden *et al.*, 1992b, Lang *et al.*, 1994).

Magnetic fields may affect the focussing of electrons onto the top of the dynode chain or the passage of electrons through the chain itself. Furthermore, as the telescope tracks through an observation, the angle between PM tube axis and the magnetic field will change. The PM tubes used in the telescope have mumetal shields around the region in which the electrons are accelerated from the photocathode. This reduces the terrestrial magnetic field penetrating the tubes.

In order to test the effects of the geomagnetic field on the performance of individual tubes, an unshielded PM tube was exposed to the flash from the radioactive pulser in the dark laboratory. The dip angle, the angle between the magnetic field and the surface of the Earth, at Durham is approximately  $60^\circ$  from the horizontal, pointing downwards towards the north. Repeated measurements of signal amplitude from the pulser were taken with the tube axis aligned perpendicular and parallel to the direction of the dip angle. Results are shown for both R1924 and XP3422 PM tubes in figure 4.15.



(a) Hamamatsu R1924 25 mm PM tube



(b) Philips XP3422-SG4 56mm PM tube

*Figure 4.15 Effect of orientation of PM tube axis relative to the geomagnetic field on PM tube gain. After a 'warm-up' period, sets of measurements were made with the tube axis aligned parallel to the geomagnetic field lines (circle) and perpendicular to the field (triangle).*

No significant variation is seen in the data from the (physically smaller) R1924 PM tube. The XP3422 however, appears to show a reduction of approximately 1% in gain when the PM tube axis is perpendicular to the geomagnetic field. The magnitude of this effect is of the order of the experimental error. It is possible that the larger XP3422 PM tube is more significantly affected by deflections of electrons caused by a magnetic field than the smaller PM tube.

The experiment was repeated with a mumetal shield applied to the XP3422 tube covering the accelerating region between the photocathode and the top of the dynode chain. The shield, which is fitted to all PM tubes on the telescope, reduces the strength of the Earth's magnetic field passing through the PM tube. Figure 4.16 shows that there is no detectable difference between measurements made with the tube parallel and perpendicular to the magnetic field when the mumetal shield is in place.

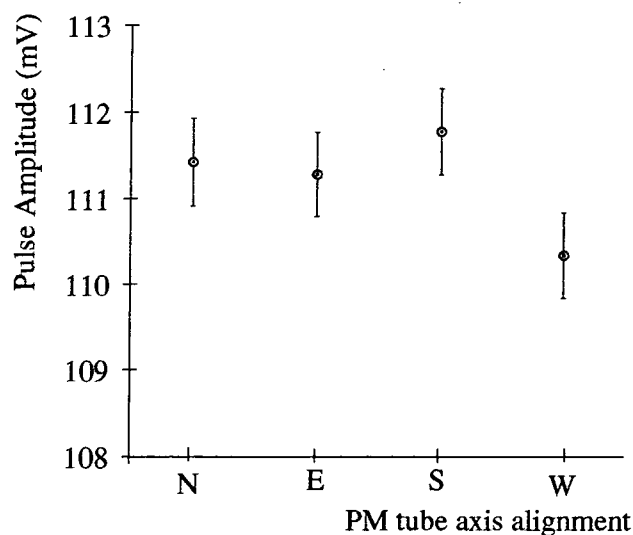


*Figure 4.16 The effect of changing the orientation of the axis of a PM tube relative to the geomagnetic field when surrounded by a mumetal shield. The experiment was carried out in Durham. The tube axis is parallel to the geomagnetic field when pointing to the north and approximately perpendicular to the field when pointing in all other directions. The tube was inclined at  $45^\circ$  to the horizontal for all measurements.*

The conclusion of this work is that any observed effects in telescope performance correlated with the geomagnetic field arise from the interaction between the field and the electromagnetic cascade and not from changes in the performance of the mumetal shielded PM tubes. A discussion on the effect of this interaction on the interpretation of data recorded with the telescope can be found in Armstrong *et al.* (1998).

#### 4.3.4 Sky Clarity

Changes in the clarity of the atmosphere are of utmost importance in determining the quality of the data recorded, although they have not previously been studied thoroughly. They cause changes in the signal (the Cherenkov light from the

cascade shower) and background (sky background induced noise). This can result in reductions in the amount of data recorded and can also reduce the efficiency of background rejection measures.

#### 4.4 Systems for Monitoring Telescope Performance and Environment

The operation of the telescope is extensively monitored. Many aspects of the performance of the telescope and its components are constantly recorded and are available to the operator in real time, as described in section 3.3. Trend monitoring is particularly important, to provide advance warning of changes in the operating conditions. Environmental data and sky clarity measurements are recorded separately and are also displayed in the control room via a video link.

##### 4.4.1 Telescope Performance Parameters

Experience has shown that it is prudent to monitor anode currents and singlefold noise rates for each PM tube. Steady readings for these parameters show that the photomultipliers and electronics are operating satisfactorily. Measurements of the threefold count rates for all 19 individual triggering channels provide an additional check on the operation of the coincidence electronics. Measurement of the total count rate of the telescope provides an overall indication of satisfactory performance of the detectors and stability of the atmospheric radiator.

These performance indicators are displayed and are recorded on a regular basis into a timestamped 'housekeeping' file which can be cross-referenced with the data files. The monitoring system has been outlined in chapter 3.

##### 4.4.2 Monitoring the Telescope Environment

Three components of the telescope have been identified as susceptible to variations in ambient temperatures. These are the photomultipliers, electronics and the laser calibration system. A number of thermistors are situated throughout the telescope, on the mirrors, in the PM tube detector packages, in the calibration laser mounting box and in the telescope control room in order to measure temperature variations.

Figure 4.17 shows the temperature variation recorded in a PM tube package by thermistors mounted at various positions in the central detector package. The large increase in temperature, up to 30°C at the centre of the detector, is caused by resistive heating effects in the dynode chain components. The effect is less at the edge of the detector due to the dissipation of heat energy through the casing into the atmosphere.

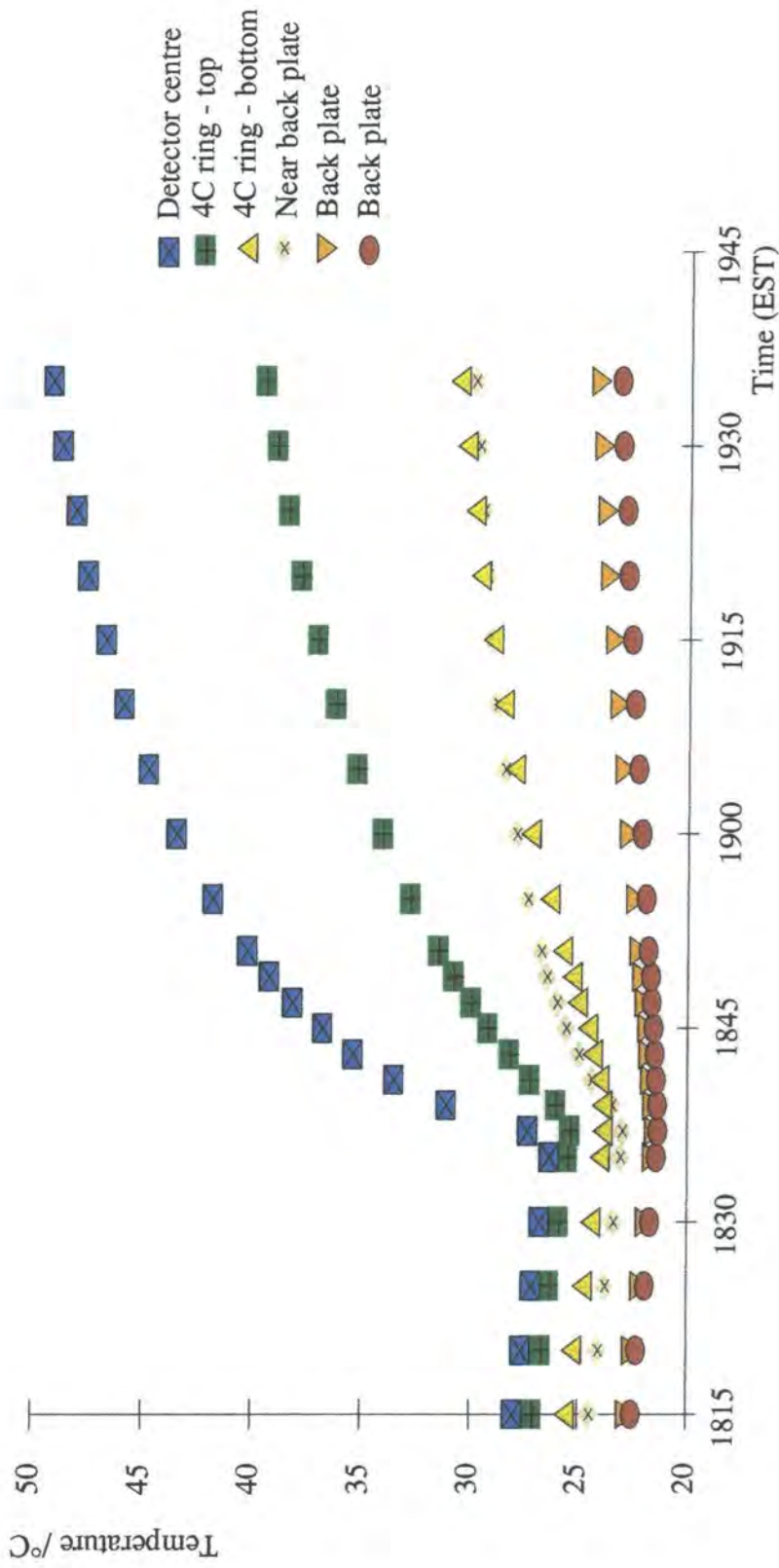
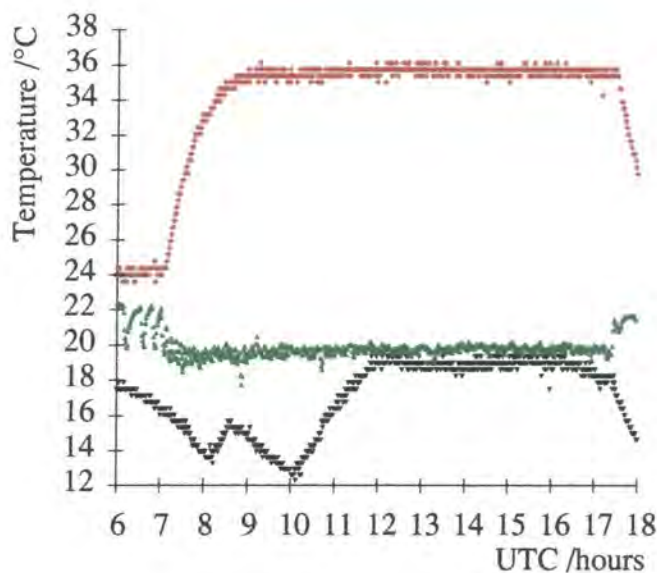


Figure 4.17 Temperature variations at various positions in PM tube detector package measured on May 9th, 1997.

Such a large temperature change could have severe implications for the gains of the PM tubes, resulting in potential changes of up to 30% in the gain of individual PM tubes, measured in terms of charge output per unit incident light, as discussed in section 4.3.3.1. We therefore prewarm the detector packages and maintain the high temperature by thermostatic control.

The laser operating temperature and temperatures within the logging electronics are also monitored and typical results are shown in figure 4.18. The temperature coefficient of the laser output requires that action be taken to minimize the variations seen here. The temperatures within the electronics suite remain stable following the prewarming and the thermostatic control of the ambient temperature in the control room.



*Figure 4.18 Temperatures as measured in the Amplifier electronics (red), EHT supplies (green) and laser box (black) during an observation on May 10th, 1997. The electronics were switched on at 0700UTC and the EHT supply to the tubes and laser at 1000UTC. The run ended at 1700UTC.*

In addition, ambient air and mirror temperatures are recorded, together with pressure, humidity, instantaneous and recent high values of windspeed and wind direction.

Figure 4.19 shows the temperature recorded at the mirror surface and the ambient air temperature, during a night in a winter month. The mirror temperature is seen to be a few degrees lower than the air temperature, due to thermal coupling of the mirror to the cold sky. The difference remains essentially constant throughout the night. When mirror temperature drops below the dew point, defined by air

temperature and humidity, condensation forms on the mirror. This process, misting, causes a dramatic reduction in the telescope count rate and the successful precautions taken to prevent it are discussed in chapter 5. Measurement of air temperature provides an indication of the onset of mirror freezing. A long term development task is to reduce the data loss due to this process, by supplying heat to the mirrors.

Humidity and changes in a long term pressure trend are logged, as they often indicate changes in the weather.

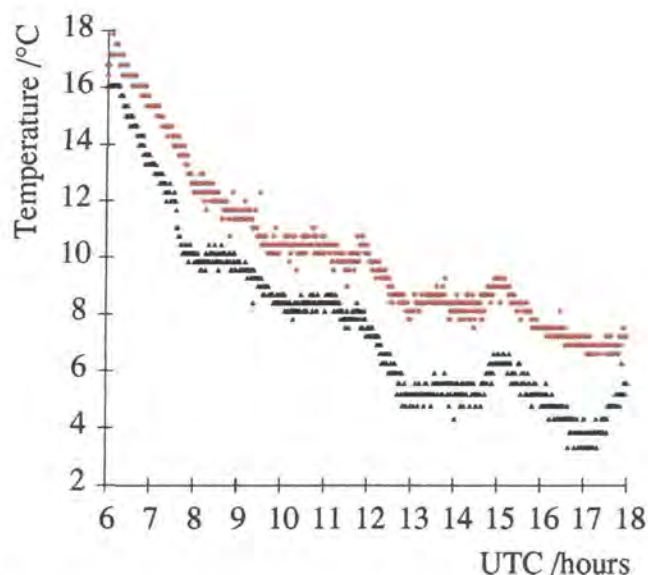


*Figure 4.19 Mirror temperature (black) tracks air temperature (red) through the course of the night of 10<sup>th</sup> May, 1997.*

#### 4.4.3 Sky Clarity

Indications of sky clarity have been provided in part from CCD measurements of the brightness of guide stars and values of the PM tube noise rates and anode currents, averaged over the 2° field of view. However, both of these methods are unsatisfactory, as they rely on having a suitable bright guide star, or using data intrinsic to the experiment. In September 1996, a Heimann KT 17 radiation thermometer (radiometer) was installed on the telescope to provide a direct measurement of sky temperature in the same field of view as the telescope.

The radiometer measures the intensity of radiation in the long-wavelength infrared region of the electromagnetic spectrum ( $\lambda = 8-14\mu\text{m}$ ), to which the atmosphere is transparent. All objects emit radiation in this waveband in the form of heat. The operation of the radiometer is discussed by Roberts (1994). The radiometer has a

field of view similar to the field of the telescope. A clear sky contains very little matter and so radiates little heat. The radiometer response is dominated by the cold sky and measures a temperature ranging from  $-30^{\circ}\text{C}$  in the summer to  $-70^{\circ}\text{C}$  in the winter. Reductions in sky clarity are caused by the presence of obscurants, such as cloud, which radiate energy according to their temperatures. The radiometer has proved capable of detecting changes in clarity invisible to the naked eye which correspond to observed reductions in telescope count rate, as shown in figure 4.20.

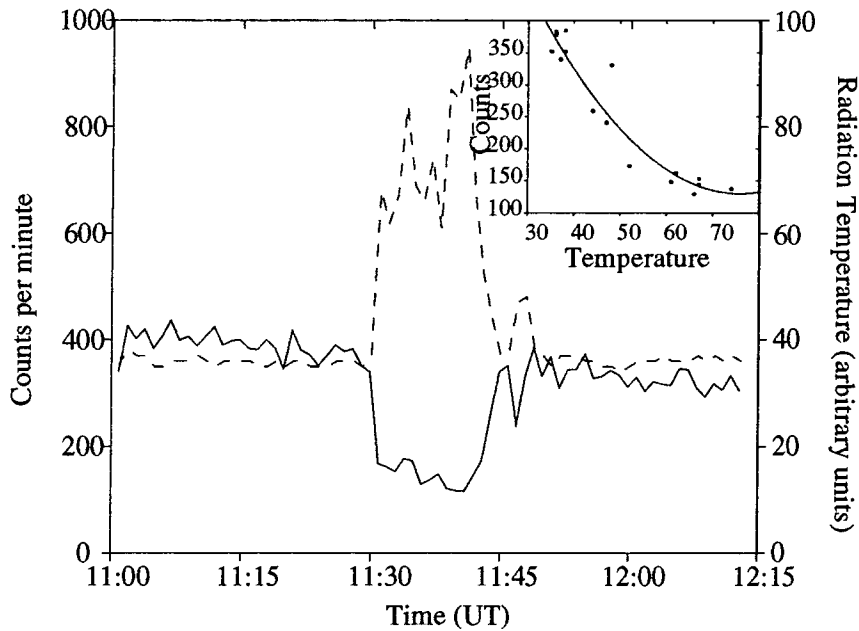


*Figure 4.20 Relationship between radiometric measurement of sky temperature and telescope count rate for a 75 minute period. The plot shows the temperature increase and associated count rate reduction when a cloud passed through the field of view (from Turver, 1998).*

The response of the radiometer is presented in  $^{\circ}\text{C}$  and corresponds to the temperature at which a blackbody (emissivity  $\epsilon = 1.0$ ) would radiate energy at the rate measured by the radiometer. The radiometer allows the operator to associate an unexpected reduction in count rate with a deterioration in sky quality, rather than with a potential change in telescope performance. The  $8\text{-}14\ \mu\text{m}$  radiometer provides a new sensitive and instantaneous measure of sky clarity, independent of the performance of the telescope itself.

## 4.5 Stabilization of Telescope Operating Conditions

The temperature variations in the detector packages, as discussed in section 4.4.2, will cause significant variations in the gains of individual PM tubes. To counter this problem, temperature servo systems were introduced to maintain a constant temperature in the PM tube environments. The temperature variations recorded in the detector package with the servo system installed are shown in figure 4.21. The temperature variation in the detector packages is seen to be reduced to less than  $3^{\circ}\text{C}$  over the course of an observation, corresponding to a change in gain of  $<3\%$ .

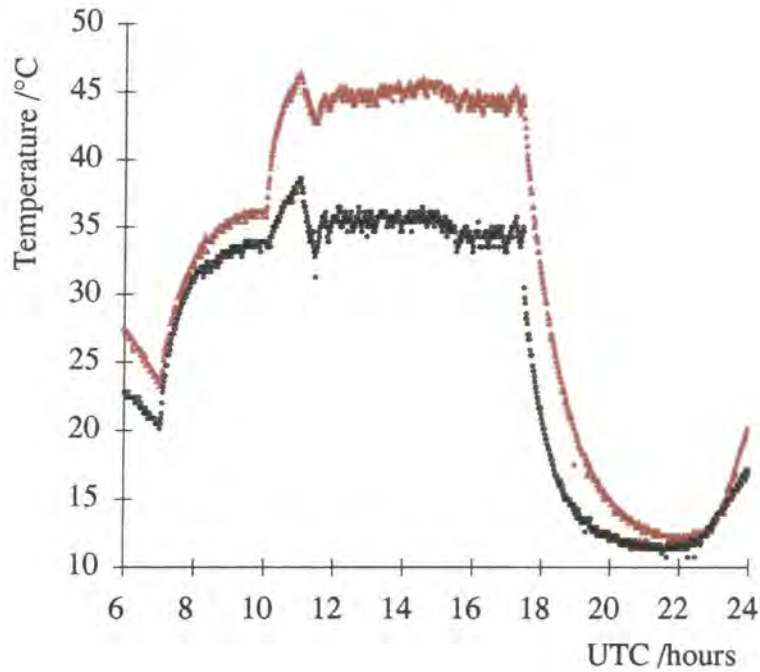


*Figure 4.21 Temperature variations at 2 points within the central detector package of the Mark 6 telescope. The red trace shows the temperature at the base of a PM tube. The temperature shown in black was measured in the space behind the tubes. The heating elements were switched on at 0700UTC. The EHT was turned on at 1000UTC, resulting in another temperature increase which was countered by the servo system in approximately 1 hour. The heaters and EHT were turned off at around 1730UTC.*

## 4.6 Conclusions

An atmospheric Cherenkov telescope is exposed to changes in a number of experimental factors both during and between observations, which may affect its performance. Furthermore, environmental conditions and, in particular, sky clarity, can have significant effects on the quality and quantity of data recorded.

Investigations have been carried out to determine how these changes in experimental and environmental conditions will affect the operation of the telescope. The critical areas of the telescope have been identified as the mirrors, photomultiplier tubes, attitude monitoring and the control and signal processing electronics. The responses of these elements to changes in the conditions under which they operate have been investigated and described.

Systems employed to monitor the operation and environment of the telescope indicate that in some cases, changes in operating conditions may lead to significant variations in telescope performance. Such variations are to be avoided if a constant approach to signal identification is to be determined. Control systems have been developed and employed to minimize temperature changes in a number of critical elements. Changes in the gain of the telescope due to a combination of all of the temperature effects discussed are shown to be <5% over the duration of an observation. Larger 'settling' effects are seen in the first ~30 minutes of operation.

The effects of variations in background illumination are restricted by the incorporation of albedo baffling, which is described in chapter 5. No discernible change in illumination is seen as zenith angle changes while tracking a field of constant brightness, implying that little light is scattered from the ground and surroundings into the PM tubes.

Variations in telescope performance due to changes in the alignment between the telescope and terrestrial magnetic field are shown to be negligible when a mumetal shield is extended around each PM tube. This shows that any measured change in the telescope performance with angle relative to the geomagnetic field is due to effects on shower propagation in the atmosphere and not on the performance of the PM tubes.

It is therefore estimated that the gain of the telescope, and therefore the energy threshold, varies by no more than 5% in stable running while observing a single starfield.

## Chapter 5. Enhancements to the Performance of the Durham Mark 6 Atmospheric Cherenkov Telescope

### 5.1 Introduction

The Mark 6 ground based gamma ray telescope was constructed in mid-1994 and has been routinely recording data for over 2 years. The aims of the project were to produce a southern hemisphere imaging telescope, located at sea level, of comparable sensitivity and threshold ( $\sim 200$  GeV) to that of mountain altitude telescopes with further capability to identify gamma ray signals at energies close to 100 GeV. The success of the project depends upon the ability to identify signals produced by gamma rays within the numerous cosmic rays which make up the dataset recorded. This chapter describes studies made since the telescope was commissioned to investigate methods of further improving the performance and sensitivity of the telescope. Three principal areas of potential improvement are identified. These are:

- A reduction in the gamma-ray energy threshold of the telescope. At lower energies, the flux of gamma ray photons increases, as shown in figure 1.3, and the hadron-induced background reduces in intensity below approximately 100 GeV, as discussed in chapter 2. The lower limit for the effective operation of a ground based gamma ray telescope is currently  $\sim 200$  GeV. Satellite detectors are generally insensitive at energies above  $\sim 30$  GeV, due to the combination of reduced flux and limited collecting area. The intervening decade is among the last regions of the electromagnetic spectrum to be exploited by astronomers.
- An improvement in the identification of lower energy gamma-rays. As shown previously, small (low energy) cascades are a potentially gamma ray rich population. It is, however, difficult to apply the same imaging techniques of signal enhancement to these events as are used to investigate larger (high energy) cascades. In order to be able to treat these small cascades effectively, it is necessary to maximise the gamma ray trigger probability and the amount of light collected for any particular cascade, and to retain as much information concerning their spatial and temporal construction as possible.
- An increase in the duty cycle of the experiment. The statistical significance of a detection is enhanced by increasing the size of the dataset from which it is extracted. Increasing observation time is possible if the effects of factors which presently limit operation, such as moonlight and inclement weather, can be minimized.

## 5.2 Reduction in the Energy Threshold of the Telescope

As a figure of merit for the performance of a gamma ray telescope, the definition of the energy threshold may be ambiguous. To allow for comparison with figures quoted for other instruments, two definitions are considered here; the energy corresponding to the peak triggering efficiency and the energy which is exceeded by 90% of observed gamma rays. Both measures are derived from a spectrum of number of detected gamma ray events as a function of primary energy. An initial derivation of the energy response of the Mark 6 telescope can be found in Holder (1997). The calculations are based on the operating condition of the telescope in December 1996, which includes many of the upgrades described in this chapter, except for the optimized light collecting cones as described in section 5.2.2.

The derivation of the energy threshold requires calibration against an absolute standard, ideally a gamma ray spectrum from a known and well documented source. In the absence at present of such a source available to southern hemisphere projects, it is necessary to rely entirely on computer-based simulations of the predicted behaviour of the telescope. The response of the telescope to the cosmic ray background is well measured. Simulation programs can be optimised to accurately recreate this behaviour, which can then be applied to a simulated flux of gamma ray photons. The method used by Holder (1997) is based on the cosmic ray trigger rate for an atmospheric Cherenkov telescope, which is given below.

$$R = \Omega \int_{E_{\min}}^{E_{\max}} \eta A_{\text{coll}} f(E) dE$$

where  $\eta$  is the triggering efficiency,  $A_{\text{coll}}$  is the collection area of the telescope and  $\Omega$  is the field of view. The differential cosmic ray flux is measured as  $f(E) = 1.7 \times E^{-2.7} \text{ s}^{-1} \text{ cm}^{-2} \text{ sr}^{-1} \text{ GeV}^{-1}$  (Gaisser, 1990). Matching observed counting rate to simulations, by varying simulated discriminator thresholds, provides a model which can then be applied to Monte Carlo simulations of gamma ray showers. Holder simulated a gamma ray flux of spectral index -2.4, that of the Crab nebula in the VHE range (Vacanti *et al*, 1991). This flux can be combined with the effective area of the telescope, which is a function of gamma ray energy, size of Cherenkov light pool and triggering probability, to determine the detected gamma ray flux as a function of energy, as shown in figure 5.1.

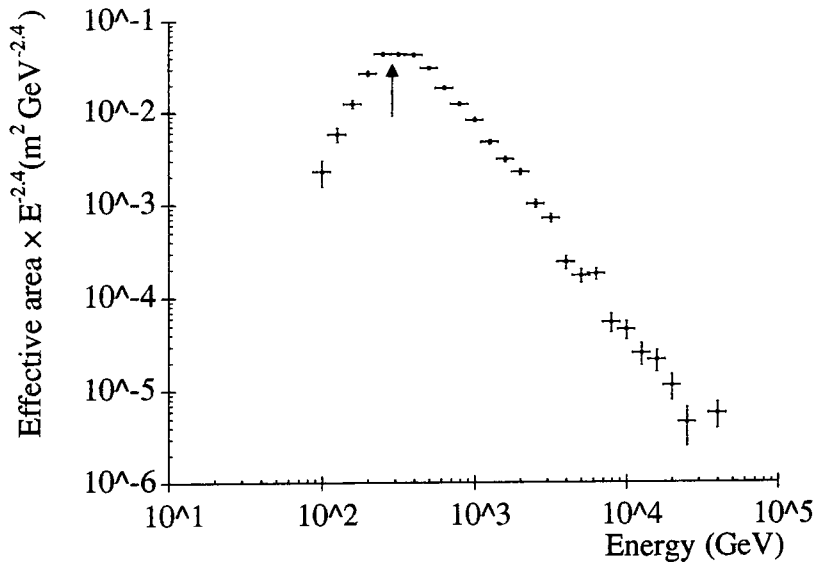


Figure 5.1 The predicted differential gamma ray response for the Mark 6 telescope. A differential source spectrum of index  $-2.4$  is assumed. The threshold energy, corresponding to the energy of the maximal differential flux is approximately  $300 \text{ GeV}$  (from Holder, 1997).

Holder shows that, using the maximum triggering efficiency definition, the energy threshold of the telescope is approximately  $300 \text{ GeV}$ . The data can also be used to show that  $90\%$  of telescope triggers correspond to gamma-ray energies in excess of  $150 \text{ GeV}$ . This demonstrates the low energy sensitivity of the telescope.  $10\%$  of gamma-ray induced triggers are due to primaries of energy  $<150 \text{ GeV}$

The smallest event which can be usefully treated, a summed PM tube response of  $100$  digital counts, corresponds to a gamma-ray energy of  $62 \text{ GeV}$ . A light pulser, comprising  $^{241}\text{Am}$  dispersed throughout a scintillator, has been used for absolute calibrations of PM tubes. It has been measured by  $3$  independent methods to provide approximately  $300 \pm 50$  photons ( $70 \pm 12$  photoelectrons) per pulse. This source has been measured to provide a mean pulse size of  $283.3 \pm 0.5$  digital counts above pedestal on the  $25 \text{ mm}$  diameter PM tubes in the imaging camera of the Mark 6 telescope. By allowing for the collecting area of each mirror ( $42 \text{ m}^2$ ) it is possible to derive a measure of the sensitivity of the telescope in terms of number of photoelectrons per square metre per digital count. Numerous computer simulations indicate a signal at sea level of  $1.5 \pm 0.1$  photons  $\text{m}^{-2}$  for a  $100 \text{ GeV}$  gamma ray over a wide range of lateral distances. For the Mark 6 telescope, a value of  $0.0062 \text{ pe m}^{-2} \text{ dc}^{-1}$  is obtained, leading to the relationship that, for a gamma ray photon,  $62 \text{ GeV} \rightarrow 100 \pm 20$  digital counts for photons near the zenith, the statistical uncertainty being dominated by the variations in light from the pulser.

### 5.2.1 Optimization of Trigger Capability by Choice of PM Tubes

The role of the left and right PM tube packages in the Mark 6 telescope, as described in chapter 3, is to contribute to a low energy, stable and noise free trigger, based on the requirement for temporal and spatial coincidence in the light detected by separated detectors. Individual detector packages can thus be operated at high noise/gain levels. Accidental triggers are precluded by the coincidence requirement, as discussed in chapter 3. The imaging camera can therefore be operated at a higher gain than a camera in a single dish system.

The PM tubes used in the left and right detectors (the triggering cameras) are chosen to have different specifications to those in the imaging camera. Good spatial coverage is important, but high resolution of the shower image is not critical, although it would offer advantages. A smaller number of PM tubes than in the central camera can therefore be used, with each tube in the triggering system providing sky coverage corresponding to more than one tube in the imaging camera. Good spatial coverage is achieved by minimizing the dead area between the PM tubes. In a conventional isometric arrangement, this requires either the use of hexagonal cross-section PM tubes or light collecting cones. The use of PM tubes of large photocathode surface area also reduces the unavoidable dead area due to tube wall thickness. Most importantly, the PM tubes in the triggering packages must have high gain/low noise characteristics.

The noise from a PM tube (in the case of a gamma ray telescope, dominated by sky noise) generally increases with tube gain. The ideal operating condition for an individual PM tube should be a high gain with low corresponding PM tube sky noise rate, in order to ensure that the telescope will record the smallest possible events while minimizing the rate of accidental coincidence triggers.

The operating conditions, particularly tube noise as a function of gain, of all PM tubes in a detector package should ideally be similar to minimize the possibility of biases favouring the recording of events in particular regions of the camera. Although a certain amount of variation between tubes is inevitable, the effects may be minimized by ensuring a large initial population from which to select photomultipliers of the desired high gain/low noise characteristics.

At construction, the left and right detector packages of the Mark 6 telescope each consisted of 19 Burle 8575 PM tubes, a type which had previously been used in the Mark 3, Mark 4 and Mark 5 telescopes. In 1996, a sample of more than 100

Philips XP3422-SG4 PM tubes became available. This type of tube has not previously been used in ground based gamma ray astronomy. Table 5.1 shows a comparison of the characteristics of the two tube types. As the Philips tubes are of comparable size to the original Burle tubes, 2 sets of 19 were required to replace the originals. It is therefore possible to select a sample from the total set which best display the required characteristics.

PM tube type	Burle 8575	Philips XP3422-SG4
Photocathode Shape	Circular	Hexagonal
Diameter (mm)	50	56 (across flats)
Photocathode Area (mm <sup>2</sup> )	1750	2350
Dead Area of Tube	12%	14%
Packing Efficiency	73%	98%
Spatial Coverage of Sensitive Area	64%	85%
Typical Operating Voltage (Volts)	1400	1700
Typical Anode Current ( $\mu$ A)	20	32
Typical Noise Rate (kHz)	1000	10
Rise Time (ns)	2	5
Available Sample	~50	>100

*Table 5.1 Comparison of the physical and operating characteristics of the samples of Burle 8575 and Philips XP3422-SG4 PM tubes.*

The Philips tubes may be preferable to the Burle tubes for two important reasons. The hexagonal sensitive area allows the light collection to be maximized without the use of cones and the noise rate at comparable gain has been shown to be significantly lower than that of the Burle tube. However, the Philips tubes have a slower temporal response, defined by pulse rise time, but for use in the telescope triggering system the effect of this disadvantage can be minimized.

### 5.2.2 Threshold Energy Reduction Using Light Collecting Cones

The use of cones as lightguides mounted in front of the PM tube photocathodes serves one of two primary purposes, depending on whether they are used in the imaging camera or the triggering detectors.

Cones are used in conjunction with the imaging camera to maximise the sensitive area of the detector by collecting light that would otherwise have fallen into the dead area between the circular tubes. This ensures that the maximum amount of light is collected, optimizing the size of the signal sample recorded.

It is also important that the left and right detectors, which form the trigger elements, collect as much of the available light as possible. For this reason, simple light collecting cones, of similar design to those fitted to the imaging camera, were initially fitted to the circular Burle PM tubes of the triggering packages in order to collect the maximum amount of available light.

However, the telescope trigger threshold is dependent on signal amplitude rather than area, since the discrimination is on the basis of voltage and not charge. Therefore, in order that the telescope should record events at low energies, it is necessary to maximise the amplitude produced by a given amount of light. Such pulse shaping gives rise to the second application of light cones, the concentration of the incident light on a small part of the photocathode with well defined, high bandwidth characteristics. The variations in spatial and temporal response across the surface of the Philips PM tubes are discussed in section 4.3.2.1. By concentrating the light in the central region of the photocathode, the effective bandwidth of the Philips PM tube can be improved allowing an increase in amplitude for a pulse of given area. The result of this is that trigger channels fitted with such light concentrators respond to smaller light pulses corresponding to lower gamma ray energies. The count rate of the telescope is governed by the threshold of the left and right detectors and so increasing the sensitivity of these detectors reduces the energy threshold of the telescope.

In this section, investigations into the optimal design of light collecting cones to improve the bandwidth of the Philips PM tubes are discussed. Laboratory measurements of the effects of using cones of different geometries are described. An initial test of the cones on the Mark 6 telescope is also described.

A secondary function of light cones is the shielding which they provide to the PM tubes against extraneous light.

In all cases, it is important that there is no 'crosstalk' between channels and that light reaches the photomultiplier corresponding to the part of the image in which it originated. The outer surface of the light cone is placed in the focal plane of the mirror. The cross section of the cone must be hexagonal at this outer surface in order to fit into an isometric grid. If the inner aperture of the cone has a circular crosssection, then a castellated outer surface results. Barriers are required between channels to ensure that no photons reach the focal plane in one channel, but then strike the photocathode of a different PM tube. Figure 5.2 is a photograph of a cone mounted inside a crosstalk shield, prior to mounting on the telescope.

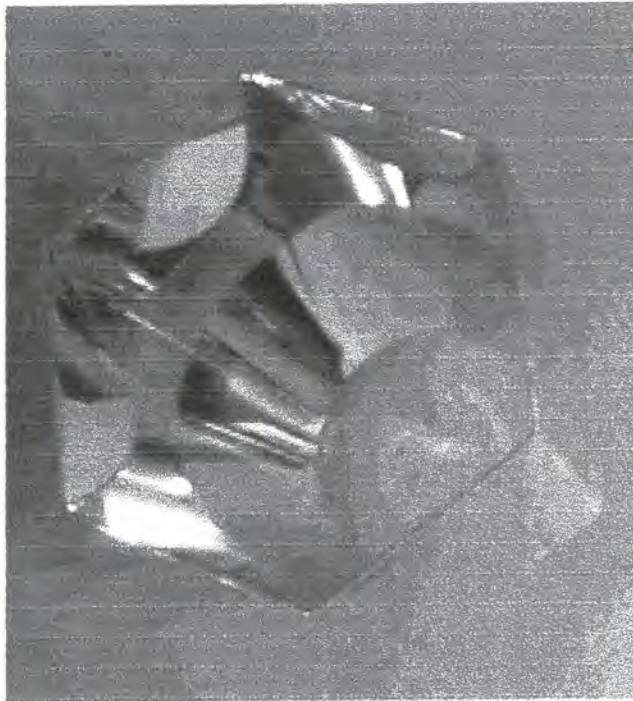


*Figure 5.2 An individual light collecting cone from a triggering detector of the Mark 6 telescope.*

The variations in sensitivity and temporal response across the photocathode of the Philips PM tube are discussed in chapter 4. From these, it is apparent that the bandwidth may be improved by restricting the area of photocathode exposed to

incident light to the central region. This results in an inevitable compromise between increasing the response speed and incurring a loss in light reaching the photocathode.

#### *5.2.2.1 Laboratory Measurement of Efficiency of Light Collecting Cones*

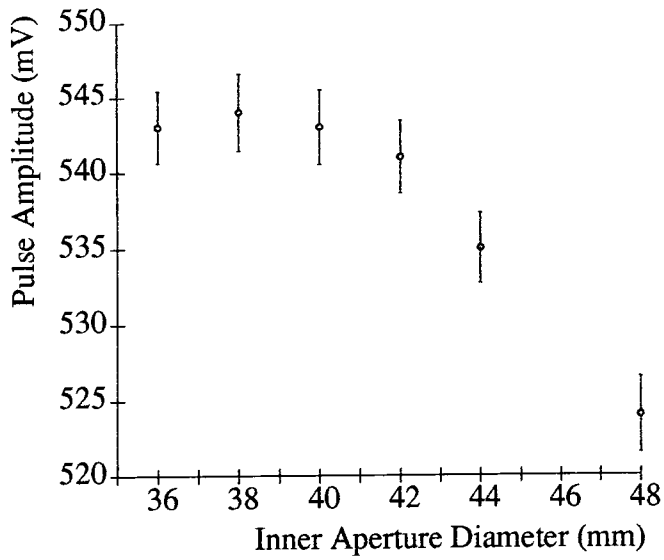
Laboratory measurements of the performance of light collecting cones of various geometries were made to investigate the effects of cone shape on PM tube output pulses. A dark laboratory, as described in chapter 4, was used. A plane signal was produced by passing laser light to the focus of a searchlight mirror, which reflected a near plane light front onto a white wall. The PM tube was exposed to this reflective surface. Diffuse background light was again provided by use of a green light emitting diode.

Cones of various lengths and inner apertures were tested. All were mounted in a hexagonal sleeve, as used on the telescopes to prevent crosstalk between channels. Each light collecting cone in turn was mounted immediately in front of the test PM tube window.

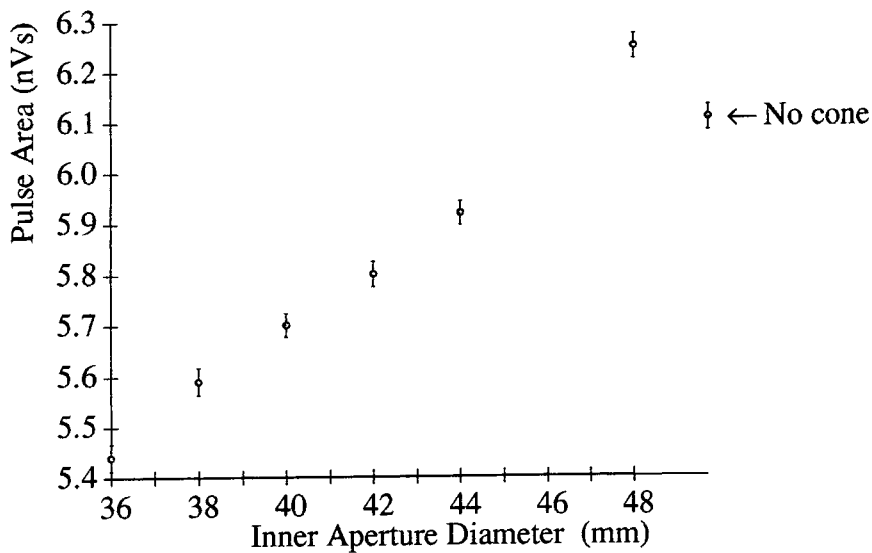
PM tube pulse outputs were measured on a LeCroy 9350 oscilloscope. The operating conditions of the experiment were defined by the background light level, PM tube operating voltage and oscilloscope trigger level. These were configured such that >95% of laser pulses were recorded and <1% of recorded pulses were not induced by the laser. Pulse amplitude was measured in order to monitor improvements in triggering. Pulse area was also measured to estimate the amount of light lost due to absorption by the cone.

Figure 5.3 shows the PM tube output pulse amplitude and area as functions of the cone inner aperture for sets of cones of constant length. Figure 5.4 shows the PM tube output pulse amplitude and area for cones of varying length and constant inner aperture.

The results suggest that the PM tube output pulse amplitude is maximised when the cone geometry is defined by an inner aperture of  $38\pm 2$  mm and a length of  $70\pm 5$  mm.

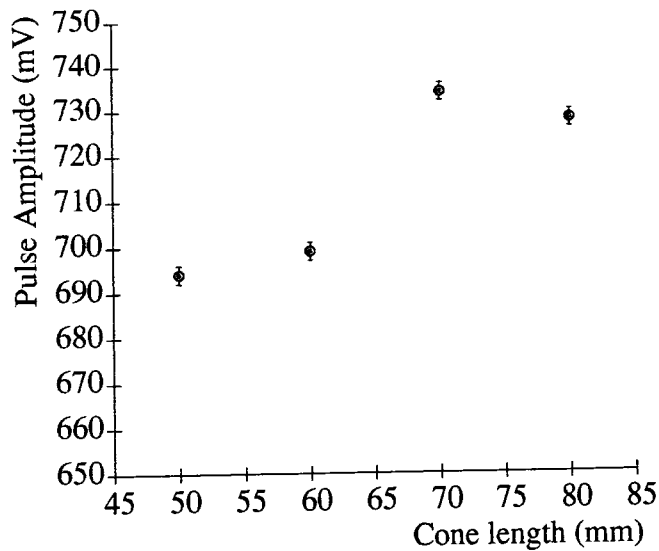


(a)

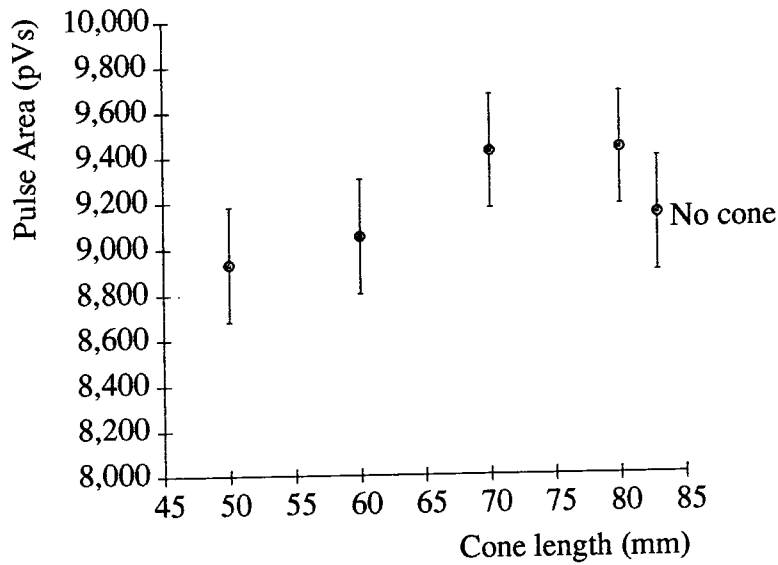


(b)

Figure 5.3 Variation of (a) amplitude and (b) area of a PM tube pulse corresponding to a standard light pulse measured using a combination of PM tube and light collecting cones of fixed length with varying inner cone aperture. The area of a pulse measured using no light cone is shown for comparison. The amplitude of a pulse measured using no cone was  $405 \pm 19$  mV.



(a)



(b)

Figure 5.4 Variation of (a) amplitude and (b) area of a output pulse corresponding to a standard input pulse measured using a combination of PM tube and light collecting cones of fixed inner aperture and varying length. A pulse measured without using a light collecting cone had amplitude  $501 \pm 2 \text{ mV}$ .

These results indicate that the initial use of light collecting cones on the left and right detectors of the Mark 6 telescope increases the light collection of the PM tubes to the extent that pulse amplitude is increased by  $\sim 25\%$ , with a corresponding

reduction in telescope energy threshold. This was found to be the case in tests made on the telescope in Australia. Furthermore, on the basis of the laboratory measurements, it may be possible to achieve a further reduction in energy threshold of ~5% by modifying the design of the cones in use.

#### 5.2.2.2 Field Testing of Light Collecting Cones

It has not been practical to carry out laboratory tests of the effects of light collecting cones on focussed light reflected off a mirror surface as is the case for Cherenkov light incident on the telescope, since it is impossible to recreate the physical mirror/detector construction of the telescope in the dark laboratory. To test the cones under these conditions, it has been necessary to carry out final testing of the cones *in situ* on the Mark 6 telescope.

This can be regarded as the ultimate test of the efficiency of the light collecting cones. Any improvement in the performance of the cones should produce a lowering of the threshold and should translate into an increase in the overall count rate of the telescope and that of the 19 individual coincidence channels. If the energy threshold of the telescope is successfully reduced, more small events should be recorded by the central camera, operating at constant gain. This would be manifest as a change in the size distribution of events seen in the camera.

There are, however, problems with field test data of this type which do not affect the laboratory measurements. Comparisons between the performance of two cone sets involve data recorded at different times through a night - before and after changing the cones. It has already been shown, in chapter 4, that telescope count rates vary systematically with the zenith angle at which a source is being observed. If the delay between observations translates into a significant change in zenith angle, or there is a secular change in contrast, the change in count rate may mask any (small) improvement due to the presence of the cones.

In January 1997, 2 sets of 7 cones were tested on the central channels of the left and right detectors of the Mark 6 telescope. Each set consisted of 3 standard cones on channels 1, 2 and 3 and reduced aperture (40 mm) cones on the channels C, 4, 5 and 6, as shown in figure 5.5. The cones were mounted on a plastic plate similar to the standard set permanently installed on the telescope. This method allows testing only of cones of the same length as the standard, as the outer aperture of the cone must be in the focal plane of the mirror. The telescope was operated without cones on the outer ring of PM tubes; all data from the 12 outer tubes were disregarded.

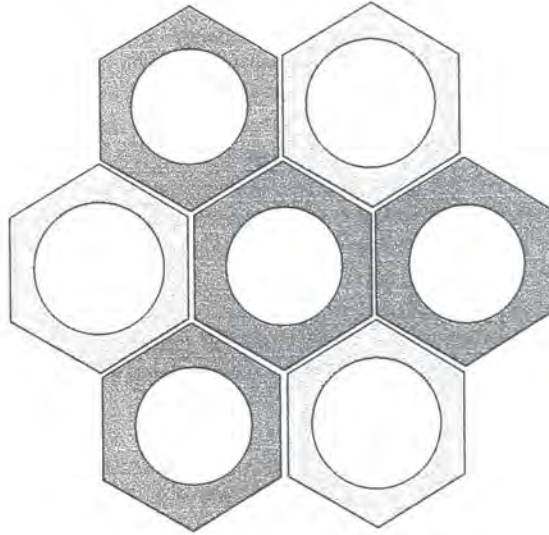


*Figure 5.5 Arrangement of test cone sets as used on the central 7 PM tubes of the left and right detector packages of the Mark 6 telescope in January, 1997. The dark grey channels (C+456) are reduced aperture cones. Channels 1, 2 and 3 had standard cones fitted.*

Cosmic ray events were recorded by the telescope using the test and standard cone sets; each observation lasted for 1 hour. The events were analysed by examining those events which any one of the six channels in the inner ring of PM tubes together with any, or no, tubes from the outer rings. Results for the central channel have been disregarded. Events which trigger only this channel are more restricted in terms of an upper size limit than events triggering tubes in the inner ring, which can extend outwards from the tube centre. An improvement in the telescope performance using the test cones would be indicated by an excess of events recorded in channels 4, 5 and 6 with the new cones over the predicted value from the response of the standard cones on channels 4, 5 and 6 in the test configuration. Results are shown in table 5.2. A second control dataset was recorded using the standard cones. Table 5.2 also includes a comparison between the two control sets taken at different times.

	Ctrl I	Test
(a) Chs 1,2,3	10126 (101)	9489 (97)
Chs 4,5,6	3304 (57)	3656 (60)

	Ctrl I	Ctrl II
(b) Chs 1,2,3	10126 (101)	12791 (113)
Chs 4,5,6	3304 (57)	4207 (65)

*Table 5.2 Events recorded triggering individual channels in the innermost ring of PM tubes in the left/right detectors and any tubes in the outer ring. Counting uncertainties are shown in brackets.*

The absolute numbers of counts seen in table 5.2 are based on the use of the 'Fire Pattern Generator' (FPG). The FPG produces a record, for each event, of those channels in which the Cherenkov light exceeded the threshold level. However, for each channel, there is some probability that the FPG will occasionally malfunction. This results in the imbalance seen in table 5.2. The method used here to compare relative count rates requires only that the probability with which the FPG accurately records the operation of an individual channel remains constant. Any variation in the relative triggering of the channels due to a cause other than the cones would manifest itself in an inconsistency between the results of the two control datasets.

For channels 1, 2 and 3 (standard cones in both control and test datasets), the ratio of the number of events in the control to the test (table 5.2a), is  $0.94 \pm 0.01$ . For the channels with the test cones, the same ratio is seen to be  $1.11 \pm 0.02$ . The ratios for the second control dataset to the first (table 5.2b) are seen to be  $1.26 \pm 0.01$  and  $1.27 \pm 0.02$ . The two control sets are therefore clearly consistent with one another. The test data suggests that a significant improvement is seen in using the test cones. However, the increased number of events is not distributed evenly over the 3 channels and some doubt remains that the improvement can be ascribed to the new cones.



Examination of the anode currents and singlefold noise rates of the PM tubes in the left/right mirrors have shown no significant increase in these quantities. This suggests no increase in the amount of light collected. The results cannot, therefore, be used as reliable evidence for improved telescope performance resulting from the installation of the modified sets of light collecting cones.

In April 1997, two full sets of reduced aperture cones (inner aperture = 40 mm) were installed on the left and right detectors of the Mark 6 telescope for a number of nights. Observations were made on 2 objects (PSR B1706-44 and PSR J1105-61). The analysis of these data was made in comparison with data taken in the same month on the same objects using the standard cone set. At the end of the observing session, the standard cone set was reinstalled on the telescope.

The data from this trial again show no significant change in telescope count rate when using the new cones. Furthermore, there is no evidence from examinations of histograms of the charge distribution of events for individual tubes of an increase in the number of 'small' events being recorded. The weather in this month was relatively stable, although sky temperature measurements using the radiometer indicated that sky clarity was not perfect and the usual uncertainty in the validity of test data taken over long periods remains.

At present, it is not possible to make a definitive statement concerning the effectiveness in providing the 5-10% reduction in threshold expected from laboratory measurements.

### 5.2.3 Minimization of Sky Noise Using Light Baffles

Exposure of the PM tubes to background light reduces the efficiency of the telescope in two ways. Firstly, increased illumination causes a reduction in PM tube gain, as shown in chapter 4. Secondly, the tube noise rate increases, with the consequence that gain must be reduced to maintain an acceptable level of triggers of the telescope due to accidental coincidences. It is therefore desirable to minimise the amount of light falling on the PM tubes originating from sources other than Cherenkov flashes. The purpose of baffles is to reduce the amount of this light falling on the PM tubes from outside the mirror area. Reduction of this source of light will result in an improvement in the signal to noise ratio.

Under normal operating conditions, baffles can only remove the albedo component of background light. They do not restrict background starlight or zodiacal light reflected in the flux collectors from the field of view of the telescope. The

photocathode of an unshielded PM tube is exposed to  $2\pi$  steradians. On the Mark 6 telescope, each mirror occupies only 1.1 steradians of the field of view. Therefore, 83% of the solid angle to which the tube is exposed is a source of noise only. The purpose of baffles is to minimize the amount of light from this area falling onto the photocathode.

In an ideal case, albedo shielding can be provided by housing the telescope in a building. Since the size of most large atmospheric Cherenkov telescopes precludes this as a viable option, three other possibilities remain. These are; to provide shielding around the flux collector, shielding around the PM tubes and to use the shielding properties of the light collecting cones described in section 5.3.2.

The presence of simple light collecting cones reduce background light levels by only a few per cent. Winston cones, incorporating a parabolic section into the design, give better results, but at the expense of the loss of signal light, increasing the energy threshold of the telescope (Punch, 1993).

Light baffles have been mounted on the Mark 6 telescope around the mirrors and the detector packages. The ideal arrangement, which has been implemented on the Mark 5 telescope, is represented in figure 5.6.

Detector mounted baffles are intended to shield the PM tubes from as much of the non-mirror aperture as possible, without obscuring any of the flux collector. The length of the detector baffle is a function of the angle subtended by the mirror and the diameter of the baffle. This defines the shape of the light collecting area and should match the mirror/detector arrangement. The baffles must also be non-reflective, so as to prevent background light being reflected onto the PM tubes. These baffles are mounted on the detector package housings and therefore are not particularly large. They were therefore designed to be rigid, constructed from aluminium sheet painted matt black. For the left and right detectors, the baffles protrude 35 cm from the detectors towards the mirrors and are 65 cm across the flat faces of a hexagonal cross-section. The central imaging detector package is protected by baffles which are only 24 cm long and 68 cm across the flats. The shield on the central detector package is shorter than those on the left and right detectors due to the increased diameter of the sensitive area of the central light detector arrangement. This is because the PM tube cluster facing the central mirror covers a wider area than the left and right detectors.

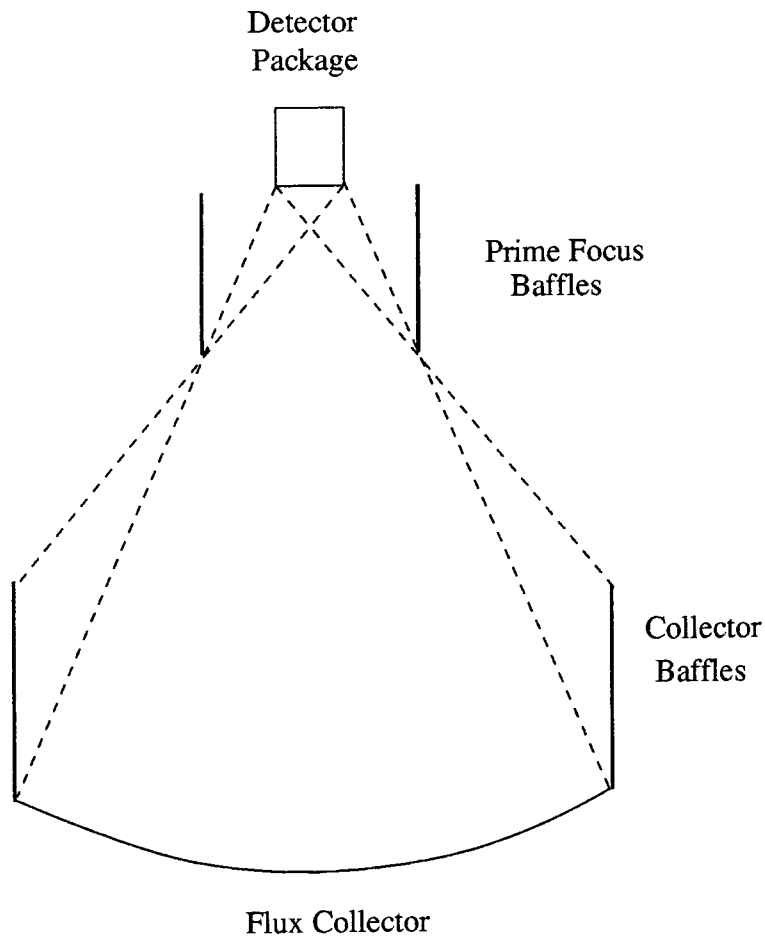


*Figure 5.6 The ideal arrangement of baffling, resulting in the total exclusion of background albedo light from the detector package.*

The baffles surrounding the mirrors are intended to cut out light from off-axis sources which would be diffusely reflected by the mirror onto the PM tubes. In the ideal case, these baffles extend out to the focal plane of the mirror, in which the detector lies. In this case, no detector baffling would be required. Construction constraints limit the length to which mirror baffles can be extended, so a combination of mirror and detector baffles is used.

Mirror baffles were tested and implemented on the Mark 6 telescope in September and October, 1995. Tarpaulins are used for the mirror baffles to minimize the weight increase to the telescope. These are fixed in a square box arrangement using the telescope structure around the mirrors. The existing structure was used, except for the central mirror, where extensions were required to provide support. Further covers were used to fill gaps around the mirrors to prevent albedo light from behind the mirrors reaching the PM tubes. The length of the baffles around

the mirrors is limited by the telescope structure. They are 1.8 m long, which is short of the ideal length represented in figure 5.6.

The effect of the baffles is to reduce the background light, with a corresponding reduction in anode current and telescope triggers due to accidental coincidences. The reduction in anode current and noise allows an increase in EHT and therefore in gain as described in chapter 4. The EHT at which the PM tubes operate can therefore be increased without causing an unacceptable number of accidental triggers. This leads to a reduction in energy threshold of the telescope, estimated to be ~15%.

### 5.3 Improving the Detection Efficiency for Smaller Events

The probability with which the telescope detects Cherenkov light flashes is significantly smaller at and around the energy threshold of the telescope than it is for light produced by higher energy primaries, as discussed in chapter 2. The sample of near threshold small events is a potentially gamma ray rich population, since the gamma ray flux increases to low energies and the hadronic background reduces at energies around 100 GeV. This section describes work done to investigate the performance of the telescope trigger system in an attempt to increase the number of low energy events measured.

Small events would not be expected to respond well to the standard analysis techniques described in chapter 3. As they contain relatively little light, the images are confined to just a few tubes in the camera. The small number of samples of the light distribution means that there are large uncertainties in the higher order moments of the images used to determine the parameters normally employed in background rejection. Because of this, the event selection must be relaxed in order to retain as many gamma rays as possible. This results in a reduction in the effectiveness of the background rejection.

#### 5.3.1 The Standard 4-fold Digital Trigger System

Telescopes designed and constructed by the Durham group have 3 flux collectors to provide independent measures of a Cherenkov light pool. Such telescopes provide robust low energy and noise free triggers. The trigger system requires that a signal exceeds a threshold value in the same  $0.5^\circ$  pixel (observing the same area of sky) of the three detectors, within a short, fixed, time interval (10 ns). This rigorous system precludes accidental triggers including ones due to the effects of muons and favours the spatial concentration of the intensity of light produced by gamma ray

events over distances comparable to the separation of the light collectors on the Mark 6 telescope, as discussed in chapter 2. The background, hadron-induced, events are more likely to fluctuate and appear significantly different between elements of the telescope and therefore likely to fail to exceed threshold in one or more detectors.

The amount of light recorded from a gamma ray event is approximately proportional to the energy of the primary photon. The variation on the signal size may be represented by a Poissonian distribution in the number of photoelectrons produced. In the case where the signal would just exceed threshold but the noise contribution is negative, the telescope trigger will reject the event, regardless of how the noise modifies the signal in the other detectors. This means that, for events for which the Cherenkov signal is exactly at the threshold, only 50% (those where the noise contribution is positive) will cause each individual detector to exceed threshold. For a multiple coincidence system ( $n$ -fold), only 1 such event in  $2^n$  will cause the telescope to be triggered. A digital trigger system, whilst having many advantages, is therefore intrinsically inefficient in dealing with events which are close to threshold energy. The inefficiency increases with the multiplicity of the system.

### 5.3.2 Alternative Methods for Telescope Triggering

The triggering system used by the Durham telescopes is described in chapter 3. In this section, investigations into two alternative methods of triggering an atmospheric Cherenkov telescope are described.

#### 5.3.2.1 Triggering on the Response of the Imaging Camera

A telescope comprising a single collector/detector package, such as the Whipple 10 m reflector (see e.g. Weekes *et al.*, 1997) must use coincidence between elements of the imaging camera in order to reduce background events to manageable levels. Experiments have been carried out to investigate the effects of such a trigger system on data recorded using the Mark 6 telescope.

The simplest coincidence requirement based only on the response of PM tubes in the imaging camera of the Mark 6 telescope is that any 2 should satisfy triggering conditions within some time interval. This is a much less rigorous trigger condition than the 3-fold spatial coincidence in regular use with the Durham telescopes, described in chapter 3. The result is that the number of accidental triggers due to

the sky noise background increases significantly. In order to compensate for this, it is necessary to reduce the gains of the PM tubes in the imaging camera. Gain is reduced to the level where accidental coincidences due to noise are at the same level as for the standard Durham trigger system. The lower gain results in a significantly reduced in telescope count rate as shown in figure 5.7.

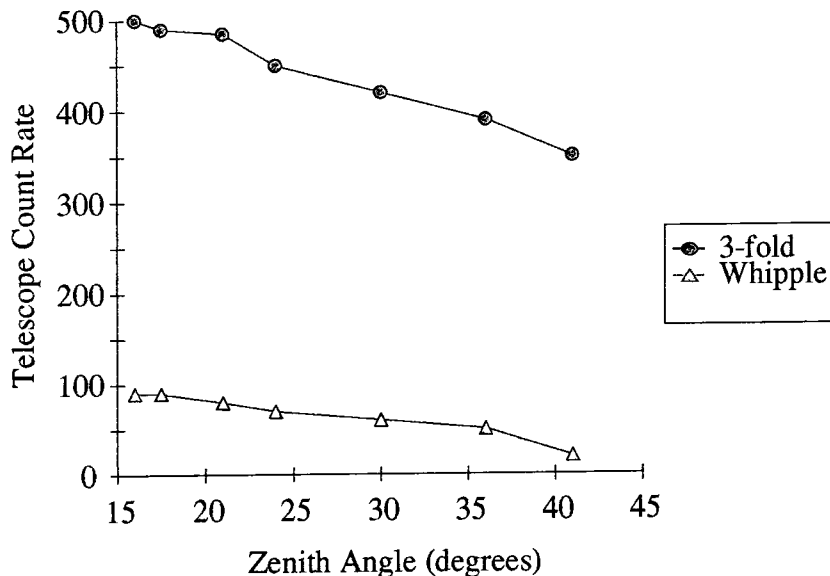
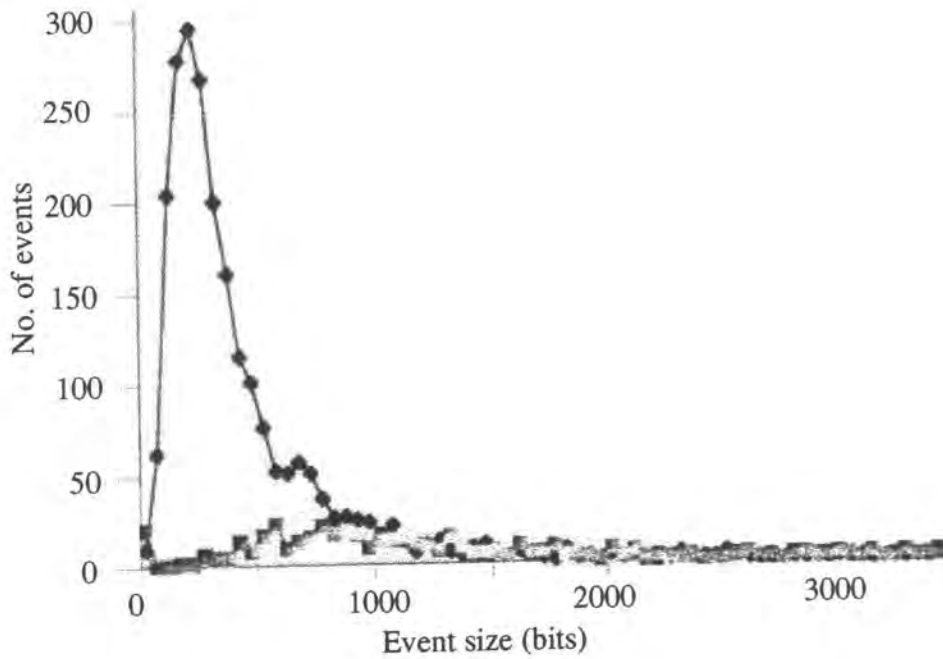


Figure 5.7 Count rate as a function of zenith angle for the Mark 6 telescope operating under 3-fold coincidence and '2-of-91' ('Whipple') trigger conditions.

Figure 5.8 shows the distributions of event sizes using the two trigger systems. The increased sensitivity to smaller events of the standard Durham trigger system is well demonstrated. This illustrates the fact that under the 'Whipple trigger' conditions, the telescope is less sensitive to low energy events.

### 5.3.2.2 An Analogue Trigger

Simulations by Orford (1995) have suggested that the energy threshold of multiple-coincidence triggered atmospheric Cherenkov telescopes can, in principle, be reduced by modification of the triggering requirement. It is proposed that the analogue sum of the squares of the signals in the detectors can be compared against a single discrimination value. This allows the telescope to trigger on events in which the noise component reduces the signal below threshold in one or more detectors depending on the contribution of the noise on the signal in the other detectors. The net effect may be a reduction of the energy threshold of a telescope utilising such a 3-fold analogue coincidence system of about 40%.



*Figure 5.8 Distributions of event sizes as recorded by the Mark 6 telescope operating under 3-fold coincidence (diamonds) and '2-of-91' ('Whipple') trigger (square) conditions. The reduced sensitivity to small events under the Whipple trigger system is clear.*

Implementation of a circuit to perform the signal processing - analogue squaring of photomultiplier pulses - was performed as part of an undergraduate project (Bleackley, 1996 (unpublished)). The further development of such a system was investigated in a recent undergraduate project (Tindale, 1997 (unpublished)). This work has been validated and extended to incorporate the effects of signal amplification on the operation of the analogue processing system and an investigation of the properties of a proposed circuit under typical operating conditions.

### 5.3.3 Comparison of Analogue and Digital Trigger Systems

In order to demonstrate that the analogue trigger system is an improvement over the standard digital method, it is necessary to show that Cherenkov events are accepted at a greater rate under identical operating conditions for the PM tubes. It is also desirable that it be shown that the extra accepted events are small and due to low energy primaries.

### 5.3.3.1 Specification of an Analogue Trigger System

The primary requirements of an analogue trigger system are that it should be of a high enough bandwidth to match that of the PM tubes to which it is connected and that it should produce an output pulse which is easily resolvable from the background noise. The unit designed in Durham was based on the Analogue Devices AD834, a four-quadrant analogue multiplier integrated circuit, designed with an input bandwidth of up to 500MHz. Two identical circuits, shielded against crosstalk, were mounted in a single width NIM unit, together with a voltage regulator to produce the necessary supply voltages (Bleackley (1996)).

Bleackley reported the successful operation of the squaring circuit and the RF shielding, showing that the dependence of the output voltage on the input voltage was of the form:-

$$|V_{out}| = |V_{in}/(2.828 \pm 0.033)|^2$$

Bleackley further showed that the intrinsic noise on the multiplier output was <1mV and therefore that for input voltages ~500mV, the noise would contribute ~3% of the signal. Further work has confirmed these results. Pulses produced by a Cherenkov flash in a PM tube under typical night sky operating conditions are typically ~3 mV in amplitude, after removal of any DC component, but prior to electronic amplification. In a conventional digital trigger system, the signal is amplified by a factor of 10 prior to discrimination. The AD834 circuit requires a signal amplification of such inputs in excess of 100 in order to operate in the regime explored by Bleackley. This can be achieved by cascading two standard  $\times 10$  amplifier units. If this amplification is not introduced, the output signal of the AD834 circuit is indistinguishable from the intrinsic noise. The extra amplification, if provided by cascaded amplifiers such as the  $\times 10$  LeCroy 612A, also causes an increase in the noise. The result is an unacceptably large number of accidental triggers, in which the current noise dominates the sky noise.

The multiplication element on the AD834 IC takes two input voltages, which in this case are identical, and determines their amplitudes as fractions of a reference voltage. It is these fractions which are processed to provide the output voltage as a fraction of the reference. In the case of this particular circuit, the reference voltage is significantly higher than the voltages being transformed, resulting in the value of the transfer function noted. For this reason, the employment of this particular analogue squaring system as the basis for an improved trigger system is

impractical. In the absence of an ADC with a more favourable transfer function, use of a low noise  $\times 100$  amplification system may provide a means by which to proceed.

### 5.3.3.2 Additional Tests of the Analogue Trigger Concept

Further testing of the principle has been carried out using a LeCroy 1GHz digital oscilloscope. The waveform processing capabilities of the instrument mean that an oscilloscope channel can be configured to square and add two input signals with a transfer function as required. Two XP3422 PM tubes were connected through  $\times 10$  LeCroy amplifiers to the inputs of the oscilloscope. Background light was produced by a green LED, with signal light being provided by the flash from the scintillator driven by the laser. Signal pulse size was adjusted to be approximately equal to the discrimination threshold of the electronics. The background light was of a level typical of normal operating conditions, and the noise contribution due to the background light dominated electronics noise. In a test, measurements showed that the signal size was 5.1 times the RMS noise on the system (mean signal size 57 mV, RMS noise 11 mV). The discrimination level was set at 50 mV. Measurements showed that, whilst a conventional digital trigger system selected 43% of these events, the analogue system selected 71%. This compares favourably with the predicted values of 40% and 69% respectively (Orford (1995)).

The results indicate that an improvement in count rate of up to 50% in these smallest events may indeed be possible. For larger events, the improvement is less marked, as the inefficiencies of the digital system become less significant. This demonstrates the potential improvements in telescope counting using an analogue method, if the practical problems outlined can be overcome.

If a circuit with a more suitable transfer function can be identified, or a suitable amplification system can be incorporated, then *in situ* testing on the telescope will become necessary.

Full implementation of such a system on the Mark 6 telescope would require significant work to be carried out on the established electronics systems. The new system would require an extra  $2 \times 19$  ADC channels and extra lengths of delay cabling due to the increased signal processing required. The potential increase in 'dead-time' will have to be offset against improvements in trigger efficiency in comparisons of the old and new systems.

## 5.4 Increasing the Duty Cycle of the Telescope

The typical duty cycle of an atmospheric Cherenkov telescope is less than 10%. This limit is a result of the requirement for good weather and the absence of the sun and moon. A Cherenkov telescope can only operate at full sensitivity in total darkness, although operation under moonlight is possible at the expense of an increased threshold and reduced sensitivity (Chantell *et al.*, 1997).

Operations in Narrabri are affected by problems of condensation and freezing of the mirror surfaces. The means by which these effects can be reduced are discussed. Poor weather prevents data recording for up to 40% of total available dark time in a year. Most of this is time lost to rain, wind etc, when observing is impossible, but it is estimated that approximately 10% of the lost time is due to freezing of the mirror surfaces. This lost time occurs mainly over a three month period during midwinter. Time losses due to mirror condensation would be similar or greater without treatment, which is applied from autumn to spring, which has been used for many years.

### 5.4.1 Prevention of Condensation on the Mirrors

Misting of the mirror surface occurs when the temperature of the mirrors falls below the dew point and results from the condensation of water vapour into droplets on the mirror surfaces. This causes increased scattering of light and therefore reduces the amount of light focussed on the PM tubes. Since the light is scattered isotropically, the reduction means that observations become impossible.

The problem is countered by spraying the mirrors with a detergent solution prior to observations when misting is expected. This does not prevent the condensation of water vapour, but breaks down the surface tension of the water, preventing drops from forming. This results in the formation of a uniform film across the mirrors, reducing the scattering effects of the water. This method has been shown to be effective for up to twelve hours and therefore serves throughout an observation. It is generally required between mid-autumn and spring, when night time temperatures are low.

Misting problems would, if not checked, cause a reduction in the telescope operating time by around 20% of total current data. Comparison of data taken on nights when demisting has been carried out and nights when the mirrors have been left dry show no evidence for any detrimental effect on telescope performance due to wet mirrors. This is a satisfactory, if inconvenient, low-cost procedure which has been used for more than 10 years.

#### 5.4.2 Mirror Heating to Prevent Freezing

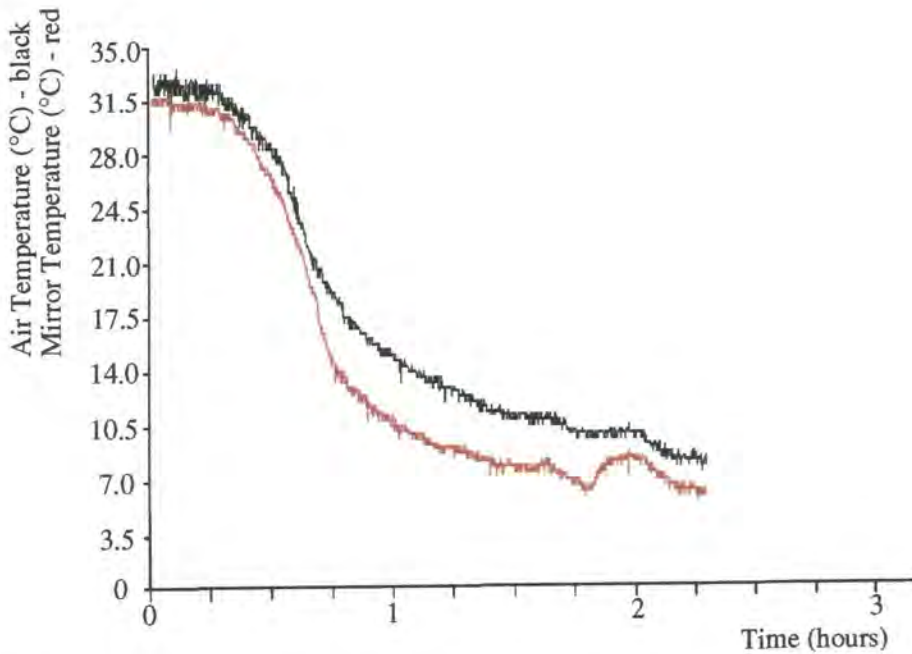
It is possible for water to condense on the mirror surfaces and then freeze when mirror temperatures drop below 0°C, causing scattering and a loss of reflectivity in the mirror surfaces and a premature end to an observation. Because the mirror surfaces are coupled to the cold sky and the thermal conductivity of the honeycomb structure of the mirror is low this may happen at air temperatures up to 3°C above freezing. Although air temperature rarely falls below freezing at Narrabri, it often reaches 2-3°C in winter, so freezing of the mirrors occurs frequently. Unfortunately, this freezing occurs under clear skies, otherwise ideal for observing. Figure 5.9 shows the relationship between mirror surface and air temperatures during a clear winter night.

The freezing problem has been exacerbated by the installation of the baffles around the mirrors. As well as reducing background light, baffles keep the air still at the mirror surface, allowing it to cool to below the ambient temperature, due to reduced mixing of the air.

Attaching heating elements to the back surface of the mirror has been investigated and found to be an unsatisfactory method of supplying heat to the mirror surfaces, due to the low thermal conductivity of the mirror structure.

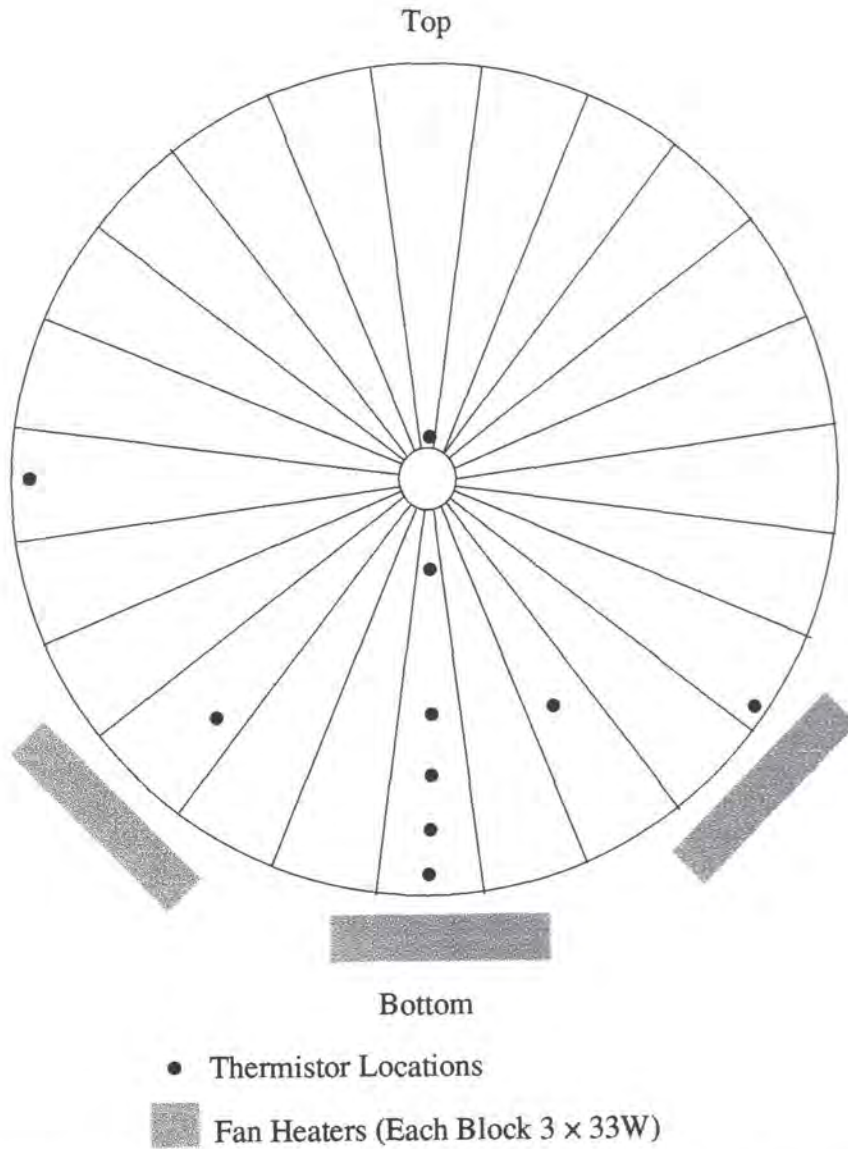
In April 1997, experiments were carried out to investigate the effects of heating and/or moving the air at the surfaces of the mirrors. A number of small fan heaters were installed around half of the circumference of the right hand mirror of the telescope. These were used to provide a continuous flow of air above ambient temperature across the face of the mirror. Thermistors were used to measure mirror temperatures at various positions on the dish, as shown in figure 5.10. Control temperatures were also measured on the surfaces of the two unheated mirrors.

Mirror temperatures were recorded at regular intervals from dusk through the early part of a number of observations made under clear and stable weather conditions. Figure 5.11 shows that, prior to the application of heating, the surface temperature of the right mirror tracks that of the left dish. During the observation, the fans and heaters were switched on. From this point, temperature measurements were made more frequently. The unheated mirror continues to cool at a relatively constant rate. The heated mirror increases in temperature by between 0°C and 2°C and is maintained at a constant temperature for a further hour. The small peak seen in both temperature curves at approximately 2215EST has been attributed to a slight breeze which is recorded in the meteorological data for the evening.



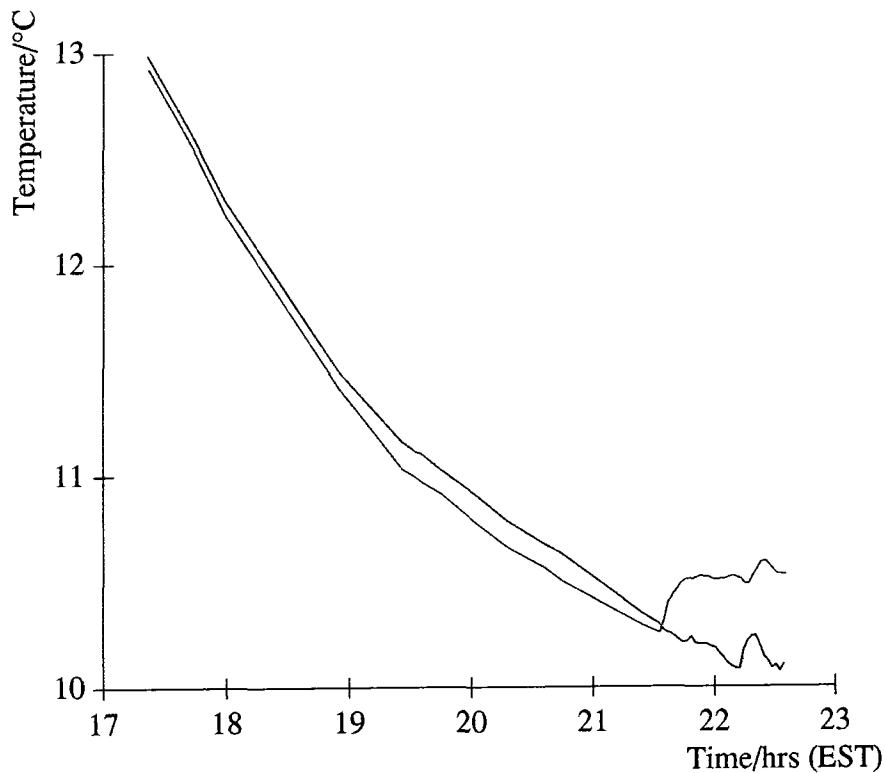
*Figure 5.9 Relationship between mirror and air temperatures at the start of an observation. The mirror temperature (red track) normally falls at the same rate as the air temperature, but stabilises at approximately 3°C below the ambient temperature.*

Figure 5.12 shows the result of removing the heating effect. Temperatures were measured approximately 1 metre from the bottom of the left and right mirrors of the telescope from just before dawn following an observation, when mirror temperatures are expected to be at a minimum. At the start of the test, the difference between mirror temperatures is seen to be  $-0.5^{\circ}\text{C}$ . At 0515 (EST) the heaters facing the right dish were switched on. The temperature of the heated mirror rises initially, then cools at approximately the same rate as the unheated mirror until 0620. At this point, both mirrors begin to warm due to the sun. At 0640, the heaters were switched off and the right mirror temperature drops quickly, stabilizing when the temperature difference between the mirrors is  $<0.5^{\circ}\text{C}$ . This process takes less than 10 minutes. At the end of the test, the right mirror temperature is seen to be warmer than the left mirror, the reverse of the case before dawn. This can be attributed to the fact that trees close to the left mirror of the telescope (when parked) shield it from the rising sun more efficiently than the right mirror.



*Figure 5.10 Locations of thermistors and heaters during the heating test, as viewing the front of the right mirror of the Mark 6 telescope. The heaters were mounted on the telescope structure, approximately 1 metre in front of the mirror surface.*

The temperature changes due to heating were also measured at different distances from the centre of the mirror in order to determine whether a system of this design (power dissipation  $9 \times 33\text{ W}$ ) is capable of increasing the temperature across the whole mirror. Figure 5.13 shows the temperature variations at a number of points on a mirror exposed to the heater/fan systems. The result shows that, as expected,



*Figure 5.11 Thermistor measurements of temperatures of the left and right mirrors. Warm air was driven across the surface of the right mirror (black) from 2100EST. A slight wind caused the temperature peak seen at approximately 2215EST.*

the heating effect is reduced towards the centre of the mirror. It appears that heaters mounted at the edge of the collector are not capable of increasing the temperature of the centre of the dish. They do, however, reduce the rate at which the mirror surface cools. This means that, even if freezing cannot be completely prevented, it may be possible to delay the onset and increase the operation of the telescope by up to two hours in a clear night.

It therefore appears that time lost due to mirrors freezing could be significantly reduced by the introduction of systems to heat and circulate the air at the mirror surface. The temperature of the perimeter of the mirror can be kept constant by the use of such a low dissipation system. At the centre of the dish, the heating effect is less, but the reduced cooling rate will delay the onset of freezing. The process described is dynamic and must be applied continually throughout the observation. If the heating process is stopped, the heating effect is lost within 20 minutes. If

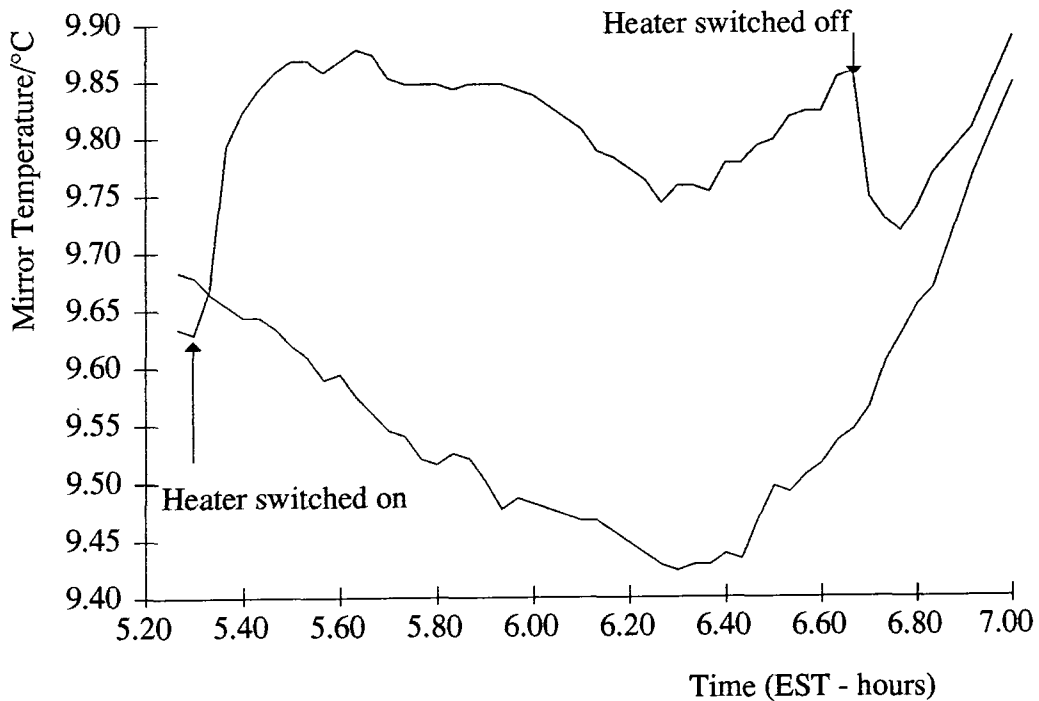


*Figure 5.12 The result of stopping the supply of warm air to the right mirror. The effect of turning on the heaters on the right mirror (red track) is seen, followed by continued cooling. Once the temperatures begin to rise after dawn, the right mirror temperature tracks that of the left mirror (black track) more closely.*

heat is applied in this way, requiring a total input of 2.5 kW (8 sets of  $3 \times 33$  W heaters per mirror), the suggestion is that a shutdown enforced by freezing could be delayed by up to two hours. Over the course of a winter month, freezing may curtail observations on between 7 and 10 nights. Increasing observations by around 2 hours per night would correspond to an increase in the monthly data taken in excess of 20% in a winter month. This corresponds to a potential increase of 5% of the total data taken per year.

A complete installation of heaters and fans on one mirror during a winter month to investigate the heating effects at low temperatures and to quantify the delay in freezing must still be carried out.

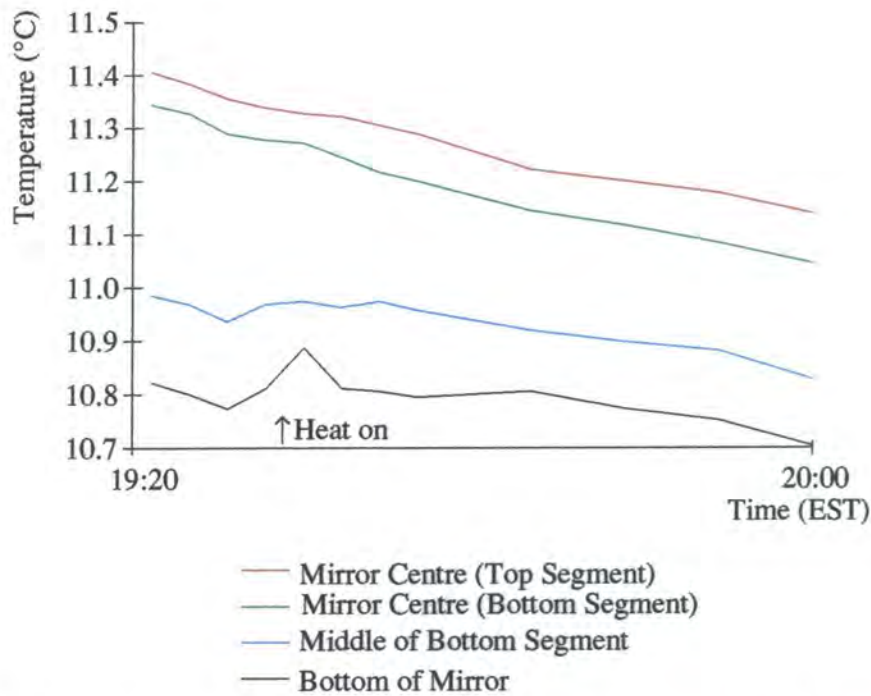


*Figure 5.13 Temperature measurements made at various points across the surface of the right hand mirror. Heating was applied for a short period at the base of the mirror. The mirror temperature is seen to rise at points up to 3.5 metres from the heaters. There is some evidence for a slowing of the cooling process at the centre of the mirror.*

The final engineering of such a system (including weather proofing of the fans) remains to be developed. Future development of the telescope, discussed in chapter 7, include resurfacing the flux collectors. This would allow heating elements to be installed inside the mirror, in contact with the front (reflective) surface and this may well be the most effective and convenient solution.

A recent (June 1998) investigation involved driving heated unducted air onto the back of one of the Mark 6 telescope flux collectors. A 35 kW industrial heater was situated on the ground under one of the collectors as the telescope tracked an object across the sky. As the air rose, the mirror was heated by about 4°C, to the extent that both mirror misting and freezing were prevented. A subsequent test will involve the installation of ducts to carry air directly to the back of all of the mirror surfaces to assess the possibility of incorporating such a system into routine telescope operations.

## 5.5 Conclusions

In the two years since its construction, efforts have been made to improve the operation of the Mark 6 telescope in three principal ways; reduction of the energy threshold, improved identification of low energy events and an increase in the telescope duty cycle.

The energy threshold of the telescope has been reduced by improving the efficiency of the light detection and by noise rejection measures including albedo rejection baffles. Further reductions may be possible if field tests of an analogue triggering system are successful.

The duty cycle of the telescope is a limiting factor in the amount of data recorded. The procedures used to minimize the effects of misting on the mirror surfaces are described. Investigations of methods to reduce time loss due to mirrors freezing have been made. Initial results suggest that the duty cycle in winter months may be increased by more than 20% by delaying the onset of freezing by use of systems to heat and circulate the air at the mirror surfaces.

## Chapter 6. Stereo Techniques in Ground Based Gamma-Ray Astronomy

### 6.1 Introduction

The light pool generated at ground level by a Cherenkov flash with its height of maximum light in the upper atmosphere is greater than 100 metres in diameter. It is therefore possible for the light pool produced by an individual primary to be detected by more than one telescope if the instruments are suitably separated from one another.

It is possible that such observations using multiple telescopes - stereoscopic studies - may provide a method of identifying those cascades initiated by gamma-ray primaries. In particular, such observations may provide more information than is available in observations using a simple telescope comprising a single detector package

In this chapter, the methods by which observations using two gamma-ray telescopes with low-resolution imaging capabilities can identify showers induced by gamma-ray primaries are discussed. The operation of the Durham Mark 3A and Mark 5A telescopes at Narrabri as a stereo pair was reported in Chadwick *et al* (1996) and is reviewed, including the results of observations of the cataclysmic variable AE Aquarii.

Development of an analysis of data acquired with the Mark 6 and Mark 5 telescope pair has been performed and is discussed. Analyses of data taken during observations of Cen X-3 with the Mark 5/Mark 6 stereo pair and with the Mark 6 telescope alone are reported. The utility of the Mark 5 telescope as a stereo counterpart to the Mark 6 telescope is discussed.

This use of stereoscopic measurement data is distinct from imaging stereo measurements such as those made using the HEGRA array of telescopes (Daum *et al.*, 1997) and proposed for the VERITAS system (Finley, 1998). Such systems are designed to discriminate between gamma-rays and background events by means of the higher order moments of the images and require high resolution capabilities in all telescopes. The methods described in this chapter can use data from low-resolution instruments such as the Durham Mark 3A and Mark 5A telescopes.

## 6.2 Event Parameterization Using Two Widely Spaced Telescopes

The analyses reported here involved the interpretation of the lower moments of a Cherenkov light flash as recorded in two or more simple telescopes with  $0.5^\circ$  pixel imaging. Only two quantities need to be measured for this analysis, the total amount of Cherenkov light (the zeroth moment) and the position of the centroid of the image within the field of view of the camera (the first moment) at each telescope. From these quantities, the parameters described below can be derived. Because higher order moments of the Cherenkov image are not used in these measurements, the observations do not require high resolution ( $\leq 0.25^\circ$  pixels) images; they are perfectly possible with data from medium resolution, low-cost, cameras such as the ones in the Durham Mark 3A and Mark 5A telescopes.

The position of the image centroid is obviously affected by the loss of light which falls outside the detector. This image truncation would result in inaccurate positioning information if not avoided or corrected. The centre of the measured image is closer to the detector centre than that of the complete image. The position of the image centroid is evaluated by applying corrections to the components of the first order moments of the image thus:

$$X_{CG} = \bar{x} \left( 1 + \frac{\exp(dist/1.48)^{3.6} - 1}{dist} \right)$$

(and similarly for  $Y_{CG}$ ) where  $X_{CG}$  is the corrected component of the image position,  $x$  is the uncorrected component and  $dist$  is the distance of the centroid from the centre of the field of view (Orford, private communication). This relationship is based on simulation work by Orford.

The correction is derived, making the assumption that the primary of the cascade is a gamma-ray photon. If this is not the case, then, as shown in section 2.3, the shower development shows greater fluctuations. As a result, the subsequent treatment may lead to a meaningless and possibly non-physical result for the derived parameter and the event being classified (correctly) as 'non-gamma ray like'.

### 6.2.1 The Geometric Height of Maximum ( $H_0$ )

The height of maximum of Cherenkov light ( $H_0$ ) of a shower is the altitude at which the light produced by the cascade process maximizes. For gamma-ray induced showers, it is a weak function of the energy of the primary gamma-ray. The related quantity, depth of maximum light ( $D_{max}$ ), is a measure of the column

density of the atmosphere through which the cascade develops before maximum light is produced. The depth of maximum light is related to atmospheric quantities including pressure and water vapour content and is a function of the energy of the primary gamma-ray. It is measured from the top of the atmosphere downwards. An empirical relationship between depth of maximum light and energy of a primary gamma ray is

$$D_{max} = 300 + 37.4 \ln((E_0/300)^{-2}) \text{ g cm}^{-2}$$

(Orford, private communication). For a well defined atmosphere,  $D_{max}$  and  $H_c$  have a singular relationship.

From knowledge of the pointing directions of both telescopes and the positions of the centroids of the images in both cameras, it is possible to reconstruct the lines-of-sight from both telescopes to the point at which the Cherenkov flash maximized. The height of maximum light is defined as the altitude at which these two lines intersect or make their closest approach.

Simulation data indicate that events recorded at zenith angle of  $30^\circ$  from 0.3-1.0 TeV gamma-ray primaries have a height of maximum light distribution centred in the range 8.8-11.5 km. Events with hadron primaries have a wider distribution. Figure 6.1 shows the  $H_c$  distribution for simulated gamma-ray events and for measured background events from off-source observations in the Cen X-3 observation discussed in section 6.6. The  $H_c$  distribution for the hadronic background is seen to extend to higher values due to the poorer definition of the shower path as described above.

The height of maximum light of a shower varies systematically with primary energy - more energetic primaries penetrate the atmosphere further before a cascade is initiated. This results in the range of values seen for  $H_c$  in figure 6.1. Such variation reduces the efficiency of any selection applied without consideration of the energy of the primary on the basis of this parameter, due to the significant overlap between the source and background distributions.

### 6.2.2 Image Centroid Separation ( $D_{miss}$ )

It is possible to account for systematic changes in  $H_c$  as a function of primary energy and hence to improve the analysis, by calculating the predicted position of a shower image in one telescope based on its measured image in the other. The separation of the predicted and measured image centroids in the second telescope yields the parameter  $D_{miss}$ .

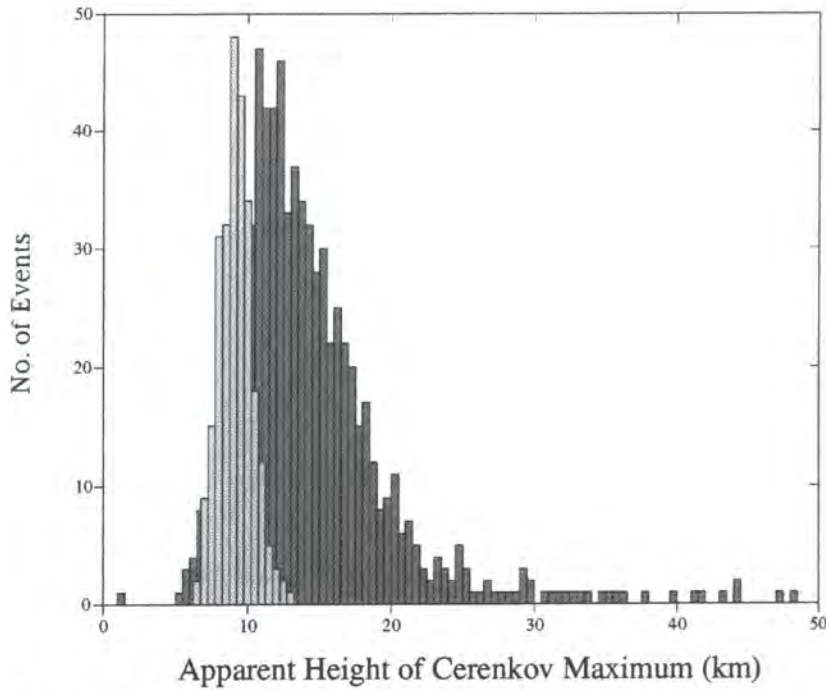


Figure 6.1 Distributions of height of maximum light for showers resulting from simulated gamma rays (light grey) and the measured hadronic background (dark grey).

The  $D_{miss}$  parameter is calculated by the following procedure:

- (1) A line in space is constructed from telescope #1, through the image centroid to give the direction to the shower maximum.
- (2) On the basis of the measured centroid position, derive the impact parameter (the distance between the telescope and shower core). This is then used in conjunction with the total amount of measured light to determine the primary energy of the initiating particle, *based on the assumption that it is a gamma ray*. From this, a value for the expected depth of maximum light is derived on the basis of simulation results.
- (3) The calculated depth of maximum light and the direction of the shower define the point in space where the light maximized. The shower axis in telescope #1 can now be redefined based on the position of shower maximum. The primary energy of the initiating particle is recalculated using the new value of the impact parameter of the shower. This process may be repeated as necessary until convergence.
- (4) A line drawn between the position of the light maximum and telescope #2 provides a prediction of the location of the image centroid in this telescope, *assuming a gamma ray primary*.

(5) The difference between predicted and actual centroid positions in telescope #2, measured in degrees, is  $D_{miss}$ .

For gamma-ray induced events,  $D_{miss}$  is expected to be close to zero. For hadron induced showers, the relationship between impact parameter and amount of light measured is less well defined than for gamma ray events. Therefore, the distribution for background events is expected to extend to larger values of  $D_{miss}$  as shown in figure 6.2.

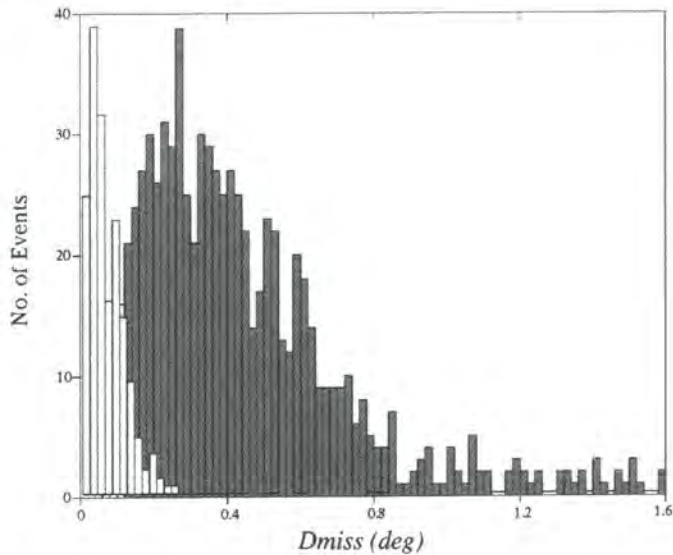


Figure 6.2 Distributions of  $D_{miss}$  for simulated gamma rays (light grey) and measured hadron initiated showers (dark grey).

### 6.2.3 Primary Energy Ratio ( $R_{ep}$ )

The ratio of measurements of the primary energy of a shower made in two telescopes is another measure which is sensitive to the primary of the cascade. For each telescope, the energy of the primary is derived based upon the amount of light measured.

The calculation of the primary energy on the basis of the measurement for each telescope requires an understanding of the relationship between measured number of digital counts (QT bits) and primary energy and how this relationship is affected by the *distance* parameter. For images with large values of *distance*, some light may be lost outside the camera. Furthermore, the 'Cherenkov shoulder' effect demonstrated in figure 2.4 affects the relationship between primary energy and measured digital counts. The measured number of digital counts is modified to account for this relationship and some estimation of the light loss outside the camera.

The primary energy ratio ( $R_{ep}$ ) is simply these ratio of the two measures, expressed so that the value always lies between 0 and 1. As the development of gamma ray induced showers is symmetric about the axis and uniform to distances in excess of 100 m from the axis, it is expected that  $R_{ep}$  will be  $\sim 1.0$  for these showers. For hadron induced showers, the development is more varied, and distance does not provide a good measure of the impact parameter, since the arrival direction is unknown. This means that the correlation between the amount of light detected and the primary energy is reduced with the result that  $R_{ep}$  is not well defined as expected and values cover the complete range from 0.0 to 1.0. Figure 6.3 shows simulated values of  $R_{ep}$  for gamma ray and hadron induced events. The peak in the lowest bins for the real events is a result of events for which the shower image lies at the edge of the camera of one or both telescopes and it is impossible to make an accurate estimate of the total light content of the image.

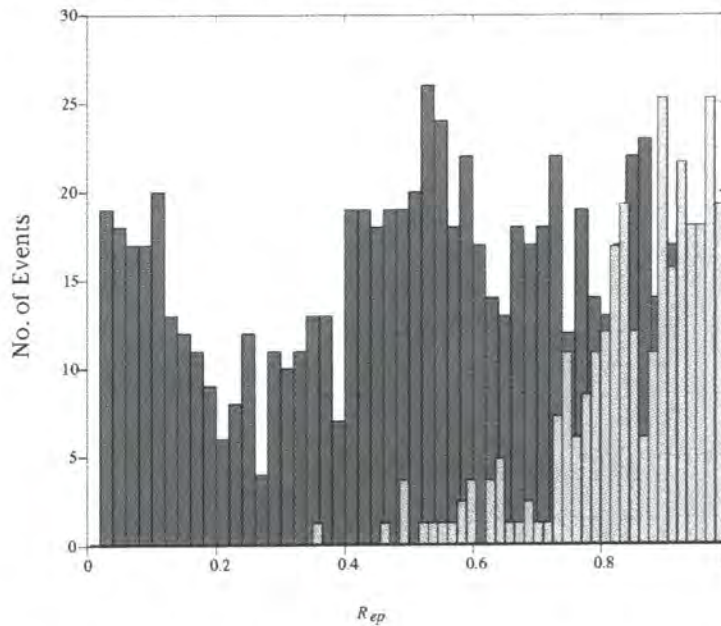


Figure 6.3 Primary energy ratio ( $R_{ep}$ ) distributions for simulated gamma rays (light grey) and hadron induced events (dark grey).

There therefore exists the possibility of using one or more of these stereoscopic parameters as a means of rejecting background events and enhancing any gamma ray signal in a dataset.

These procedures, involving low resolution images, should not be confused with the interpretation of multiple high-resolution images, which forms the basis of numerous experiments under proposal and construction (e.g. VERITAS (Finley, 1998), HESS (Hofmann, 1998)).

## 6.3 Stereo Observations Using the Durham Mark 3A and Mark 5A Telescope Pair

The Durham Mark 3A and Mark 5A telescopes are described in Holder (1997) and Dickinson (1995) respectively. The telescopes are similar in terms of mirror area, limited imaging capability and are separated by 100 metres in an east-west direction. Triggering of each telescope occurs individually at a rate of  $\sim 2$ Hz, of which about 45% are common to both telescopes. This fraction changes little with zenith angle from  $0^\circ$  to  $60^\circ$ .

The Durham telescopes are operated independently of one another, in accordance with the procedures discussed in chapter 3. An event is recorded when the 3-fold coincidence requirements of the individual telescope are satisfied. Datasets are extracted from the records by offline examination of the event times as recorded by the individual telescopes. A stereo event, defined as a light flash which satisfies the triggering conditions in both telescopes, is deemed to have occurred if the individual telescopes record events within a predefined time interval of  $10 \mu\text{s}$ . Datasets are produced for the individual telescopes containing only those events which have a counterpart recorded in the other telescope. These events have a sixfold spatial coincidence requirement and are therefore free of accidental coincidence events.

The images formed in the individual telescopes can be used together to reconstruct the shower and determine its axis and the energy of the initiating primary as described in section 6.2. Typical stereo events, as recorded by the Mark 3A and Mark 5A telescopes are shown as grey scale schematics in figure 6.4. Figure 6.4(a) shows the images of a shower whose axis passed almost equidistant from the two telescopes. The images in figure 6.4(b) were produced from a shower falling much closer to the Mark 5A telescope.

### 6.3.1 Observations of the Cataclysmic Variable AE Aquarii

Observations of the cataclysmic variable AE Aquarii were made on the 11th October, 1993, using both the Durham Mark 3A and Mark 5A telescopes. Analysis of the data recorded by the individual telescopes showed a burst of events with a periodicity consistent with the 2<sup>nd</sup> harmonic of the White Dwarf rotation period. The burst lasted for 4200 seconds (Chadwick *et al*, 1995).

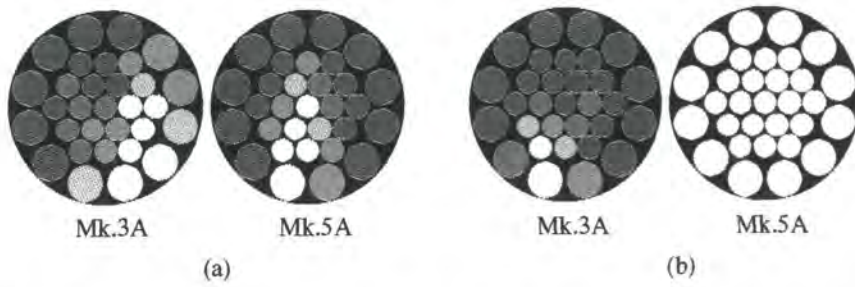


Figure 6.4 Grey scale representation of typical stereo events recorded by the Durham Mark 3A and Mark 5A telescopes (from Chadwick et al., 1996).

A total of 5038 events were observed in one or other (but not both) of the telescopes. A periodicity, at 16.477 seconds, was observed in these events with a chance probability of  $10^{-3}$ . This corresponded to a signal strength for gamma-rays of 3.7% of the cosmic ray background. These data were subject to conventional imaging analyses as applied to data from medium resolution instruments. The process retained 72% of the candidate gamma rays, while rejecting 77% of the background, a Q-factor of 1.5. The probability that the periodicity in the data of the outburst after enhancement was due to chance reduced to  $6 \times 10^{-7}$ .

A dataset of events triggering both telescopes was formed which was independent of the data used for the above result. A total of 2786 events were common to both telescopes during the outburst. Prior to any enhancement, these independent data showed a pulsed signal strength of 4.5% of background, with a chance probability of  $3 \times 10^{-3}$ .

Figure 6.5 shows the differences between the on- and off-source distributions of the various stereo parameters for the pulsed events. The excess is shown to be concentrated in a region described by  $\log(R_{ep})$  in range -0.5 to 0.5,  $D_{miss} < 0.2$  and  $H_c$  between 7.5 and 15km. This is consistent with the behaviour of gamma-ray events as described above.

### 6.3.2 Limitations of the Durham Mark 3A and Mark 5A Telescopes as a Long Baseline Stereo Pair

The utility of long baseline stereo observations made with telescopes separated by  $\sim 100$  metres is limited primarily by the pointing accuracy of the telescopes. In 1993, the Durham Mark 3A and Mark 5A telescopes had relative pointing accuracies of  $0.1^\circ$  and absolute accuracies of  $< 0.1^\circ$ , resulting in an overall uncertainty in image cross-correlation of  $0.15^\circ$ . This has subsequently been

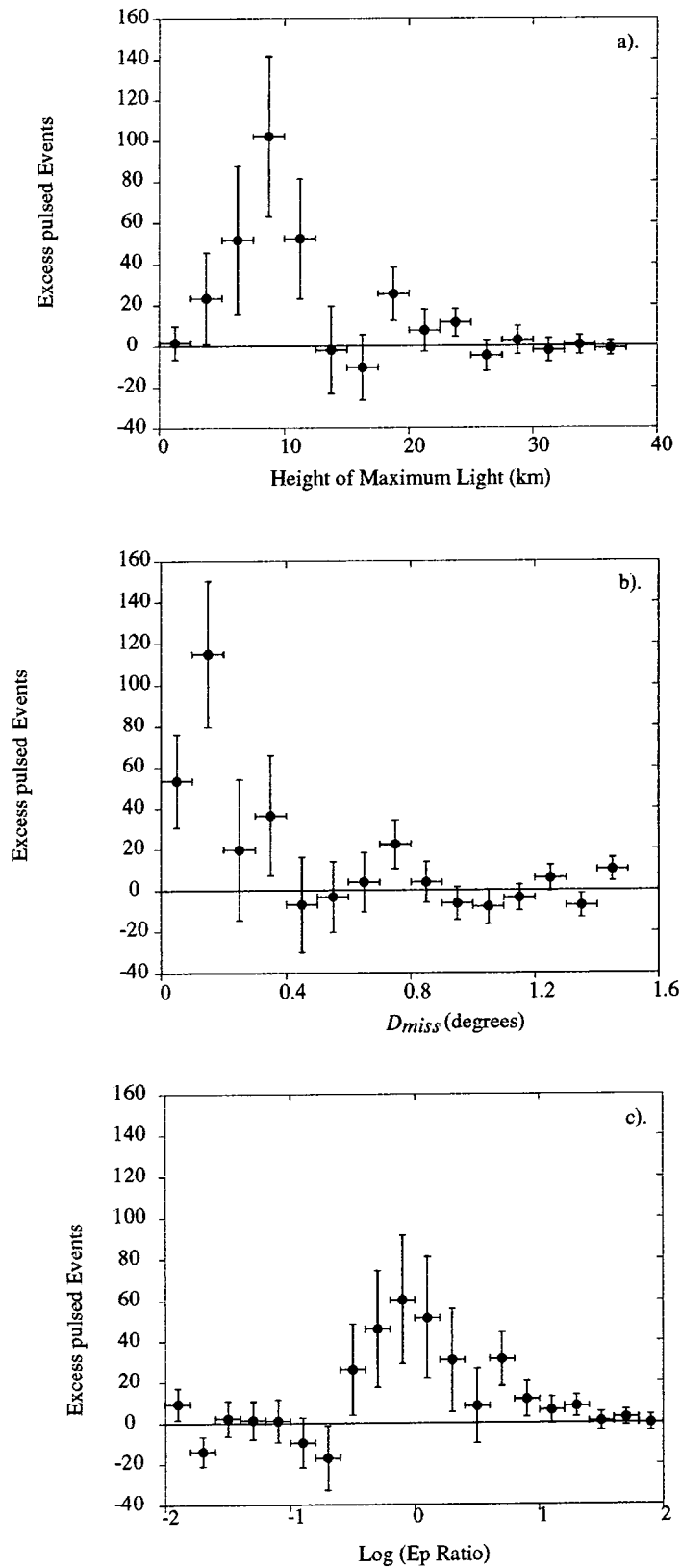


Figure 6.5 Distributions of the three stereo parameters for the excess pulsed events from the AE Aquarii dataset (taken from Chadwick et al., 1995)

significantly improved by the incorporation of information from the paraxial CCD camera. The  $D_{miss}$  distribution for gamma rays shown in figure 6.2 requires a measurement accuracy much better than this if it is to be exploited. Consequently, the full power of the  $D_{miss}$  parameter cannot be used by low resolution telescopes. Examination of the  $x$ - and  $y$ - components of the  $D_{miss}$  distribution in the focal plane allows corrections to be made to ensure that each has a mean value of zero. This means that the uncertainty can be reduced to  $\sim 0.08^\circ$ . Further improvements have since been made with the implementation of CCD cameras on both telescopes as described in chapter 3, allowing  $D_{miss}$  to be determined to sufficient accuracy to be fully used in any further observations.

#### 6.4 Adapting Stereo Techniques to Data from the Mark 5A and Mark 6 Telescope Pair

The utility of stereo observations in enhancing data from two similar, small, low resolution telescopes has been demonstrated. The construction of the Durham Mark 6 telescope in 1994 afforded the opportunity to investigate the use of long baseline stereo parameters where the two telescopes are significantly different in terms of size, energy threshold and imaging resolution.

The separation of the Mark 5A and Mark 6 telescopes is similar to that of the Mark 3A and Mark 5A telescopes ( $\sim 80$  m), also along an approximately east-west baseline. The Mark 6 telescope is capable of measuring more information about a cascade image than the Mark 5 telescope due to the increased light collecting area and improved resolution of the imaging camera.

#### 6.5 Analysis of Mark 6 Telescope Data from Centaurus X-3

Centaurus X-3 is a high mass accreting X-ray binary containing a 4.8 second period pulsar orbiting an O-type supergiant. VHE gamma rays (TeV) have been observed from this source (Carraminana *et al.*, 1989; Raubenheimer *et al.*, 1989; Brazier *et al.*, 1990). A GeV gamma ray outburst was also detected by the EGRET instrument on the *CGRO* at 100 MeV (Vestrand, Sreekumar and Mori, 1997).

Centaurus X-3 was observed using the Durham Mark 6 telescope in March and June, 1997 (Chadwick *et al.*, 1998b) and the results are reviewed here. The Durham Mark 5A telescope was also used during the March observations and a discussion of the distributions of the stereo parameters is presented in the next section.

Centaurus X-3 was observed using the Durham Mark 6 telescope on March 1, 3 and 4 and June 1, 2, 4, 5 and 7, 1997 for typically 3 hours per night. Many observations were targetted to be close to orbital phase 0.8 relative to the X-ray eclipse, where TeV emission has been previously detected. Data were taken in alternate 15-minute on- and off-source segments. For the on-source observations, the telescope was pointed such that the source was close to, but not at, the centre of the camera, to avoid any biases that may be introduced by camera symmetries.

Data were analysed only for segments where the sky was clear and stable and where the total number of events in the on- and off-source segments were within  $2.5\sigma$  of one another. These requirements produced a dataset of 10 hours of on-source data. These data were calibrated for gains, pedestals and CCD positioning and 'software padded' as described in chapter 3.

Prior to the application of gamma ray selection measures, low brightness images and those whose centroids lie close to the camera edge ( $>1.1^\circ$  from the camera centre) are removed from the dataset, as these do not respond well to parameterization. After application of this procedure, known colloquially as 'tidying', there were 64713 on-source events and 65171 background. This corresponds to a source deficit of 458 events ( $1.3\sigma$ ).

Image parameters were derived for the Mark 6 telescope data using standard 'image and border' techniques. The parameters used in selection were *BRIGHTNESS*, the total number of digital counts in the image, image *ECCENTRICITY* (width/length),  $D_{dist}$ , the single telescope analogy to the stereo parameter  $D_{miss}$ , described in section 6.3 and the Hillas parameters *DISTANCE*, *ALPHA* and *WIDTH*, as discussed in chapter 3. Gamma ray selection was carried out based on the following parameter limits.

1.  $800 > BRIGHTNESS/digital\ counts > 20000$ . 1 digital count corresponds to 0.5GeV.
2.  $0.3 < ECCENTRICITY < 0.8$ . This is required to allow accurate estimation of *ALPHA*.
3.  $0.35^\circ < DISTANCE < 0.75^\circ$ . The lower limit allows shower images to become elongated while the upper limit reduces camera edge effects.
4.  $D_{dist} < 0.07^\circ$ .
5.  $WIDTH < 0.28^\circ$ .

The application of these parameter limits produce a dataset comprising 4429 on-source events and 4087 off-source. The 342 event excess has a 3.7s significance. The difference in the *ALPHA* distributions of the on- and off-source distributions is shown in figure 6.6. This shows that the excess is concentrated at small values of *ALPHA*, which is consistent with the expectation from a true gamma ray source. Imposition of an upper limit of 30° on *ALPHA* leaves 1546 on-source events and 1208 off-source. The excess is significant at the 6.4s level ( $338 \pm 52$  events). The 30° upper limit for rejection of events based on *ALPHA* is currently common to all sources observed with the Mark 6 telescope. It is believed to be due to image distortion in the detectors as a result of spreading of images in the direction of the transverse component of the geomagnetic field (Chadwick et al, 1999b)

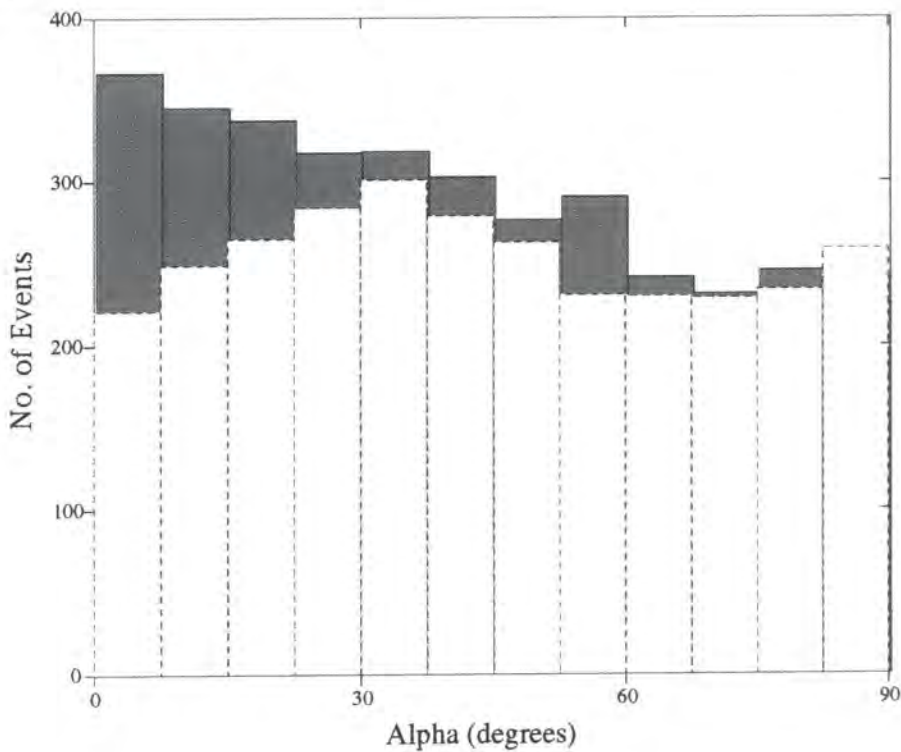
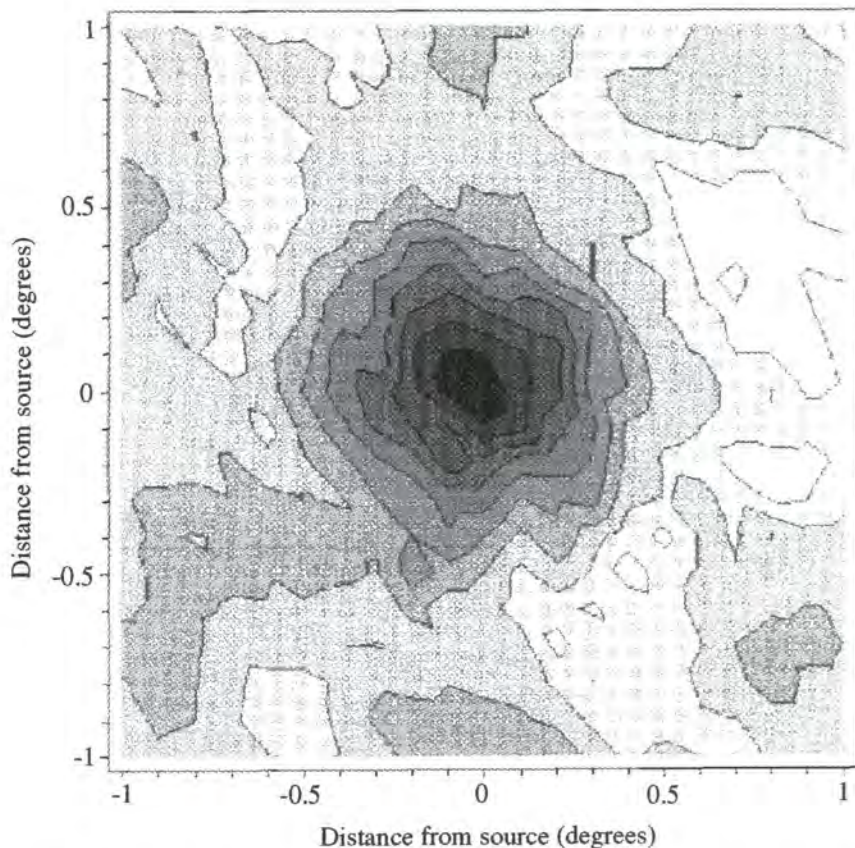


Figure 6.6 Difference between *ALPHA* distributions of on- (dark grey) and off-source (light grey) events after application of gamma ray selecting cuts.

A false source analysis, as described in chapter 3, has been performed. For each combination of event and putative source position, *DISTANCE* and *ALPHA* are recalculated. The origin of the plot, shown in figure 6.7, corresponds to the position of Cen X-3 and not the camera centre, which is offset by 0.1-0.2°. The result shows that the maximum significance corresponds to the location of the candidate source.



*Figure 6.7 False source analysis showing excess events with  $\alpha < 30^\circ$ . The contours are spaced at  $0.6\sigma$  intervals. The black region, which is colocated with the source, represents an excess of events significant at the  $6\sigma$  level.*

The Mark 6 telescope has therefore been used to identify a population of events which exhibit behaviour of the high resolution image consistent with that expected from gamma-ray induced showers. This allows an investigation to be carried out into the usefulness of the Mark 5A and Mark 6 telescopes as a stereo pair.

## 6.6 Observations of Centaurus X-3 using the Mark 5A and Mark 6 Telescopes

Centaurus X-3 was observed using both the Durham Mark 5A and Mark 6 telescopes on March 3 and 4, 1997. All observations were made with both telescopes working in the 'ON/OFF/OFF/ON' mode with each interval being 15 minutes. The leading and trailing off source fields were used alternately as background, so minimizing residual secular effects.

Both telescopes recorded data samples as follows:

03/03/1997	7 ON/OFF pairs
04/03/1997	4 ON/OFF pairs

### 6.6.1 Analysis Procedures

The dataset contains 2.75 hours of on-source data. For these observations, the data from the two telescopes were stereo matched by identifying and selecting events recorded by both with timestamps within 10 microseconds of each other. The stereo parameters developed for the Mark 3/5 pair of telescopes, addressed in section 6.2, were then calculated for each of these events. In deriving these parameters, the data from the Mark 6 telescope and its high resolution camera are of much greater accuracy.

A procedure has been developed to remove events for which one or more of the parameters lie outside physically reasonable bounds. The criteria for rejection were;

(a)  $R_{ep}$  less than 0.2.

Figure 6.8 shows the relationship between  $R_{ep}$  and *DISTANCE* (image centroid-camera centre), as recorded by the Mark 6 telescope.  $R_{ep}$  is only a meaningful measure if the images of the shower are neatly contained within the cameras of both telescopes. A very small value of  $R_{ep}$  suggests that some of the light forming the shower image may have fallen outside one camera, particularly for events with large values of *DISTANCE*. Small values of  $R_{ep}$  are indeed shown to correlate with large values of *DISTANCE*. This selection of events, on the basis of  $R_{ep}$ , is therefore analogous to the rejection of events with large values of *DISTANCE* as applied in the analysis of imaging telescope data.

(b)  $H_c$  greater than 25 km.

For large values of  $H_c$ , the paths joining the telescopes to the shower maximum are almost parallel and therefore small uncertainties in pointing accuracy can translate into very large variations in inferred height of maximum. A maximum value of  $H_c$  has been chosen such that it is well into the high value 'tail' of the distribution. Since very few genuine events are expected with such heights, it is likely that the events discarded as a result of this limit are subject to large measurement errors.

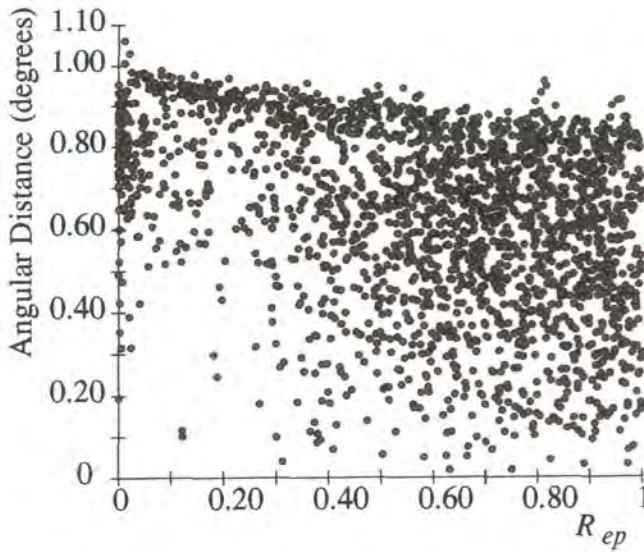


Figure 6.8 Angular Separation between image centroid and camera centre for events recorded by the Mark 6 telescope as function of  $R_{ep}$ .

(c)  $D_{miss}$  greater than 1.0 degree.

The distribution of  $D_{miss}$  values is similar for both on- and off-source fields, as shown in figure 6.9. The only preliminary processing performed on the basis of this parameter is to reject a few (<1%) events with  $D_{miss}$  values greater than  $1.0^\circ$ . These events are seen to lie well outside the standard distribution shown in figure 6.9 and are unlikely to be accurate parameterizations of the showers they represent.

Figure 6.9 shows the distributions of the stereo parameters for the on-source and background observations for the March dataset after application of these selection criteria. Figure 6.10 shows the differences between the two sets of plots.

### 6.6.2 Discussion of Results

The complete dataset for the 2.75 hours of observation on the two nights was considered. The expected distributions for gamma-ray and hadron induced events, shown in figures 6.1, 6.2 and 6.3 suggest that 4 possible parameter limits should be applied to the dataset in order to enhance any gamma-ray signal;

1. An upper limit on  $D_{miss}$ ,
2. An upper limit on  $H_c$ ,
3. A lower limit on  $H_c$ ,
4. A lower limit on  $R_{ep}$ .

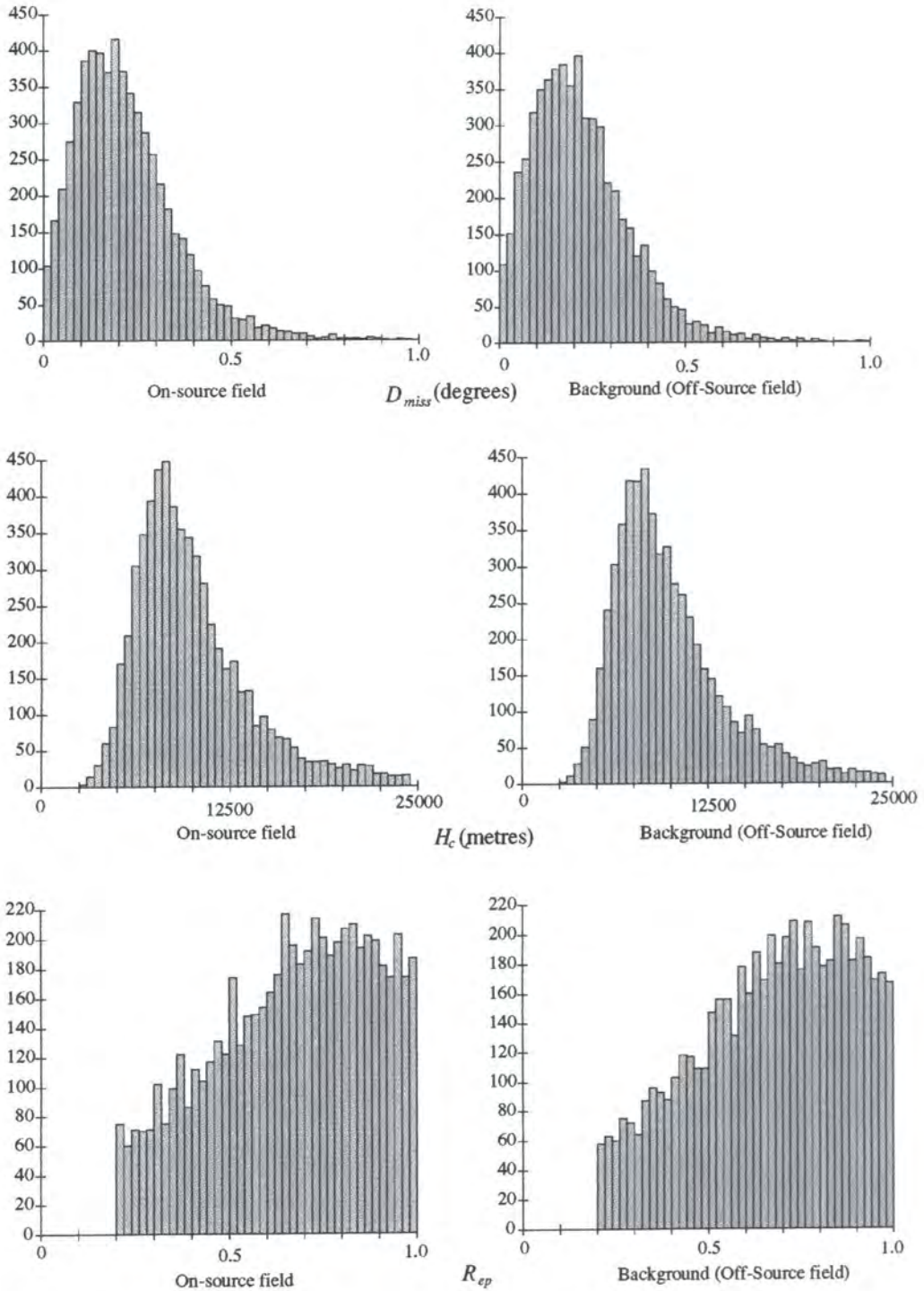


Figure 6.9 Distributions of stereo parameters for the Cen X-3 dataset taken on March 3 and 4, 1997.

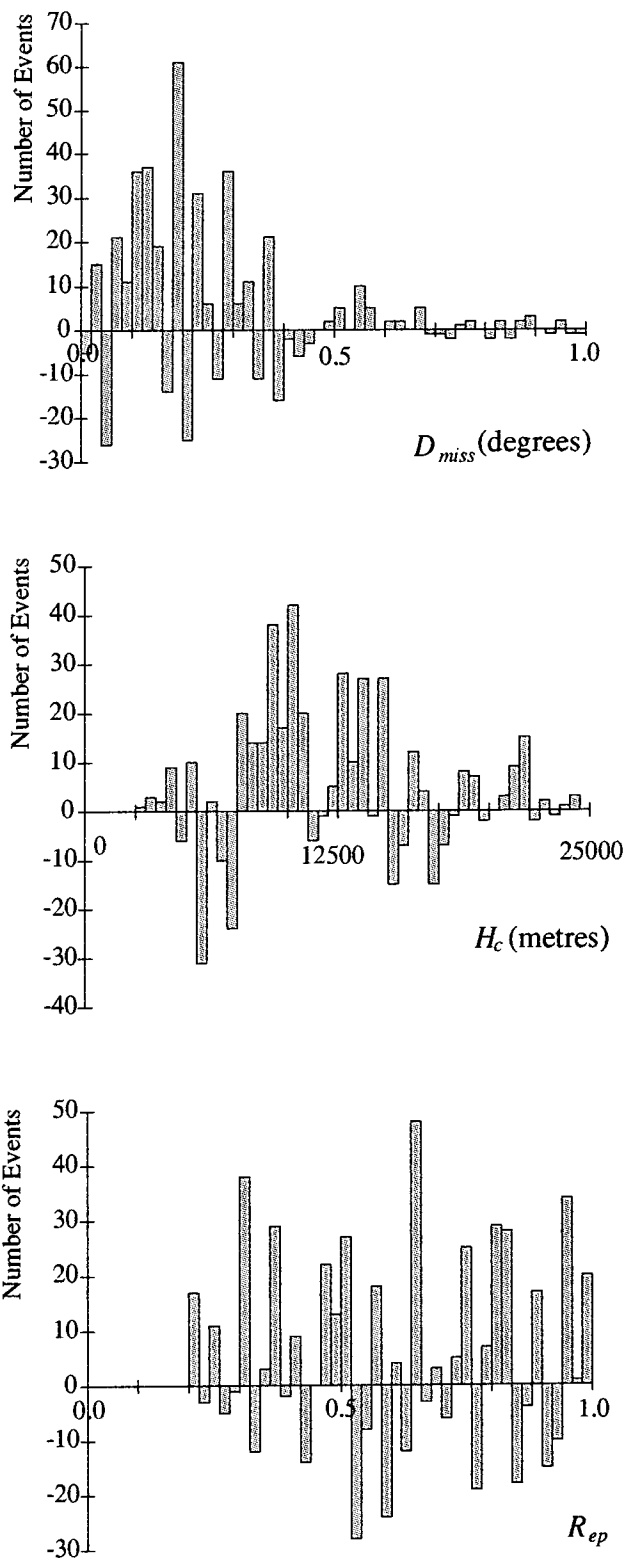


Figure 6.10 Differences between on- and off-source stereo parameter distributions for Cen X-3 data taken on March 3 and 4, 1997.

$D_{miss}$  and  $H_c$  are dependent on the zeroth and first order moments and are related to one another. The height of maximum light distribution for gamma-ray induced events lies in the middle of that for the hadronic background. However, gamma-rays are expected to result in images with smaller values of  $D_{miss}$  than the background.  $D_{miss}$  is also the more robust of the two parameters (it does not have a residual variation with primary energy).  $R_{ep}$  is derived only from the zeroth order moments of the two images. It is therefore to be expected that  $R_{ep}$  and  $D_{miss}$  provide the best combination of independent measures to enhance any gamma-ray signal.

Selection limits were applied at intervals through the dataset for various values of  $R_{ep}$  and  $D_{miss}$ . The optimal choice of parameter limits was defined as that which produced the greatest increase in significance of the size of the excess of on-source gamma-ray candidates. As can be seen from table 6.1, no selection significantly enhances the excess over the background.

	ON	OFF	EXCESS
Raw Stereo events	6552	6306	+242 (2.2 $\sigma$ )
'Tidy' Stereo events	6046	5823	+223 (2.0 $\sigma$ )
$R_{ep} > 0.30$	5156	4952	+204 (2.0 $\sigma$ )
$D_{miss} < 0.20^\circ$	2713	2540	+173 (2.4 $\sigma$ )
$H_c > 7\ 500\text{ m}$	3917	3646	+271 (3.1 $\sigma$ )
$H_c < 21\ 500\text{ m}$	5383	5163	+220 (2.1 $\sigma$ )

*Table 6.1 Numbers of events remaining after the imposition of optimum stereo parameter limits on the March dataset, as described in the text.*

In a further attempt to differentiate between the on- and off-source data, the shapes of the stereo parameters have been considered. The  $\chi^2$  test (Batschelet, 1981) has been used to compare the on- and off-source distributions for each of the three parameters. The results of such tests show no evidence that the on- and off-source distributions are drawn from different parent populations. This is supported by an application of the K-S test to the data .

### 6.6.3 Expectation of a Successful Detection of Gamma-Rays with the Mark 5 and Mark 6 Telescopes

The detection of a strong outburst from AE Aquarii, using stereo parameters recorded by the Mark 3 and Mark 5 telescopes to enhance the signal, was based on a dataset comprising 2784 stereo events. Application of stereo parameter selection to this dataset reduced it to 787 events, after approximately 75% hadronic background rejection. A Rayleigh test applied to the remaining events suggest a pulsed component of 11%, compared to 3.7% in the unselected data. The key to this detection was the strength of the outburst combined with a modest but effective background rejection.

The Cen X-3 Mark 5/6 dataset comprised 6306 off-source stereo events. Rejecting data at the same 75% level as for the AE Aquarii dataset would reduce this to 1577 background events. A detection at the  $3\sigma$  confidence level would require the identification of 173 gamma-ray events against this background, a signal strength of 2.7% of background.

A knowledge of the strength of the Cen X-3 emission is available from the (independent) high resolution imaging data from the Mark 6 telescope. For example, the Mark 6 Cen X-3 dataset after imaging analysis contains 338 candidate gamma rays. Application of imaging selection means that >99% of background are rejected and also approximately 50% of gamma-ray events, so the original dataset (at the 'tidied' stage) can be estimated to contain 676 gamma-rays on a background of ~65000 events. The signal derived from a single telescope imaging analysis is therefore 1% of the cosmic ray background. This is only a third of the signal strength required for a detection at the  $3\sigma$  confidence level on the basis of the simple stereo parameters. It is therefore not surprising that no significant evidence of gamma-ray emission is seen in the data in table 6.1.

It may be that an observation using 2 telescopes inherently rejects a greater number of background events than during a single telescope observation, due to the differences in the distribution of light within the light pool, as described in chapter 2. This would have the effect of enhancing the signal strength prior to the application of any selection procedure. Such an enhancement can indeed be seen by comparing the Mark 5 single telescope and Mark 3/5 stereo datasets for the AE Aquarii outburst. The signal strength in the stereo dataset (4.5%) is a little over twice that in the dataset recorded by the Mark 5 telescope alone (2.1%).

The Mark 5A telescope is much less sensitive than the Mark 6 telescope (background count rates at the zenith  $\sim 350$  minute<sup>-1</sup> and  $\sim 800$  minute<sup>-1</sup> respectively), so it would not be expected to provide the same degree of enhancement as it provides for data taken with the similarly sensitive Mark 3A telescope.

These results suggest that the use of the Mark 5A telescope as a stereo partner to the Mark 6 telescope does not and should not improve the significance of a gamma-ray detection. However, while the Mark 5A/Mark 6 telescope pair may not be able to identify a subset of events as being gamma-ray candidates, it may be possible to use data from the Mark 5 telescope to provide independent confirmation that a dataset selected on the basis imaging by a single telescope (the Mark 6) may be gamma-ray rich. To this end, the events remaining after the application of the imaging analysis to the Mark 6 data, as described in section 6.7, have been subject to stereo analysis in conjunction with the full Mark 5 dataset. The image-selected Mark 6 dataset contains 189 on-source events and 106 off-source events. Of these, 98 on-source and 54 off-source events have counterparts in the Mark 5 dataset. This is a reduction of  $\sim 49\%$  in the size of the dataset for both on- and off-source data. In such a small dataset, it is difficult to identify significant differences between the on- and off-source population parameter distributions. For example, figure 6.11 shows the  $D_{miss}$ ,  $R_{ep}$  and  $H_c$  distributions for on- and off-source events. The shapes of the distributions for signal and background are clearly similar. Figure 6.12 shows the differences between these two distributions.

The small size of this resulting dataset makes selection on the basis of the stereo parameters impractical. This result further suggests that the Mark 5A telescope cannot contribute to the identification of gamma ray events within the Mark 6 dataset.

## 6.7 Short Baseline Stereo Measurements Using the Mark 6 Telescope

The centres of the left and right flux collectors of the Mark 6 telescope are separated by 14 m. Comparison of the lower moments of the images of showers formed on the detectors facing these mirrors affords the opportunity to investigate differences between gamma and hadron induced showers over a short baseline. The gamma-ray selection parameters which can be developed for such a system are analogous to those used for the long baseline parameters discussed above.

This sensitivity to the cascade primary has also been developed and exploited as a means of gamma-ray signal enhancement by the Crimean Astrophysical Observatory group (e.g. Vladimirovsky *et al.*, 1989, Kornienko *et al.*, 1993).

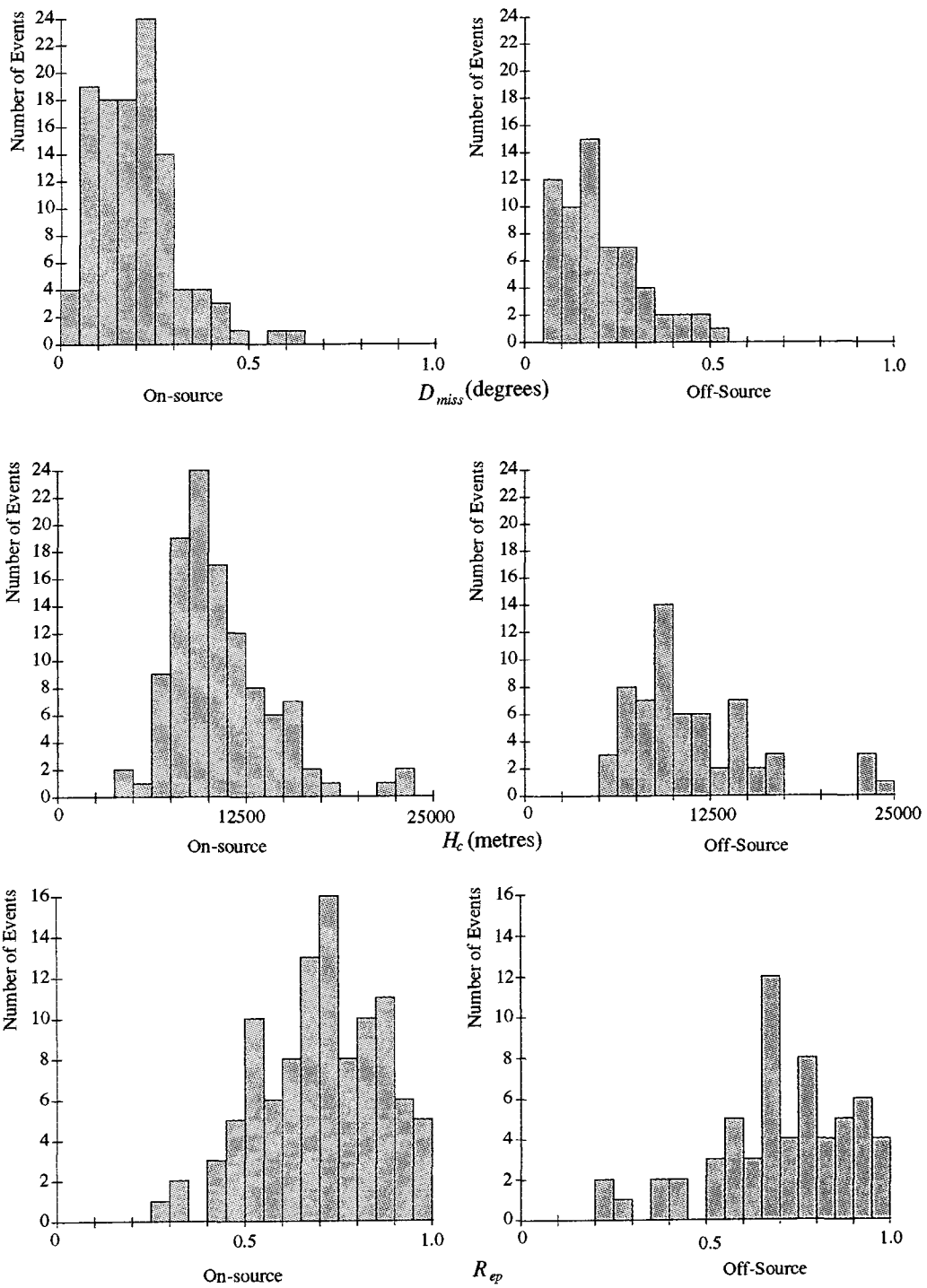


Figure 6.11 Distributions for  $D_{miss}$ ,  $R_{ep}$  and  $H_c$  for stereo datasets formed from Mark 6 single telescope gamma-ray enhanced data and the total Mark 5A telescope data.

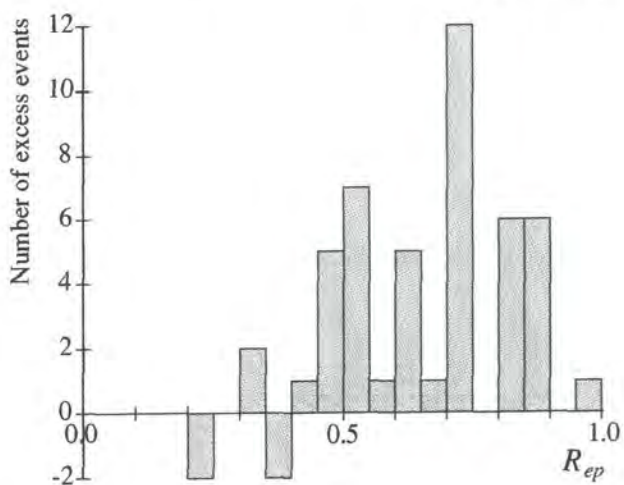
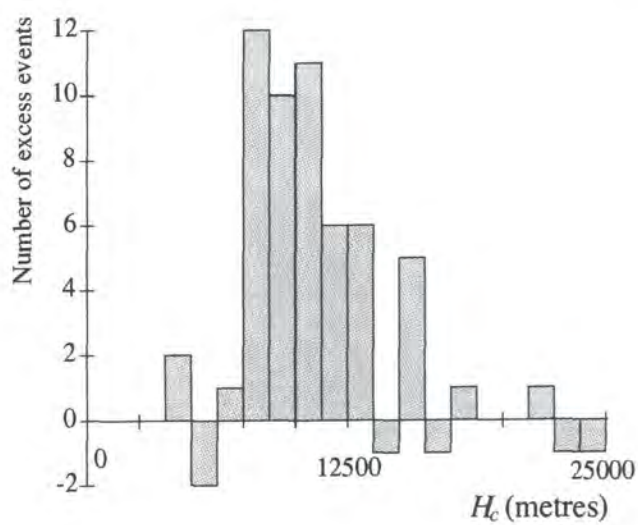
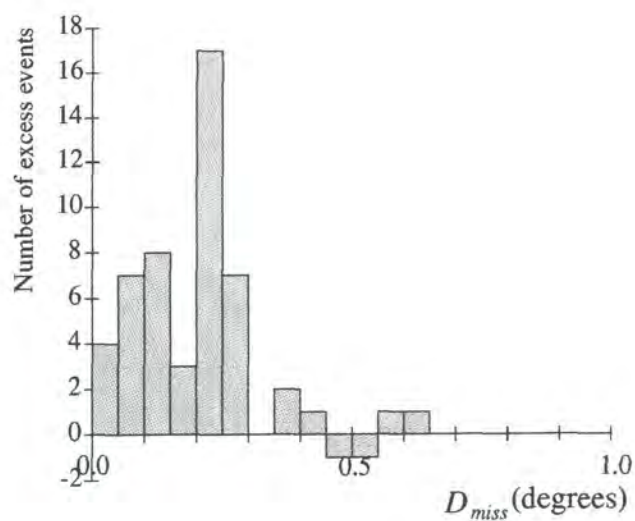


Figure 6.12 Differences between on- and off-source distributions of the stereo parameters formed from a dataset incorporating only imaging-selected Mark 6 telescope data.

These short baseline stereoscopic measurements also use the spatial uniformity of the gamma-ray light pool as opposed to the more irregular light distribution from hadron-induced showers. For detectors which are located close to one another, the differences will be less marked. For example, trigonometrical reconstruction of the shower axis is more susceptible to error where the baseline on the ground is shorter. Despite these limitations, short baseline stereoscopic measurements with the Mark 6 telescope may prove to be an attractive and powerful discrimination tool due to the size of the dataset available (65000 'tidied' on-source Mark 6 events in the Cen X-3 dataset available for short baseline studies, compared to 7000 long baseline stereo events).

Qualitatively, *D-dist* and *Left-Right ratio* are the Mark 6 short baseline equivalents of the long baseline parameters  $D_{miss}$  and  $R_{ep}$  respectively. The distributions of these parameters and their utility in analysis of Mark 6 telescope data are discussed in Shaw (1999).

## 6.8 Summary

The light created in a shower initiated by a gamma-ray primary is generally of more uniform intensity across the light pool than that of a shower resulting from a cosmic-ray primary. This difference can be used with measurements made with more than one telescope to distinguish between gamma-rays and cosmic-rays.

Measurements with the Durham Mark 3A and Mark 5A telescopes have shown the power of stereoscopic parameters recorded using simple telescopes to distinguish between gamma-rays and the cosmic ray background. In 1993, a burst of gamma rays from the cataclysmic variable AE Aquarii was observed. Selection of data based on the stereo parameter  $D_{miss}$  allowed the signal strength to be enhanced from 4.5% to 11.2%, which is a worthwhile improvement in the significance of the detection.

While it appears that the application of such parameters to a system comprising instruments of dissimilar sensitivity (the Mark 5A/Mark 6 telescope pair) is of limited benefit, stereoscopic studies remain a viable tool in the application of short baseline studies using the data recorded by the triggering detectors of the Mark 6 telescope, which are separated by 14 metres.

## Chapter 7. Conclusions and Future Work

### 7.1 Introduction

This thesis has described the commissioning of the Durham Mark 6 atmospheric Cherenkov telescope, and the improvements in equipment and practice which have been developed since the telescope was constructed.

The use of the Mark 6 telescope, in conjunction with the smaller Mark 5 telescope, as a stereo system for enhanced gamma-ray detection has also been investigated.

This chapter summarises the achievements made with the Mark 6 telescope up to the time of writing. The success of the telescope in its use to detect a number of VHE gamma-ray sources is briefly described. It also outlines and discusses further possible developments to the telescope and a brief overview of possible future developments in the wider VHE gamma-ray astronomy field.

### 7.2 Achievements to Date

In the period covered by the work described in this thesis, the Mark 6 telescope has been used to observe a total of 17 objects during about 1500 hours of operation. Detections of TeV gamma-rays from PSR B1706-44, Cen X-3 and Mrk 501 have been reported. Observations have also been made on a number of further AGNs in view of the successful detection of close AGNs by groups working in the northern hemisphere. A recent detection of PKS2155-304 (Chadwick *et al.*, 1998c) is the first report of an X-ray selected BL Lac observed from the southern hemisphere and -very importantly- the most distant AGN yet detected ( $z = 0.117$ )

Observations of SN1006 have also been made with a view to confirming the TeV detection by Tanimori *et al.* (1998). This would confirm the important discovery that this SNR, and by inference others, are responsible for at least some fraction of the cosmic ray flux.

A number of important technical developments have been made to the telescope in the same period.

- The introduction of light baffles around the flux collectors and detectors has reduced the effect of background light on data recorded with the telescope.
- A laser based calibration system for PM tube gain calibration provides a significant improvement over the previous system based on a radioactive light pulser.

- A CCD sky camera has been incorporated into the telescope to improve the knowledge of the pointing accuracy of the telescope, to  $<0.02^\circ$  for each individual event.

- The effects of temperature variations on elements of the telescope (laser, PM tubes, electronics) have been investigated. Temperature control systems have been implemented in cases where the variation causes significant changes in telescope operation.

- The effects of heating the mirrors have also been investigated, in order to reduce the data lost due to freezing and misting of the mirrors. This investigation is ongoing.

- Atmospheric clarity is now measured routinely using an infrared radiometer, which detects the radiation from clouds or other matter in the field of view. This measure is more sensitive and consistent than the personal assessment of clarity by an observer. It is also an instantaneous measure of the sky clarity independent of the performance of the telescope.

### 7.3 Detections of VHE Gamma-Ray Sources

AE Aquarii is a cataclysmic variable which has been detected by the Potchefstroom and Durham groups (e.g. Meintjies *et al.*, 1992, Bowden *et al.*, 1992). In 1993, a 4200 s burst of VHE emission was observed using the Mark 3A and Mark 5A telescopes (Chadwick *et al.*, 1995). In addition to standard imaging techniques, stereoscopic techniques were applied to these data. The successful application of such stereo parameters, reviewed in chapter 6, demonstrated the potential of studies using multiple telescopes.

PSR B1706-44 is a radio pulsar detected at VHE energies by the CANGAROO collaboration (Kifune *et al.*, 1995). Analysis of data taken with the Mark 6 telescope has confirmed this detection (Chadwick *et al.*, 1998a). Imaging analysis techniques were applied to the data and an excess of events were seen in the on-source data significant at the  $5.9\sigma$  level. The flux at  $E > 300$  GeV was estimated to be  $(3.9 \pm 0.7) \times 10^{-11} \text{ cm}^{-2}\text{s}^{-1}$ .

Cen X-3 is a high mass accreting X-ray binary. VHE emission has been previously detected from this object (Brazier *et al.*, 1989, Raubenheimer *et al.*, 1989). A 100 MeV outburst also been detected by the *EGRET* experiment (Vestrand *et al.*, 1997). Cen X-3 was observed using the Mark 6 telescope during March and June, 1997. Imaging analysis techniques were applied to the dataset (Chadwick *et al.*, 1998b and reviewed in chapter 6). After the application of such measures to both

on-source and background data, the number of excess on-source events was  $338 \pm 52$ , a  $6.4\sigma$  excess.

Mrk 501 has been detected, during a strong outburst in July/August 1997, as a TeV source using the Mark 6 telescope in observations at zenith angles in excess of  $70^\circ$ . This is important as an example of the continued sensitivity of the telescope for observations at large zenith angles. It may also be important in investigating the highest energies of gamma-rays ( $> \sim 15$  TeV) as probes of the intergalactic IR background density.

PKS 2155-304 is the brightest BL Lac object in the sky. It is also one of only two X-ray selected BL Lac objects detected by the *EGRET* experiment (the other is Mrk 421). It was observed in September-November 1996 and October/November 1997. The application of imaging analysis techniques produced an excess of  $729 \pm 107$  on-source events, a  $6.8\sigma$  excess. The flux of gamma-rays at energies  $> 300$  GeV is found to be  $(4.2 \pm 0.7_{\text{stat}} \pm 2.0_{\text{sys}}) \times 10^{-11} \text{ cm}^{-2} \text{ s}^{-1}$ .

## 7.4 Further Modifications to the Durham Atmospheric Cherenkov Telescopes

Any future modifications to the telescopes will be made with the same motivations as those which drove the construction process discussed in chapter 4 and the improvements described in chapter 5. Improvements to the telescope will be carried out with the aim of increasing the duty cycle or reducing the energy threshold of gamma ray detection. Increases in duty cycle will be achieved by modifications which allow the telescope to operate under conditions which currently preclude data taking. Reduction of the telescope energy threshold may be achieved by increasing the number of low energy showers recorded and increasing the accuracy with which they are parameterized. It may also be reduced by improving the ability to distinguish between gamma-ray and hadron induced events.

As a result of experience gained during operation of the Mark 6 telescope, methods of further improving the capabilities of the telescope have become apparent. Some of these, such as laser calibration of the PM tubes and correction of steering measurements using a CCD sky camera, have been implemented early in the lifetime of the instrument, discussed in chapter 3. Others, such as methods of reducing data loss due to mirror freezing/misting have been the subject of preliminary investigations discussed in chapter 5. Further possibilities for enhancing the telescope performance remain and these are discussed in section 7.5.

The Mark 6 telescope development program has seen successful implementation of a number of measures to improve telescope operation by reducing the energy threshold and increasing the duty cycle. Such measures have produced a telescope capable of detecting gamma-ray induced events at energies  $\geq 100$  GeV, albeit with low detection probability.

Future possible upgrades to the Mark 6 telescope include replacement of the mirrors and enhancement of the imaging capability in all three detector packages by improving the PM tube arrangements. Further improvements in telescope capability may be possible, for example, by using optical (high bandwidth) signal cables between the detector packages and the telescope electronics.

#### 7.4.1 Future Improvements to the Mark 6 Telescope

A phased upgrade plan has been proposed for the Mark 6 telescope to improve the quality and quantity of data recorded. The phases are outlined below.

- Replacement of the 'guard ring' of 2" diameter PM tubes with 2 rings of 1" tubes (an extra 78 tubes) to provide uniform camera coverage over a diameter of  $3^\circ$ . This would require a significant redesign of the imaging detector package and also the incorporation of extra electronics to monitor and process the signals. It would improve the parameterization of events recorded at the edge of the camera by providing uniform resolution across a wider field of view. The additional PM tubes would not have corresponding PM tubes in the left and right triggering packages, and so would not form part of the telescope triggering mechanism. The improved parameterization would reduce the uncertainty in the calculation of the Hillas parameters for events containing light detected at the camera edge and therefore improve the ability to discriminate between gamma-ray and background events. This is an obviously beneficial, but expensive ( $\sim$  £50 000) development.

- Replacement of the central flux collector with one of similar design but improved quality and reduced point spread function (PSF). An improvement in the quality of the collector would reduce the extent to which light is dispersed over the surfaces of the PM tubes in the light detector packages. This would have the effect of concentrating the light from a given shower onto a smaller number of PM tubes. The result would be a reduction in telescope energy threshold. There would also be an enhancement in event parameterization due to the improved optical quality. This would allow improved discrimination between gamma-ray and hadron induced events based on imaging parameters.

Replacement of the central collector may also provide the opportunity to

incorporate heating elements into the surface of the mirror in order to prevent freezing as discussed in chapter 5. This is an important and low cost (~£7 000) development.

- Replacement of the left and right flux collectors in a similar fashion to the central collector. An improvement in the PSF of these collectors offers a reduction in energy threshold and an improvement in the parameterization of the image recorded in the triggering detectors, allowing further development of the short baseline stereoscopic analysis parameters discussed in chapter 6. Addition of heating elements in conjunction with similar work on the central collector offers the potential of increased duty cycle due to reduced time loss due to freezing. This is a worthwhile improvement at a cost of £15 000.

- Upgrade the left and right triggering detector packages to 91 PM tubes providing  $0.25^\circ$  pixellation, similar to the current central detector package. This would provide a true triple-imaging system. This modification would improve the background rejection characteristics of the telescope by allowing the coincidence trigger requirements to be even more closely matched to the behaviour of gamma-ray induced showers. The spatial non-uniformity of the light in a hadron-induced shower is already utilised. Events are rejected where the spatial coincidence of light between the three collectors is poorer than  $0.5^\circ$  (taking into account the spread of light in the image plane). Improving the resolution of the triggering detector packages as described would increase the severity of the coincidence requirement to  $0.25^\circ$ . This would reduce the number of small hadron-induced events which cause the system to trigger. The result would be an increase in the telescope sensitivity to low energy gamma-rays relative to the sensitivity to low energy background events. This would be an expensive modification (~ £100 000).

- Upgrade the central detector package to a 500 element camera with  $0.1^\circ$  resolution. This would use the full potential of the improved PSF of the new central collector to further improve the definition of the shape of the image of the shower. This will lead to increased effectiveness of the parameterization of the event and provide a state of the art telescope at a cost of £250 000.

However, no provision for this upgrade plan is included in the programme for 1998/9.

## 7.5 Future Prospects for VHE Gamma-Ray Astronomy

Gamma-ray observations in the TeV region of the electromagnetic spectrum are currently being made by a number of groups in both hemispheres. In the northern hemisphere, the Whipple collaboration (Finley, 1998) and the HEGRA collaboration (Daum *et al.*, 1997) are in the process of developing multiple telescope array systems. Such systems have the potential to exploit multiple imaging measurements for event discrimination. These systems comprise a central detector (or detectors) surrounded by a number of similar instruments. The sensitive area of the central instrument is therefore also covered by those of the surrounding detectors. In arrays such as those described above, the majority of events detected by the central instrument will also fall within the sensitive area of one (or more) of the others. The dataset available will therefore be of comparable size to that available for imaging analysis from an individual instrument.

In the southern hemisphere, the Durham group and CANGAROO collaboration (Tanimori *et al.*, 1998) have concentrated on developing single, efficient instruments, utilising well refined background rejection techniques. The existence of two instruments provides the important opportunity for independent corroboration of all detections.

The EGRET experiment on board the *Compton Gamma-Ray Observatory* is nearing the end of its useful life, and no satellite based experiments are due to launch before GLAST, proposed for sometime in the first decade of the next century (e.g. Gehrels and Michelson, 1997). The high energy and medium energy (HE, ME) parts of the gamma-ray region of the electromagnetic spectrum will therefore not be well served for some years. The requirement to improve the lower energy limits of ground based gamma-ray astronomy into these regions will therefore become of increased importance.

The Durham Mark 6 telescope is now established and operating routinely. The capabilities of the instrument have been demonstrated by observations of a number of objects, including Cen X-3 (Chadwick *et al.*, (1998b)), PSR B 1706-44 (Chadwick *et al.*, 1998a) and numerous AGNs including PKS 2155-304 (Chadwick *et al.*, 1998d). The enhancements described in this thesis have improved the operating characteristics of the telescope significantly from those at the time of construction. Preliminary work has been done on further improvements to increase the sensitivity and duty cycle of the telescope. A plan for future upgrades to the telescope and its control, logging and monitoring systems has been described. These improvements will ensure that the Mark 6 telescope could remain a highly sensitive scientific instrument, capable of offering a significant contribution to the field, for many years to come.

## References

- Allan, H.R., 1971, *Prog. Elem. Part. and Cosmic Ray Physics*, **10**, 170
- Armstrong, P., *et al.*, 1999, *Experimental Astronomy* in press
- Batschelet, E., 1981, *Circular Statistics in Biology*, Acad. Press, London
- Blackett, P.M.S., 1948, *Rep. Gassiot Comm. of the Roy. Soc.*, **34**, Physical Society, London
- Bleackley, P., 1996, *M.Sci report (unpublished)*, University of Durham
- Bowden, C.C.G., *et al.*, 1992a, *Astroparticle Physics*, **1**, 47
- Bowden, C.C.G., *et al.*, 1992b, *J. Phys. G.: Nucl. Part. Phys.*, **18**, L55
- Bradbury, S.M., *et al.*, 1995, *Towards a Major Atmospheric Cherenkov Detector IV*, (Ed. Cresti, M.) 182
- Bradbury, S.M., *et al.*, 1997, *Astronomy and Astrophysics*, **320**, L5
- Brazier, K.T.S., *et al.*, 1989, *Experimental Astronomy*, **1**, 77
- Brazier, K.T.S., *et al.*, 1990, *Proc. 21st int. Cosmic Ray Conf. (Adelaide)*, **2**, 292
- Brazier, K.T.S., *et al.*, 1994, *MNRAS* **268**, 517
- Carraminana, A., 1991, *Ph.D. Thesis*, University of Durham
- Carraminana, A., *et al.*, 1989, *Astrophys. J.*, **346**, 967
- Carter, D.A., 1990, *Experimental Astronomy*, **1**, 4
- Catanese, M., *et al.*, 1998, *Astrophysical Journal*, **501**, 616
- Cawley, M.F., *et al.*, 1989, *Experimental Astronomy*, **1**, 173
- Cawley, M.F. *et al.*, 1990, *Irish Astronomical Journal*, **19**, 51
- Cawley, M.F., *et al.*, 1993, *Towards a Major Atmospheric Cherenkov Detector II*, (Ed. Lamb, R.C.), 176
- Chadwick, P.M., 1987, *Ph.D. thesis*, University of Durham
- Chadwick, P.M., *et al.*, 1995, *Astroparticle Physics*, **4**, 99
- Chadwick, P.M., *et al.*, 1996, *Space Science Reviews*, **75**, 153
- Chadwick, P.M., *et al.*, 1996, *Astron. Astropys. Supp.*, **120**, 657.
- Chadwick, P.M., *et al.*, 1998a, *Astroparticle Physics*, **9**, 131
- Chadwick, P.M., *et al.*, 1998b, *Astrophysical Journal*, **503**, 391
- Chadwick, P.M., *et al.*, 1999a, *Astrophysical Journal*, in press
- Chadwick, P.M., *et al.*, 1999b, *J. Phys. G.*, accepted for publication
- Chantell, M.R., *et al.*, 1997, *Astroparticle Physics*, **6**, 205

- Charles, P. A. and Seward, F.D., 1995, *Exploring the X-ray Universe*, Cambridge University Press, Cambridge
- Cherenkov, P.A., 1937, *Phys. Rev.*, **52**, 378
- Daum, A., *et al.*, 1997, *Astroparticle Physics*, **8**, 1
- Dickinson, J.E., 1995, *Ph.D. thesis, University of Durham*
- Fegan, D.J., 1992, *Towards a Major Atmospheric Cherenkov Detector* (Ed. Fleury, P., & Vacanti, G.), Editions Frontiers, Gif-sur-Yvette, 3
- Fegan, D.J., 1996, *Space Sci. Rev.*, **75**, 137
- Fierro, J.M., *et al.*, 1993, *Astrophysical Journal*, **413**, L27
- Finley, J.P., 1998, *American Astronomy Society Meeting*, 192, #81.05
- Frank, I.M., & Tamm, Ig., 1937, *Dokl. Acad. Nauk*, **14**, 109
- Galbraith, W. & Jelley, J.V., 1953, *Nature*, **171**, 349
- Gaisser, T.K., 1990, *Cosmic Rays and Particle Physics*, Cambridge University Press, Cambridge
- Gehrels, N. & Michelson, P., 1997, *American Astronomical Society Meeting*, **191**, #64.08
- Gibson, A.I., *et al.*, 1982, *Nature*, **296**, 883
- Goeckel, 1910, *Phys. Zeits.*, **11**, 280
- Gould, R.J. & Schröder, G.P., 1966, *Phys. Rev. Lett.*, 16, 252
- Greissen, K., 1956, *Progress in Cosmic-Ray Phys.*, **3**, North Holland Publishing, Amsterdam
- Halzen, F., 1998, *American Astronomical Society Meeting*, **192**, #62.28
- Hamamatsu R1924 PM tube data sheet
- Heaviside, O., 1892, *Electrical Papers*, **2**, 494
- Hess, V.F., 1911, *Phys. Zeits.*, **12**, 998
- Hillas, A.M. & Patterson, J.R., 1987, *Very High Energy Gamma-Ray Astronomy* (Ed. Turver, K.E.), D. Reidel, Dordrecht, 243
- Hillas, A.M., 1982, *J. Phys. G: Nucl. Part. Phys.*, **8**, 1475
- Hillas, A.M., 1985, *Proc. 19<sup>th</sup> Int. Cosmic Ray Conf.*, La Jolla, **3**, 445
- Hillas, A.M., 1996, *Space Science Reviews*, **75**, 17
- Hofmann, W., 1997, *Towards a Major Atmospheric Cherenkov Detector V* (Ed. de Jager, O.C.), 405
- Holder, J., 1997, *Ph.D. thesis, University of Durham*
- Horowitz, P. and Hill, W., 1980, *The Art of Electronics*, Cambridge University Press, Cambridge

- Jelley, J.V., 1958, *Cerenkov Radiation and its Applications*, Pergamon Press, London
- Jelley, J.V., 1966, *Phys. Rev. Lett.*, **16**, 11
- Kifune, T., *et al.*, 1995, *Astrophysical Journal*, **438**, L91
- Kohnle, A., *et al.*, 1996, *Astroparticle Physics*, **5**, 119
- Konopelko, A., *et al.*, 1996, *Astroparticle Physics*, **4**, 199
- Kornienko, A.P. *et al.*, 1993, *Experimental Astronomy*, **4**, 77
- Lang, M.J., *et al.*, 1994, *J. Phys. G: Nucl. Part. Phys.*, **20**, 1841
- Lang, M.J., 1995, *Proc. 24<sup>th</sup> Int. Cosmic Ray Conf.*, Rome, **3**, 754
- Leahy, D.A., *et al.*, 1983, *Astrophysical Journal*, **272**, 256
- Mallet, L., 1926, *C. R. Acad. Sci. (Paris)*, **183**, 274
- Mallet, L., 1928, *C. R. Acad. Sci. (Paris)*, **187**, 222
- Mallet, L., 1929, *C. R. Acad. Sci. (Paris)*, **188**, 445
- Mannings, V., 1990, *Ph.D. Thesis, University of Durham*
- Mattox, J.R., *et al.*, 1992, *Astrophysical Journal*, **401**, L23
- Meintjes, P.J., 1992, *Astrophysical Journal*, **401**, 325
- Mirzoyan, R. and Lorenz, E., 1994, *HEGRA preprint*, MPI-PhE/94-35
- Nolan, P.L., *et al.*, 1993, *Astrophysical Journal*, **409**, 697
- Ong, R.A., *et al.*, 1996, *Astroparticle Physics*, **5**, 353
- Orford, K.J., 1995, *Experimental Astronomy*, **6**, 1
- Petry, D., *et al.*, 1996, *Astronomy and Astrophysics*, **311**, L13
- Pinkau, K., 1996, *Astronomy and Astrophysics Supplement*, **120**, 43
- Pohl, M., 1996, *Astronomy and Astrophysics*, **307**, L57
- Punch, M. *et al.*, 1992, *Nature*, **358**, 477
- Punch, M., 1993a, *Towards a Major Atmospheric Cherenkov Detector III* (Ed. Kifune, T.), 215
- Punch, M., 1993b, *Ph.D. Thesis, University College Dublin*
- Quinn, J., *et al.*, 1996, *Astrophysical Journal*, **456**, L83
- Raubenheimer, B.C. and Smit, H.J., 1997, *Astroparticle Physics*, **7**, 63
- Raubenheimer, B.C. *et al.*, 1989, *Astrophysical Journal*, **336**, 349
- Raubenheimer, B.C. *et al.*, 1994, *Astrophysical Journal*, **428**, 777
- Lord Rayleigh, 1894, *Theory of Sound*, Macmillan, **1**, 35
- Reynolds, P.T., 1991, *Proc. 22<sup>nd</sup> Int. Cosmic Ray Conf.*, Dublin, **1**, 496
- Roberts, I.D., 1994, *M.Sc. thesis, University of Durham*

- Rossi, B. & Greisen, K., 1941, *Rev. Mod. Phys.*, **13**, 240
- Rossi, B., 1952, *High Energy Particles*, Prentice Hall, New York
- Rutherford & Cooke, 1903, *Phys. Rev.*, **16**, 183
- Schubnell, M.S., *et al.*, 1996, *Astrophysical Journal*, **460**, 644
- Shaw, S.E., 1999 (in preparation), *Ph.D. Thesis, University of Durham*
- Standish, E.M., 1982, *Astron. Astrophys.*, **114**, 297
- Stecker, F.W. & de Jager, O.C., 1996, *Space Sci. Rev.*, **75**, 401
- Stecker, F.W., *et al.*, 1992, *Astrophysical Journal*, 390, L49
- Tanimori, T., *et al.*, 1997, *Towards a Major Atmospheric Cherenkov Detector V* (Ed. de Jager, O.C.), 158
- Tanimori, T., *et al.*, 1998, *Astrophysical Journal Letters*, **497**, L25
- Thompson, D.J., *et al.*, 1995, *Astrophysical Journal Supplement*, **101**, 259
- Tindale, M.J., 1997, *M.Sci report (unpublished), University of Durham*
- Turver, K.E., 1997, *Towards a Major Atmospheric Cherenkov Detector V* (Ed. de Jager, O.C.), 389
- Turver, K.E. and Weekes, T.C., 1978, *Nuovo Cimento*, **45B**, 99
- Vacanti, G. *et al.*, 1991, *Astrophysical Journal*, **377**, 467
- Vestrand, W., *et al.*, 1997, *Astrophysical Journal Letters*, **483**, L49
- Vladimirsky, B.M. *et al.*, 1989, *Proc. Int. Workshop Very High Gamma Ray Astronomy* (Ed. Stepanian, A.A., Fegan, D.J. & Cawley, M.F.), Crimea, **21**
- Weekes, T.C., *et al.*, 1989, *Ap. J.*, **342**, 379
- Weekes, T.C., *et al.*, 1997, *Towards a Major Atmospheric Cherenkov Detector V* (Ed. de Jager, O.C.), 202
- Yoshii H., *et al.*, 1996, *Astrophysical Journal*, **472**, 800
- Yoshikoshi, T., *et al.*, 1997, *Astrophysical Journal Letters*, **487**, L65

